Multiple scattering of classical waves: microscopy, mesoscopy, and diffusion

M. C. W. van Rossum

Department of Neuroscience, University of Pennsylvania, Philadelphia, Pennsylvania 19104-6058

Th. M. Nieuwenhuizen

Van der Waals-Zeeman Instituut, Valckenierstraat 65, 1018 XE Amsterdam, The Netherlands

A tutorial discussion of the propagation of waves in random media is presented. To a first approximation the transport of the multiple scattered waves is given by diffusion theory, but important corrections are presented. These corrections are calculated with the radiative transfer or Schwarzschild-Milne equation, which describes intensity transport at the ''mesoscopic'' level and is derived from the ''microscopic'' wave equation. A precise treatment of the diffuse intensity is derived which automatically includes the effects of boundary layers. Effects such as the enhanced backscatter cone and imaging of objects in opaque media are also discussed within this framework. This approach is extended to mesoscopic correlations between multiple scattered intensities that arise when scattering is strong. These correlations arise from the underlying wave character. The derivation of correlation functions and intensity distribution functions is given and experimental data are discussed. Although the focus is on light scattering, the theory is also applicable to microwaves, sound waves, and noninteracting electrons. [S0034-6861(99)00601-7]

CONTENTS

I. INTRODUCTION

Transport of waves through opaque media is a subject of interest in daily life. Examples are light transported through fog, clouds, milky liquids, white paint, paper, and porcelain, as well as electromagnetic waves transported through stellar atmospheres and interstellar clouds. Nowadays the transport of visible light through human tissue is being used as a noninvasive technique to detect, for instance, breast cancer.

Some basic properties of diffuse light are well known. On a cloudless day we see the immediate radiation from the sun. When a cloud passes in front of the sun, the light first becomes weaker and diffuse. When the cloud has become thick enough, the sun becomes invisible; this happens when the cloud thickness is of the order of a mean free path. On a cloudy day there is no direct view of the sun, but there is still light: it is diffuse light coming from many directions. It has propagated diffusely through the cloud and leaves it in random directions, partly in the direction we are looking.

The study of diffuse wave transport was first undertaken by astrophysicists. They wanted to understand how radiation created in the center of stars is affected when it traverses as interstellar cloud. Well-known books in this field were written by Chandrasekhar (1960) and Van de Hulst (1980). For more mundane applications, such as the detection of a school of fish using acoustic waves, see Ishimaru (1978).

It is the purpose of this review to present a comprehensive, self-contained text intended for laboratory applications of diffuse wave transport. We explain how the transfer equation follows from the wave equation and how radiative corrections can be calculated. Though the approach can be applied to any geometry, we shall focus mainly on slab geometries.

In Sec. II we discuss some general aspects of wave scattering, such as diffusion and Anderson localization. In Sec. III we review the basic concept of the radiative-transfer equation. Next we begin a detailed analysis in Sec. IV with the underlying wave equation in the scalar approximation. We explain the notions of the t matrix and the cross section. In Sec. V we consider the amplitude or dressed Green's function. We discuss how extinction is related to the self-energy. Next we consider propagation of intensity via the Bethe-Salpeter equation. We use the simplest case, the ladder approximation, to derive a transport equation equivalent to the radiative transfer equation. This equation then describes not only diffusion in the bulk, but also the precise behavior at the boundaries. Various experimentally relevant situations are considered in detail: transport in a bulk medium, through very thick (semi-infinite) and through finite slabs; the enhanced backscatter cone; exact solutions of the Schwarzschild-Milne equation; the regime of large index mismatch; semiballistic transport; and imaging of objects hidden in opaque media (Secs. VI–XIII).

With these ingredients we consider in the latter half of the article correlations of intensities. This leads to three kinds of observable correlation functions, the angular correlation function C_1, the correlation of total transmission C_2, and the correlation of the conductance C_3. We explain how these functions are calculated and then consider correlations between three intensities (third cumulants) and the full distribution of intensities.

A. Length scales

The diffuse regime is formulated in the three inequalities (Kaveh, 1991)

$$\lambda \ll l \ll L \ll L_{\rm abs},\ L_{\rm inc}, \tag{1}$$

where λ is the wavelength, l the mean free path, L the sample size, $L_{\rm abs}$ the absorption length (for optical systems), and $L_{\rm inc}$ the incoherence length (for electronic systems). The first inequality ensures that localization effects (see below) are small; the second inequality implies that many scatterings occur if the wave traverses the system; the third inequality ensures that not all radiation is absorbed.

The description of radiation transport can occur on roughly three length scales:

• *Macroscopic:* On scales much larger than the mean free path the average intensity satisfies a diffusion equation. The diffusion coefficient D enters as a system parameter that has to be calculated on mesoscopic length scales.

• *Mesoscopic:* On length scales of the mean free path l, the problem is described by the radiative transfer equation or Schwarzschild-Milne equation. This is the Boltzmann-type equation for the system. At this level

one needs as input the mean free path l and the speed of transport v, which should be derived from microscopics. In the diffusive regime this approach leads to the diffusion coefficient $D = vl/3$.

• *Microscopic:* The appropriate wave equation, such as Maxwell's equations, the Schrödinger equation, or an acoustic-wave equation, is used on this length scale. The precise locations and shapes of scatterers are assumed to be known. Together with the wave nature they determine the interference effects of scattered waves. In light-scattering systems the scatterers often have a size in the micron regime, comparable to the wavelength λ, which could lead to important resonance effects. The mesoscopic or Boltzmann description follows by considering the so-called ladder diagrams.

The microscopic approach will be the starting point for this review. Fundamental quantities, such as the self-energy and the Hikami box, can only be calculated on this level. The drawback of the microscopic approach is that it is too detailed. In practice the precise shapes and positions of the scatterers often are not known and a mesoscopic or macroscopic description is necessary.

B. Weak localization, closed paths, and the backscatter cone

The diffusion equation is a classical equation that fully neglects interference effects inherent in wave propagation. At this level of description there is no difference between diffusion of particles and of wave intensity. Whereas a transmission pattern of monochromatic (laser) light through an opaque medium is known to consist of speckles (bright spots on a dark background), the diffusion equation and the radiative transfer equation describe only the average intensity.

The wave nature of light immediately leads to a reduction in transmission due to interference effects. Following Rayleigh (1880) we suppose that the transmission amplitude E for a certain experiment is composed of many terms C_p arising from physically different interference paths p.

Some paths have closed loops, i.e., loops that return to the same scatterer. When such loops contain two or more common intermediate scatterers, they can be traversed in two directions. Let us consider one of these loops C_p, and denote the contribution of the second, reversed loop by D_p. Summing over all paths we have

$$E = \sum_p (C_p + D_p). \tag{2}$$

The intensity is

$$E^2 = \sum_p (C_p^* C_p + D_p^* D_p) + \sum_p (C_p^* D_p + D_p^* C_P) + \sum_{p \neq p'} (C_p^* + D_p^*)(C_{p'} + D_{p'}). \tag{3}$$

When applied to electrons, quantum mechanics tells us that the C^*C and D^*D terms are probabilities, while C^*D and D^*C terms are interference contributions. Naively, one expects the second and third terms to be small. Thus in Boltzmann theory only probabilities are taken into account, that is to say the first term.

However, if there is time-reversal invariance, the second term $\Sigma_p(C_p^* D_p + D_p^* C_p)$ will be equally large: *there is a factor of 2 for each closed loop*. As a result, for the wave intensity there is a larger probability of return.

In optics there is a simply measurable effect due to this, namely the enhanced backscatter cone. When the incoming and outgoing light are in exactly the same direction, the light path may be considered closed. As predicted by Barabanenkov (1973) and detected by several groups (Kuga and Ishimaru, 1985; Van Albada and Lagendijk, 1985; Wolf and Maret, 1985) the *average* intensity in the backscatter direction has a small cone of height almost one and an angular width of $\delta\theta \sim \lambda/l$. This observation has given an enormous push to research on weak-localization phenomena in optics.

This effect, the so-called weak-localization effect, occurs if $\lambda/l \ll 1$ and is the precursor of the so-called strong-localization effects that occur if $\lambda/l \sim 1$. Both effects are also known as "mesoscopic," indicating length scales between macroscopic (the diffusion equation) and microscopic (individual scattering events). Indeed, in electron systems these effects only show up in rather small samples due to inelastic scattering. For optical systems there is no such size restriction. The study of mesoscopic effects began in the field of electronic systems, and we shall use many results derived there.

For electronic systems weak-localization effects were first analyzed by Altshuler, Aronov, and Spivak (1981) in order to explain the Sharvin-Sharvin fluctuations of resistance as a function of the applied magnetic field (Sharvin and Sharvin, 1981). These so-called "magnetofingerprints" show a seemingly chaotic conductance as the applied field is varied, but are perfectly reproducible as they are solely determined by the location of the scatterers. (Only at very low temperatures is electron scattering dominated by impurity scattering; at higher temperatures scattering arises mainly from phonons.)

C. Anderson localization

If scattering is very strong, the "weak-localization" effects become of order unity, i.e., $l \sim \lambda$ (λ/l is of the order of 0.001–0.01 for visible light in standard laboratory situations). According to the criterion of Ioffe and Regel (1960) the diffusion constant will tend to zero at that point. The scattering process that causes the enhanced backscatter also reduces the diffusion constant. The amplitudes that make up the intensity split and one of the amplitudes visits some of the scatters in reverse sequence, thus forming a loop. The diffusion constant is lowered by these processes. (The loop is somewhat similar to the renormalization of the effective mass in field theories.) If scattering is increased, the contribution of these loops becomes more and more important. It is not simply that the diffusion constant tends linearly to zero as scattering increases. Rather, the return probability of

the intensity becomes higher and higher, reducing the diffusion constant in a stronger fashion. The diffusion constant can thus become zero at finite scatterer strength, meaning that the wave can no longer escape from its original region in space. This is the transition to the well-known Anderson localization (Anderson, 1958).

In the Anderson-localization regime there are only localized states. In the delocalized regime there exist extended states, responsible for diffusion. In the localized regime the intensity typically decays exponentially over one localization length, whereas in the diffuse regime the wave function extends up to infinity. There are thus two different phases, the diffuse, metallic regime and the localized, insulating regime. In three dimensions a phase transition from the extended to the localized state can occur. In one and two dimensions the states are always localized, provided the waves are noninteracting (for electrons spin-orbit scattering also has to be absent). Yet for a finite sample the localization length can be much larger than the system size, in which case the states appear to be extended and the conductance does not vanish. Note that the localization is solely the result of the interference of the waves scattered by the disorder. [This is not the only scenario for a metal-insulator transition in electron systems. Due to their fermionic nature and interactions, electron systems allow for a whole range of possible transitions between the conducting and insulating regimes; see Mott (1990)]. Anderson localization is also called strong localization.

The precise behavior near and at the transition is not fully understood. The standard diagrammatic perturbation technique we use, works well for the description of diffusion and low-order corrections, but it is not suited for the study of the transition. Therefore various techniques have been developed to study behavior near the transition and the phase transition itself.

An important step was the scaling theory of localization put forward by Abrahams, Anderson, Licciardello, and Ramakrishnan (1979), which states that near the localization the only parameter of importance is the dimensionless conductance g (the conductance measured in units of e^2/h). The scaling of g as a function of sample size was studied earlier (Thouless, 1974, 1977; Wegner, 1976). Abrahams *et al.* extended those ideas and derived renormalization-group equations. They concluded that in one and two dimensions there is no real phase transition; the states are always localized. In three dimensions a phase transition can occur.

Classical diffusive transport is described by the ladder diagrams. The so-called *maximally crossed diagrams* are the next most important diagrams in the diffuse regime. They describe the leading interference terms responsible for the backscatter cone and reduction of the diffusion constant. Vollhardt and Wölfle summed self-consistently combinations of the ladder diagrams and the maximally crossed diagrams in the diffuse regime (Vollhardt and Wölfle, 1980a, 1980b, 1992). They found that the diffusion constant vanishes at a strong enough scatterer strength, thus providing a microscopic picture of the Anderson transition. As the maximally crossed diagrams yield loops of intensity, the approach can be seen as a self-consistent one-loop summation. Although a self-consistent approach will certainly not include all diagrams of higher order, the method works fine even close to the transition (Kroha, 1990; Kroha, Kopp, and Wölfe, 1990) because the first few higher-order correction terms vanish.

Another approach is to perform an exact average over the disorder within a field-theoretic approach. Next, one integrates over the fast fluctuations and is left with the slow variables of the system. This technique yields the so-called *nonlinear sigma model* (Wegner, 1979; Hikami, 1981; Efetov, 1983; Altshuler, Kravtsov, and Lerner, 1991). With the resulting action it is possible to generate systematically all corrections to the diffusion process (in $2+\epsilon$ dimensions), allowing for an explicit foundation of the scaling theory.

A recent approach is that of the *random-matrix theory*. The basic assumption here is that the total scattering matrix of the system, although very complicated, can be described by random matrix elements respecting the symmetries of the system. Surprisingly, this method works well, and from the assumption of the random ensemble it predicts many features of the systems correctly and in a simple way. It is, unfortunately, only applicable to quasi-one-dimensional situations. An overview of the theory and applications of random-matrix theory is given by Stone, Mello, Muttalib, and Pichard (1991) and Beenakker (1992).

Although some years ago there was hope that the Anderson transition might soon be reached for light scattered on disordered samples, it had not yet been observed when this review was written. One did observe that in time-resolved transmission measurements the average transmission time became very long. This was interpreted as an indication that the mean free path was very small, which would mean that the light was close to localization. It turned out, however, that the long transmission times were due to the light's spending much time inside the scatterers. This meant that the Anderson localization was still out of reach (Van Albada, Van Tiggelen, Lagendijk, and Tip, 1991).

D. Correlation of different diffusions

Another interaction effect is the interference of one diffuse intensity with another that has, for instance, a different frequency or position. In this work we shall concentrate on such processes, which lead to correlations in, for instance, the transmitted beams. There are advantages to studying the correlations above the loop effects. The correlations can be measured more accurately and easily in experiments than can renormalization effects. Secondly, it is an interesting feature of optical systems that there are three different transmission measurements:

- Coming in with a monochromatic beam in one direction (we call this "channel a") one can measure the intensity in the outgoing direction b and define the *an-*

gular transmission coefficient T_{ab}. Its correlation function is called the C_1 correlation and is of order unity, describing the large intensity difference between dark and bright transmission spots.

• One can also measure all outgoing light. In practice one uses an integrating sphere. This leads to the measurement of the *total transmission*,

$$T_a = \sum_b T_{ab}. \tag{4}$$

Its correlation function is called the C_2 correlation function.

• Finally, one can also add the results coming in from all possible directions, either by repeating the experiment under many different incoming angles or by using diffuse incoming light. This leads to a quantity

$$T = \sum_a T_a = \sum_{ab} T_{ab}, \tag{5}$$

called the *conductance* in analogy with electronic systems. Its fluctuations are called C_3 fluctuations in optics. In electronics (where, for instance, the magnetic field is varied), they are called universal conductance fluctuations (UCF). Notice that these fluctuations are not temporal but static, since the scatterers are fixed. Both C_2 and C_3 correlations are low-order corrections in $1/g$, which acts as the small parameter giving the relative strength of the interference effects.

There are various books and proceedings on localization and mesoscopics in electron systems (Nagaoka and Fukuyama, 1982; Ando and Fukuyama, 1988; Kramer and Schön, 1990; Van Haeringen and Lenstra, 1990, 1991, Altshuler, Lee, and Webb, 1991; Hanke and Kopaev, 1992) and classical waves (Kirkpatrick, 1985; Sheng, 1990; Soukoulis, 1993). Many aspects of the Anderson transition have been discussed by Lee and Ramakrishnan (1985).

II. MACROSCOPICS: THE DIFFUSION APPROXIMATION

A. Transmission through a slab and Ohm's law

Consider the propagation of light through a slab of thickness L ("plane-parallel geometry"). As indicated in Fig. 1 a plane wave impinges on the surface of an opaque medium at an angle θ_a. The index of refraction of the medium is n_0, and that of the surroundings is n_1. The ratio of the indices of refraction,

$$m = \frac{n_0}{n_1}, \tag{6}$$

is larger than unity if a dry substance is placed in air ($n_1 \approx 1$). If the substance is placed in a liquid, one may have $m < 1$. If $m \neq 1$ the refracted beam inside the medium will have an angle θ_a' different from θ_a.

Due to multiple scattering the incoming beam decays exponentially,

$$I_{\text{in}}(z) = I_0 e^{-z/l \cos\theta_a}, \tag{7}$$

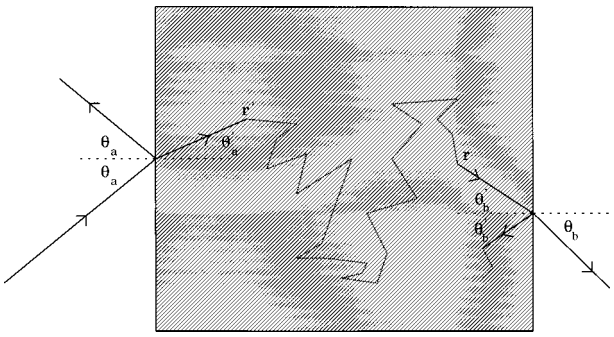

FIG. 1. Schematic representation of multiple scattering in a slab. A plane wave, impinging at an angle θ with respect to the z axis, is refracted to an angle θ' inside the multiple-scattering medium, while it is partly specularly reflected. After diffusive transport in the bulk, a wave arriving under angle θ_b' at one of the boundaries partially leaves the medium under angle θ_b and is partially reflected internally.

where the cosine is a geometrical factor expressing the total path length in terms of z. This exponential decay is known as the Lambert-Beer law. It describes the decay of direct sunlight in clouds or of car headlights in fog. The light source becomes invisible when the thickness of the diffuse medium is greater than one mean free path. The decay of direct-light intensity occurs because it is transformed into diffuse light.

The scattering of the incoming beam into diffuse light occurs in a skin layer with characteristic thickness of one mean free path. Later on this will be discussed at greater length when we solve the Schwarzschild-Milne equation. In the diffusion approach one simply assumes that the incoming beam is partly reflected and partly converted into a diffuse beam in the skin layer. Next one assumes that effectively diffuse intensity enters the system in a trapping plane located at distance $z_0 \sim l$ outside the scattering medium. The value of z_0 is phenomenological, but a precise analysis of the Schwarzschild-Milne equation reveals that this picture is valid. One usually takes $z_0 = 0.7104l$, the exact value for isotropic point scattering of scalar waves. Van de Hulst (1980) investigated many possible cross sections and always found values very close to this. Amic, Luck, and Nieuwenhuizen (1996) considered the limit of very strong forward scattering and found that z_0 lies only 1.1% above the quoted value for isotropic scattering.

Once the light has entered the bulk, the diffuse intensity obeys the diffusion equation

$$\frac{\partial}{\partial t} I(\mathbf{r},t) = D\nabla^2 I(\mathbf{r},t). \tag{8}$$

In the steady state the time derivative vanishes and the diffusion coefficient plays no role. For a slab geometry with plane waves there is no x,y dependence, and we have to solve $I''(z) = 0$. The trapping-plane boundary conditions are $I(-z_0) = I_0$, $I(L+z_0) = 0$. The solution is a linear function of z,

$$I(z) = I_0 \frac{L + z_0 - z}{L + 2z_0}. \tag{9}$$

The transmitted intensity is essentially equal to this expression at $z=L$ (at a distance $z_0 \sim l$ from the trapping plane at $L+z_0$) and equal to z_0 times the derivative at that point; this estimate will turn out to be qualitatively correct,

$$T=\frac{I(z=L)}{I_0}=-\frac{z_0}{I_0}\frac{dI(z)}{dz}\bigg|_{z=L+z_0}$$

$$=\frac{z_0}{L+2z_0}\approx\frac{z_0}{L}. \tag{10}$$

Without having paid attention to details we find the behavior $T\sim l/L$, equivalent to Ohm's law for conductors. Generally a conductor has conductance e^2/h per channel. Here there are A/λ^2 channels of which a fraction T is open. This yields the conductance

$$\Sigma\sim\frac{e^2}{h}\frac{A}{\lambda^2}T\sim\frac{e^2 lA}{h\lambda^2 L}. \tag{11}$$

B. Diffusion propagator for slabs

In the presence of absorption the diffusion equation reads

$$\partial_t I(\mathbf{r},t)=D\nabla^2 I(\mathbf{r},t)-D\kappa^2 I(\mathbf{r},t)+S(\mathbf{r},t), \tag{12}$$

where S is a source term, the second term on the right-hand side describes absorption, and the absorption length is $L_{\rm abs}=1/\kappa$. In a bulk system the solution with initial conditions $I(\mathbf{r},0)=\delta(\mathbf{r})$ and $S=0$ reads

$$I(\mathbf{r},t)=(4\pi Dt)^{-3/2}e^{-(r^2/4Dt)-D\kappa^2 t}. \tag{13}$$

Its Fourier-Laplace transform,

$$I(\mathbf{q},\Omega)=\int d^3r\, e^{-i\mathbf{q}\cdot\mathbf{r}}\int_0^\infty dt\, e^{-i\Omega t}I(\mathbf{r},t), \tag{14}$$

takes the form

$$I(\mathbf{q},\Omega)=\frac{I(\mathbf{q},\mathbf{t}=0)}{D\mathbf{q}^2+D\kappa^2+i\Omega}. \tag{15}$$

For $\kappa=0$ these expressions diverge in the limit $\mathbf{q}$, $\Omega\to 0$. This divergency is called the "diffusion pole" or "diffuson."

For a slab geometry there will only be translational invariance in the $\rho=(x,y)$ plane. Suppose we have a source $S(\mathbf{r})=\tilde{S}(x,y)\,\delta(z-z')$. Denoting the perpendicular wave vector by $\mathbf{q}_\perp$ we have for diffusion from z' to z

$$I''(z,z')=M^2 I(z,z')-\frac{\tilde{S}(\mathbf{q}_\perp)}{D}\,\delta(z-z'), \tag{16}$$

with the "mass" M defined by

$$M^2=\mathbf{q}_\perp^2+\kappa^2+i\,\frac{\Omega}{D}. \tag{17}$$

M is the inverse depth at which a given intensity contribution $\psi_a^*\psi_b$ of an incoming beam $\psi=\Sigma_a\psi_a$ has decayed by a factor $1/e$, due to spatial dephasing of the amplitudes (encoded in $\mathbf{q}_\perp$), temporal dephasing (expressed by Ω), or absorption (expressed by κ).

By realizing that the diffusion equation (16) is just a wave equation with complex frequency, one sees that the solutions to the diffusion equation are a linear combination of hyperbolic sines and cosines. (The solution can also be obtained using the method of "image charges" known from electrostatics.) The diffuse-intensity propagator has the form (Zhu, Pine, and Weitz, 1991; Lisyansky and Livdan, 1992)

$$I(z,z';\mathbf{q}_\perp;\Omega)=\frac{\tilde{S}(\mathbf{q}_\perp)}{D}\,\frac{[\sinh Mz_<+Mz_0\cosh Mz_<][\sinh M(L-z_>)+Mz_0\cosh M(L-z_>)]}{(M+M^3z_0^2)\sinh ML+2M^2z_0\cosh ML}, \tag{18}$$

where

$$z_<=\min(z,z'),\quad z_>=\max(z,z'). \tag{19}$$

In the stationary limit, in the absence of absorption ($\Omega=\kappa=0$, $\mathbf{q}_\perp=\mathbf{0}\to M=0$), Eq. (21) reduces to a tent-shaped function,

$$I(z,z';\mathbf{q}_\perp=\mathbf{0};\Omega=0)=\frac{\tilde{S}(\mathbf{q}_\perp)}{D}\,\frac{[z_<+z_0][L-z_>+z_0]}{L+2z_0}. \tag{20}$$

The propagator describes the diffuse propagation from one point in the slab to another. With roughly equal indices of refraction inside and outside the sample, the extrapolation length z_0 is a few mean free paths and thus the terms involving z_0 yield contributions of order l/L. For optically thick samples ($L\gg l$), this is negligible and one has

$$I(z,z';\mathbf{q}_\perp;\Omega)=\frac{\tilde{S}(\mathbf{q}_\perp)}{D}\,\frac{\sinh(Mz_<)\sinh(ML-Mz_>)}{M\sinh(ML)}. \tag{21}$$

The diffusion equation does not hold if the intensity gradient is steep, i.e., if $ql\sim 1$. It therefore cannot describe properly the diffuse intensity near the surface of the medium. Nevertheless, in a heuristic manner one often makes the following assumptions in the diffusion approach (Ishimaru, 1978): (1) The diffuse intensity from an outside plane-wave source is assumed to be given by

substituting $z=l$ in Eq. (18), as if all diffuse intensity originated from this $z=l$ plane. Likewise, the coupling outwards is obtained by taking $z'=L-l$. In this way two extra propagators, the incoming ($z<0$, $0<z'<L$) and the outgoing ($0<z<L$, $z'>L$) are constructed from the internal diffusion ($0<z$, $z'<L$). (2) The boundary conditions are (Zhu *et al.*, 1991)

$$I(z,z';M)|_{z=0+,L-}=z_0\partial_z I(z,z';M)|_{z=0+,L-}. \quad (22)$$

The form of Eq. (18) fulfills these conditions. The extrapolation length z_0 is determined by the reflectance at the surface. In the following we calculate it precisely.

III. MESOSCOPICS: THE RADIATIVE TRANSFER EQUATION

The study of multiple light scattering was initiated in astrophysics with the goal of deriving, on the basis of energy conservation, the radiative transfer equation. This is the ''Boltzmann'' transport equation of the problem (i.e., the mesoscopic balance equation that neglects all memory effects). It has been solved in particular for slabs (plane-parallel geometries). This approach has been described by Chandrasekhar (1960) and van de Hulst (1980). An elegant method was introduced by Ambartsumian (1943); it is based on the observation that for semi-infinite slabs quantities are invarient if extra layers are added. It will be shown below that the radiative transfer equation can also be derived from the ladder approximation to the Bethe-Salpeter equation. In other words: there exists a microscopic derivation of the radiative transfer equation. Once this is shown, more details can be incorporated in the microscopics, and more subtle effects, such as backscatter and correlations, can be derived microscopically in a way closely related to the radiative transfer equation.

A. Specific intensity

The specific intensity $\mathcal{I}(\mathbf{r},\mathbf{n})=\mathcal{I}(\mathbf{r},\theta,\phi)$ is defined as the radiation density emitted at position $\mathbf{r}$ in direction $\mathbf{n}=(\sin\theta\cos\phi,\sin\theta\sin\phi,\cos\theta)$ in a system with density n of scatterers. Let dU be the radiation energy in a given frequency interval $(\omega-\frac{1}{2}\Delta\omega,\omega+\frac{1}{2}\Delta\omega)$, transported through a surface $d\sigma$ in directions lying within a solid angle $d\mathbf{n}$ centered on $\mathbf{n}$, during a time interval dt. This energy is related to the specific intensity as (Chandrasekhar, 1960)

$$dU=\mathcal{I}\cos\Theta\,\Delta\omega\,d\sigma\,d\mathbf{n}\,dt, \quad (23)$$

where Θ is the angle between the director $\mathbf{n}$ of the emitted radiation and the normal of $d\sigma$. The energy depends in general on the position $\mathbf{r}=(x,y,z)$, the direction $\mathbf{n}$, the frequency ω, and the time t.

We are mainly interested in stationary, monochromatic situations for a slab with axial symmetry. Then $\mathcal{I}$ depends only on z and $\mu=\cos\theta$, where θ is the angle between the z axis and the direction of emitted radiation. We consider propagation in a medium with density n of rotationally symmetric scatterers with extinction cross section σ_{ex} and phase function $p(\mathbf{n},\mathbf{n}')=p(\mathbf{n}\cdot\mathbf{n}')=p(\cos\Theta)$. Thus $p(\mathbf{n}\cdot\mathbf{n}')d\mathbf{n}'\,d\mathbf{n}$ is the fraction of radiation entering inside a narrow cone of width $d\mathbf{n}'$ around incoming direction $\mathbf{n}'$ and leaving inside a narrow cone $d\mathbf{n}$ around $\mathbf{n}$. For spherically symmetric scatterers p is a function of $\mathbf{n}'\cdot\mathbf{n}=\cos\Theta$.

If radiation propagates over a distance ds, there is a loss of intensity due to scattering into other directions, and due to absorption (both are incorporated in σ_{ex}),

$$d\mathcal{I}=-n\sigma_{ex}\mathcal{I}\,ds. \quad (24)$$

There is also a gain term $n\sigma_{ex}\mathcal{J}ds$ with the *source function* $\mathcal{J}$,

$$\mathcal{J}(\mathbf{r};\theta,\phi)=\int_0^\pi\int_{-\pi}^{\pi}p(\theta,\phi;\theta'\phi')\,\frac{\sin\theta'\,d\theta'\,d\phi'}{4\pi}\,\mathcal{I}(\mathbf{r};\theta',\phi'). \quad (25)$$

$\mathcal{J}$ describes the radiation arriving at $\mathbf{r}$ in direction $\mathbf{n}'$ and scattered there in direction $\mathbf{n}$. The *radiative-transfer equation* expresses the net effect of the gain-loss mechanism,

$$\frac{1}{n\sigma_{ex}}\frac{d\mathcal{I}}{ds}=\mathcal{J}-\mathcal{I}. \quad (26)$$

Here it is derived from phenomenological considerations; later we shall provide a microscopic derivation.

The loss term $-\mathcal{I}$ leads to the Lambert-Beer law. Indeed, for a unidirectional beam $\mathcal{I}(0,\mathbf{n})=I_0\delta(\mathbf{n}-\mathbf{n}_0)$, simple integration yields $\mathcal{I}(\mathbf{r},\mathbf{n})=I_0\delta(\mathbf{n}-\mathbf{n}_0)\exp(-r/l_{sc})$ +''scattered,'' which is again the Lambert-Beer law with scattering mean free path

$$l_{sc}=\frac{1}{n\sigma_{ex}}. \quad (27)$$

B. Slab geometry

For homogeneous illumination of a slab $0\leq z\leq L$, physical quantities depend only on the depth z. It is useful to introduce the ''optical depth''

$$\tau=\frac{z}{l_{sc}}. \quad (28)$$

The optical thickness of the slab is then

$$b=\frac{L}{l_{sc}}. \quad (29)$$

Let θ be the angle between the direction of radiation and the positive z axis, and ϕ its angle with respect to the positive x axis. This allows us to introduce the dimensionless form of the radiative transfer equation,

$$\mu\,\frac{d\mathcal{I}(\tau,\mu,\phi)}{d\tau}=\mathcal{J}(\tau,\mu,\phi)-\mathcal{I}(\tau,\mu,\phi), \quad (30)$$

where

$$\mu=\cos\theta. \quad (31)$$

For a plane wave with intensity I_0 incident under an angle $\mathbf{n}_a(\theta_a,\phi_a)$ on the interface $z=0$, the boundary condition is $\mathcal{I}(0,\mu,\phi)=I_0\delta(\mu-\mu_a)\delta(\phi-\phi_a)$, where $\mu_a=\cos\theta_a>0$.

1. Isotropic scattering

The radiative transfer equation (30) can be written as an integral equation. For a slab this is usually called the Schwarzschild-Milne equation or, for short, the Milne equation. Let us consider a semi-infinite medium. For $\mu<0$, Eq. (30) yields for the radiation in the $-z$ direction (backward direction)

$$\mathcal{I}(\tau,\mu,\phi)=\int_\tau^\infty \mathcal{J}(\tau',\mu,\phi)e^{-(\tau'-\tau)/|\mu|}\frac{d\tau'}{|\mu|}, \tag{32}$$

while for $\mu>0$ the specific intensity in the $+z$ direction satisfies

$$\mathcal{I}(\tau,\mu,\phi)=\mathcal{I}(0,\mu,\phi)e^{-\tau/\mu}+\int_0^\tau \mathcal{J}(\tau',\mu,\phi)e^{-(\tau-\tau')/\mu}\frac{d\tau'}{\mu}. \tag{33}$$

Of special interest is the case of *isotropic scattering* or *s*-wave scattering for which

$$p(\cos\Theta)=1. \tag{34}$$

Isotropic scattering occurs for electron scattering from small impurities. For isotropic scattering $\mathcal{J}$ does not depend on μ and ϕ. It is common to introduce the dimensionless intensity

$$\Gamma(\tau)=\frac{1}{I_0}\int d\mu' d\phi' \mathcal{I}(\tau,\mu'\phi'), \tag{35}$$

which here equals $4\pi\mathcal{J}/I_0$. Combining the last two equations yields for a plane-wave incident in direction (μ_a,ϕ_a)

$$\Gamma(\tau)=e^{-\tau/\mu_a}+\int_0^\infty d\tau'\int_0^1\frac{d\mu}{2\mu}e^{-|\tau'-\tau|/\mu}\Gamma(\tau'). \tag{36}$$

This Boltzmann equation will also be found from the ladder approximation to the Bethe-Salpeter equation, which provides a microscopic foundation. Corrections to the ladder approximation then yield the limit of validity of the Boltzmann approach.

The precise solution of Eq. (36) can be obtained numerically. See Van de Hulst (1980) and Kagiwada, Kalaba, and Ueno (1975) for details. We have plotted it in Fig. 2 for a relatively thin slab ($L=4l$), using the data from Table 17 in Van de Hulst (1980). The albedo is unity, and there is no index mismatch. The form of the solution near the incoming surface is quite different for the three cases drawn: $\mu_a=1$, or perpendicular incidence; $\mu_a=0.1$ (angle with the z axis is 84 degrees); and diffuse incidence uniformly distributed over all angles. At the outgoing surface all solutions are alike: there is only a small deviation from the straight line crossing zero at $L+z_0$.

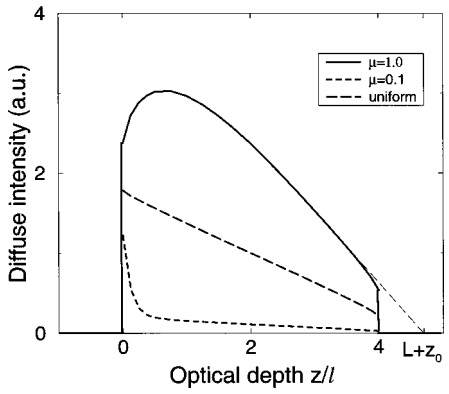

FIG. 2. Solution of the Schwarzschild-Milne equation as taken from Table 17 in Van de Hulst (1980) for a slab of thickness $L=4l$ with no internal reflection, $a=1$. The precise solution near the incoming plane strongly depends on $\mu=\cos\theta'$, where θ' is the angle of the incoming beam. Apart from a multiplication factor, the bulk behavior is the same; all lines extrapolate to $L+z_0$ (thin dashed line).

2. Anisotropic scattering and Rayleigh scattering

For acoustic or electromagnetic waves scattered from particles much smaller than the wavelength there is no *s*-wave scattering. Instead, one has to leading order the dipole-dipole or *p*-wave scattering. It is expressed by the phase function for *Rayleigh scattering*,

$$p(\cos\Theta)=\frac{3}{4}(1+\cos^2\Theta). \tag{37}$$

Scattering from spherically symmetric particles is usually anisotropic, but cylindrically symmetric with respect to the incoming direction. For arbitrarily shaped scatterers this symmetry holds only after averaging over their possible orientations. In such situations the phase function $p(\cos\Theta)$ depends only on $\phi-\phi'$, and the average over ϕ can be carried out. This leads to the projected phase function, with $\mu=\cos\theta$,

$$p_0(\mu,\mu')=\int\frac{d\phi}{2\pi}p(\theta\phi;\theta'\phi')=\int\frac{d\phi}{2\pi}\frac{d\phi'}{2\pi}p(\theta\phi;\theta'\phi'). \tag{38}$$

For Rayleigh scattering one has, using the equality $\cos\Theta=\mathbf{n}\cdot\mathbf{n}'=\sin\theta\sin\theta'\cos(\phi-\phi')+\cos\theta\cos\theta'$,

$$p_0(\mu,\mu')=\frac{3}{8}(3-\mu^2-\mu'^2+3\mu^2\mu'^2). \tag{39}$$

Because of the form of the $\mathcal{J}$ integral, it is useful to introduce

$$\Gamma(\tau)=\frac{2\pi}{I_0}\int_{-1}^1 d\mu\ \mathcal{I}(\tau,\mu),$$

$$\Delta(\tau)=\frac{2\pi}{I_0}\int_{-1}^1 d\mu\ \mu^2\mathcal{I}(\tau,\mu). \tag{40}$$

The radiative-transfer equation yields the coupled integral equations:

$$\Gamma(\tau)=e^{-\tau/\mu_a}+(\tfrac{9}{16}E_1-\tfrac{3}{16}E_3)\Gamma+(\tfrac{9}{16}E_3-\tfrac{3}{16}E_1)\Delta,$$
$$\Delta(\tau)=\mu_a^2 e^{-\tau/\mu_a}+(\tfrac{9}{16}E_3-\tfrac{3}{16}E_5)\Gamma+(\tfrac{9}{16}E_5-\tfrac{3}{16}E_3)\Delta. \tag{41}$$

Here we introduced the exponential integrals E_k,

$$E_k(\tau)=\int_0^1 \frac{d\mu}{\mu}\,\mu^{k-1}e^{-\tau/\mu}=\int_1^\infty \frac{dy}{y^k}\,e^{-\tau y}, \tag{42}$$

and the product:

$$(Ef)(\tau)=\int_0^\infty d\tau' E(|\tau-\tau'|)f(\tau'). \tag{43}$$

Equations (41) involve two coupled functions and represent the simplest extension of isotropic scattering. They have been analyzed by Van de Hulst (1980).

3. The transport mean free path and the absorption length

We have discussed how unscattered intensity decays exponentially as a function of the distance from the source. This occurs because more and more light is scattered out of the direction of the beam. The characteristic distance between two scattering events is the scattering mean free path l_{sc}. Now suppose that scattering is rather ineffective, so that at each scattering the direction of radiation is not changed much. The diffusion constant must then be large. In other words, the factor l in the identity $D=\frac{1}{3}vl$ cannot be the scattering mean free path. Intuitively one expects that l is the distance over which the direction of radiation gets lost. This length scale is called the transport mean free path. We show now how it follows from the radiative transfer equation.

The time-dependent radiative transfer equation has the form

$$t_{sc}\frac{\partial}{\partial t}\mathcal{I}(\mathbf{r},\mathbf{n},t)+l_{sc}\mathbf{n}\cdot\nabla\mathcal{I}(\mathbf{r},\mathbf{n},t)$$
$$=\int \frac{d\mathbf{n}'}{4\pi}\,p(\mathbf{n},\mathbf{n}')\mathcal{I}(\mathbf{r},\mathbf{n}',t)-\mathcal{I}(\mathbf{r},\mathbf{n},t), \tag{44}$$

where t_{sc} is the mean time between two scatterings. We can now introduce the local radiation density I and the local current density $\mathbf{J}$ as

$$I(\mathbf{r},t)=\int d\mathbf{n}\,\mathcal{I}(\mathbf{r},\mathbf{n},t),\quad \mathbf{J}(\mathbf{r},t)=\frac{l_{sc}}{t_{sc}}\int d\mathbf{n}\,\mathcal{I}(\mathbf{r},\mathbf{n},t)\mathbf{n}. \tag{45}$$

Integration of Eq. (44) yields the continuity equation

$$\partial_t I(\mathbf{r},t)+\nabla\cdot\mathbf{J}(\mathbf{r},t)=-\frac{1-a}{t_{sc}}I(\mathbf{r},t). \tag{46}$$

Here we introduce the albedo (from the Latin *albus*, white), the whiteness of the scatterer,

$$a=\int \frac{d\mathbf{n}}{4\pi}\,p(\mathbf{n},\mathbf{n}'). \tag{47}$$

For $a=1$ there is no absorption. If we multiply Eq. (44) by $\mathbf{n}$ and integrate over $\mathbf{n}$ we obtain

$$\frac{t_{sc}^2}{l_{sc}}\partial_t\mathbf{J}+\frac{t_{sc}}{l_{sc}}\mathbf{J}+l_{sc}\nabla\cdot\int d\mathbf{n}\,\mathcal{I}(\mathbf{r},\mathbf{n},t)\mathbf{n}\mathbf{n}$$
$$=\int d\mathbf{n}\,d\mathbf{n}'p(\mathbf{n},\mathbf{n}')\mathcal{I}(\mathbf{r},\mathbf{n}',t)\mathbf{n}. \tag{48}$$

If scattering is (on the average) spherically symmetric, the integral $\int d\mathbf{n}p(\mathbf{n},\mathbf{n}')\mathbf{n}$ can only be proportional to $\mathbf{n}'$. If one takes the inner product with $\mathbf{n}'$, one finds the average cosine of the scattering angle,

$$\langle\cos\Theta\rangle=\langle\mathbf{n}\cdot\mathbf{n}'\rangle$$
$$=\int\frac{d\mathbf{n}}{4\pi}\,p(\mathbf{n},\mathbf{n}')\mathbf{n}\cdot\mathbf{n}'$$
$$=\int\frac{d\mathbf{n}}{4\pi}\,p(\cos\Theta)\cos\Theta$$
$$=\int_{-1}^1\frac{d\mu}{2}\,p(\mu)\mu. \tag{49}$$

Therefore Eq. (48) can be written as

$$\frac{t_{sc}^2}{l_{sc}}\partial_t\mathbf{J}+\frac{t_{sc}}{l_{sc}}(1-\langle\cos\Theta\rangle)\mathbf{J}=-l_{sc}\nabla\cdot\int d\mathbf{n}\,\mathcal{I}(\mathbf{r},\mathbf{n},t)\mathbf{n}\mathbf{n}. \tag{50}$$

The right-hand side depends on $\mathcal{I}$ and $\mathbf{J}$. If one assumes that the intensity distribution is almost isotropic, then the current is much smaller than the density. This allows one to make the approximation (Ishimaru, 1978)

$$\mathcal{I}(\mathbf{r},\mathbf{n},t)\approx I(\mathbf{r},t)+\frac{3t_{sc}}{l_{sc}}\mathbf{n}\cdot\mathbf{J}(\mathbf{r},t)+\cdots, \tag{51}$$

since higher-order terms are smaller. Under these approximations it follows that

$$\frac{t_{sc}^2}{l_{sc}}\partial_t\mathbf{J}+(1-\langle\cos\Theta\rangle)\frac{t_{sc}}{l_{sc}}\mathbf{J}=-\frac{l_{sc}}{3}\nabla I. \tag{52}$$

For processes that change slowly in time we thus find

$$\mathbf{J}(\mathbf{r},t)=-D\nabla I(\mathbf{r},t). \tag{53}$$

When inserted in the continuity equation, Eq. (53) leads to the desired diffusion equation for the density. Thus under the above assumptions the radiative transfer equation leads to the diffusion equation,

$$\partial_t I(\mathbf{r},t)=D\nabla^2 I(\mathbf{r},t)-\frac{1-a}{t_{sc}}I(\mathbf{r},t)$$
$$\equiv D\nabla^2 I(\mathbf{r},t)-D\kappa^2 I(\mathbf{r},t). \tag{54}$$

The diffusion constant D is given by

$$D=\frac{l_{sc}^2}{3t_{sc}(1-\langle\cos\Theta\rangle)}\equiv\frac{1}{3}vl_{tr}, \tag{55}$$

where $v=l_{sc}/t_{sc}$ is the transport speed. We wish to stress that in principle t_{sc} has two contributions: the time to travel from one scatterer to the next and the dwell time spent in the neighborhood of one scatterer (Van Albada *et al.*, 1991). In Eq. (55) the *transport mean free path* occurs as

$$l_{\rm tr}=\frac{1}{1-\langle\cos\Theta\rangle}\,l_{\rm sc}. \tag{56}$$

It is the mean distance after which the direction of radiation gets lost. For strongly forward scattering $\langle\cos\Theta\rangle$ will be close to unity so that the transport mean free path becomes large. In this exercise we also found an explicit expression for the absorption length $L_{\rm abs}$ and the inverse absorption length κ,

$$L_{\rm abs}\equiv\frac{1}{\kappa}\equiv\sqrt{\frac{l_{\rm sc}l_{\rm tr}}{3(1-a)}}. \tag{57}$$

C. Injection depth and the improved diffusion approximation

In the previous section we avoided the problem of how an incoming plane wave becomes diffusive inside the medium. We introduced a ''trapping plane'' at the injection depth $z_0\sim l$. The precise statement is that the solution of the transfer equation, or Milne equation, of a semi-infinite medium starting at $z=0$ behaves as $I(z)=z+z_0$ for $z\gg l$; formally this expression vanishes at $-z_0$ outside the medium. This can also be expressed as

$$I(0)=z_0I'(0). \tag{58}$$

If there is an index mismatch between the system and its surroundings, the walls of the system will partially reflect the light. Therefore the light will remain longer in the system. The transmission coefficient will become smaller by a factor of order unity. This effect is of practical importance, as the scattering medium usually has a different index of refraction from its surroundings, usually air or liquid. Only in the special case of index-matched liquids is the mismatch minimized.

The first to point out the importance of internal reflections were Lagendijk, Vreeken, and De Vries (1989). They also noted that z_0 changes. For a one-dimensional medium they give the expression

$$z_0=\frac{1+\overline{R}}{1-\overline{R}}\,l_{\rm sc}, \tag{59}$$

in which $\overline{R}$ is the mean reflection coefficient.

For the three-dimensional situation, an analogous result was worked out by Zhu *et al.* (1991): For a system in which only the z dependence is relevant, Eq. (51), relating the specific intensity $\mathcal{I}$ to the radiation density I and the current density $\mathbf{J}$, reads

$$\mathcal{I}(z,\mu)=I(z)+\frac{3}{v}\,\mu J_z(z), \tag{60}$$

with velocity $v=l_{\rm sc}/t_{\rm sc}$, where $t_{\rm sc}$ is the scattering time. It follows that

$$J_z(z)=\frac{v}{4\pi}\int_{-1}^{1}\mu\,d\mu\int_0^{2\pi}d\phi\,\mathcal{I}(z,\mu). \tag{61}$$

From this one reads off that the radiation current per unit of solid angle $d\Omega=d\mu\,d\phi$ equals

$$\frac{dJ_z}{d\Omega}=v\cdot\mu\cdot\frac{\mathcal{I}}{4\pi}=\frac{1}{4\pi}\{\mu vI(z)+3\mu^2J(z)\}. \tag{62}$$

The total radiation at depth $z=0$ in the positive z direction is thus

$$\begin{aligned}J_{+z}(0)&=\frac{v}{4\pi}\int_0^1\mu\,d\mu\,2\pi\mathcal{I}(0,\mu)\\&=\frac{v}{4}\,I(0)+\frac{1}{2}\,J_z(0)\\&=\frac{v}{4}\,I(0)-\frac{vl_{\rm tr}}{6}\,I'(0),\end{aligned} \tag{63}$$

where the diffusive current (53) has been inserted.

In the absence of internal reflections $dJ_z/d\Omega$ must vanish for all $\mu>0$. If we impose that J_{+z} vanishes and if we compare with Eq. (58), we obtain

$$z_0=\frac{2}{3}\,l_{\rm tr}. \tag{64}$$

For isotropic scattering this expression is not far from the exact value $z_0=0.710\,44l$ that follows from the radiative transfer equation (see Sec. X).

Let us now assume that the refractive index of the scattering medium n_0 differs from that of its surroundings n_1. The ratio

$$m=\frac{n_0}{n_1} \tag{65}$$

exceeds unity for a dry medium in air, but can be smaller than unity if the medium is in between glass plates with a high refractive index. In both cases internal reflections will appear at the interface. The reflection coefficient is given by

$$R(\mu)=\left|\frac{\mu-\sqrt{m^{-2}-1-\mu^2}}{\mu+\sqrt{m^{-2}-1-\mu^2}}\right|^2. \tag{66}$$

$R(\mu)$ equals unity in the case of total reflection, namely, when the argument of the square root becomes negative. We can now calculate the current that is internally reflected at the interface $z=0^+$:

$$\begin{aligned}J_{+z}^{\rm refl}&=-\int_{-1}^{0}d\mu\int_0^{2\pi}d\phi\;R(\mu)\,\frac{dJ_z}{d\Omega}\\&=-\int_{-1}^{0}\frac{d\mu}{2}\,R(\mu)[v\mu I(0)+3\mu^2J_z(0)]\\&=\frac{v}{2}\,C_1I(0)-\frac{3}{2}\,C_2J_z(0)\\&=\frac{v}{2}\,C_1I(0)+\frac{vl_{\rm tr}}{2}\,C_2I'(0),\end{aligned} \tag{67}$$

where

$$C_1=\int_0^1d\mu\;\mu R(\mu),\quad C_2=\int_0^1d\mu\;\mu^2R(\mu). \tag{68}$$

By equating this angular average to the angular average in Eq. (63), Zhu, Pine, and Weitz derive Eq. (58) with

$$z_0=\frac{2}{3}\frac{1+3C_2}{1-2C_1}\,l_{\rm tr}. \tag{69}$$

It was later pointed out by Nieuwenhuizen and Luck (1993) that this result becomes exact in the limit of large index mismatch ($m\to 0$ or $m\to\infty$). The reason is that then the interfaces are good mirrors, so that the outer world is not seen, and hence close to the mirrors the intensity is diffusive.

In the derivation of Eq. (69) the phase function has only been used in the expression for the diffusion coefficient. This led to the occurrence of the transport mean free path. One would therefore expect that Eq. (69) remains valid for arbitrary anisotropic scattering in the limit of large index mismatch. This can be explained as follows: The interfaces act as good mirrors. Therefore many scatterings also occur close to the wall before the radiation can exit the medium. After many scatterings the radiation has become isotropic. Evidence for this point will be given in Sec. X.D.

IV. MICROSCOPICS: WAVE EQUATIONS, *t* MATRIX, AND CROSS SECTIONS

A. Schrödinger and scalar wave equations

Light scattering is described by the Maxwell equations. The vector character of the amplitudes leads to a tensor character of the intensity. In regard to sound waves or Schrödinger waves, this introduces extra complications, which we do not address here. For discussions of the vector case see, for example, Van de Hulst (1980), MacKintosh and John (1988), Peters (1992), and Amic, Luck, and Nieuwenhuizen (1997). The vector character is especially important in the case of multiple scattering of light in a Faraday-active medium in the presence of a magnetic field. For fundamental descriptions, see MacKintosh and John (1989) and Van Tiggelen, Maynard, and Nieuwenhuizen (1996). This field also includes the so-called photonic Hall effect, a light current that arises, under these conditions, perpendicular to the magnetic field. From studies of the diffuse intensity Nieuwenhuizen (1993) proposed that such a mechanism should exist. This was indeed shown by Van Tiggelen (1995) and confirmed experimentally by Rikken and Van Tiggelen (1996). Another interesting application is multiple scattering of radiation emitted by a relativistic charged particle in a random environment; see Gevorkian (1998) for diffusion and Gevorkian and Nieuwenhuizen (1998) for enhanced backscatter.

Acoustic waves and spinless electrons are described by scalar waves and for various aspects this turns out to be a good approximation for light as well. The Schrödinger equation reads, in units in which $\hbar^2/2m=1$,

$$-\nabla^2\Psi+V\Psi=E\Psi. \tag{70}$$

As potential we choose a set of point scatterers,

$$V(\mathbf{r})=-\sum_i u\,\delta(\mathbf{r}-\mathbf{R}_i). \tag{71}$$

Here $-u$ is the bare scattering strength and $\mathbf{R}_i$ are the locations of the scatterers.

Acoustic waves are described by the classical wave equation

$$\nabla^2\Psi-\frac{\varepsilon(\mathbf{r})}{c^2}\frac{\partial^2}{\partial t^2}\Psi=0, \tag{72}$$

where ε is the normalized local mass density and c is the speed of sound in a medium with $\varepsilon=1$. We shall apply the same equation to light, thereby neglecting its vector character. ε is then the dielectric constant, and c is the speed of light in vacuum where $\varepsilon=1$. For monochromatic waves $\Psi(\mathbf{r},t)=\Psi(\mathbf{r})e^{i\omega t}$, the time derivatives are replaced by frequency $i\omega$. In practice this applies to a stationary experiment with a monochromatic beam. For classical waves we can also introduce point scatterers by setting $\varepsilon(\mathbf{r})=1+\Sigma_i\,\alpha\delta(\mathbf{r}-\mathbf{R}_i)$, where α is the polarizability of the scattering region that we approximate by a point. The Schrödinger equation and the scalar wave equation then both take the form

$$-\nabla^2\Psi-u\sum_i\,\delta(\mathbf{r}-\mathbf{R}_i)\Psi=k^2\Psi,\quad \text{where}\quad \begin{cases} u=\text{constant in the Schrödinger equation;}\ \ k=\sqrt{E},\\ u=\alpha k^2\ \text{ in the classical wave equation;}\ \ k=\omega/c. \end{cases} \tag{73}$$

Many static results can be derived without specifying the kind of waves being discussed. However, the dynamics of acoustic waves will be different from those of Schrödinger waves due to the frequency dependence of u.

B. The *t* matrix and resonant point scatterers

To elucidate the notion of the t matrix, we begin our microscopic description with a simple example: scattering of an incoming beam from one scatterer in one dimension. The quantum-mechanical wave equation in $d=1$ with a scatterer in $x=x_0$ reads

$$-\Psi''(x)-u\,\delta(x-x_0)\Psi(x)=E\Psi(x),\quad \text{with}\ \ E=k^2. \tag{74}$$

Assuming that a wave e^{ikx} comes in from $x=-\infty$, we look for a solution of the form

$$\Psi=\begin{cases} e^{ikx}+Ae^{-ik(x-x_0)}, & x\leqslant x_0,\\ Be^{ik(x-x_0)}, & x\geqslant x_0. \end{cases} \tag{75}$$

The constants A and B are determined by the continuity of ψ and the cusp in ψ' at $x=x_0$. The solution can then be represented as

$$\Psi = e^{ikx} - \frac{u}{u+2ik}\, e^{ik|x-x_0|} e^{ikx_0}$$
$$= e^{ikx} + G(x,x_0) t e^{ikx_0}. \tag{76}$$

The first term is just the incoming wave. The second term represents the wave at the scatterer in x_0, where it picks up a scattering factor t,

$$t = \frac{u}{1-iu/(2k)}, \tag{77}$$

and is transported to x by the medium without scatterers. The Green's function in the medium without scatterers, defined as $(-\partial^2/\partial x^2 - k^2) G(x,x') = \delta(x-x')$, reads

$$G(x,x') = \frac{e^{ik|x-x'|}}{-2ik}. \tag{78}$$

Note that we have chosen the sign of $i\epsilon$ such that the Fourier representation of the pure Green's function reads $G(p) = 1/(p^2 - k^2 - i\epsilon)$.

C. The *t* matrix as a series of returns

In the above example Eqs. (77) and (78) show that the t matrix can be expressed as

$$t(x_0) = \frac{u}{1-uG(x_0,x_0)}. \tag{79}$$

Expansion in powers of u yields the "Born series," a series that has a clear physical interpretation: the term of order u^k describes waves that arrive at the scatterer, return to it $k-1$ times, and then leave it for good:

$$t = u + uGu + uGuGu + uGuGuGu + \cdots \tag{80}$$

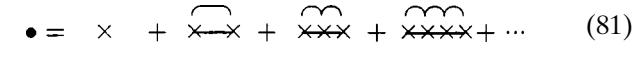

(81)

The curved lines in the equation indicate that scattering occurs from the same scatterer (so far there is only one). The t matrix is indicated by a ●. For an extended scatterer this expression reads

$$t(\mathbf{r},\mathbf{r}') = -V(\mathbf{r})\delta(\mathbf{r}-\mathbf{r}') + V(\mathbf{r})G(\mathbf{r},\mathbf{r}')V(\mathbf{r}') - \int d^3\mathbf{r}'' V(\mathbf{r})G(\mathbf{r},\mathbf{r}'')V(\mathbf{r}'')G(\mathbf{r}'',\mathbf{r}')V(\mathbf{r}') + \cdots . \tag{82}$$

Except for the case of point scatterers, this iterative solution of the single-scatterer problem is not very helpful. The problem of vector wave scattering from a sphere was solved by Mie (1908), but the result is quite involved, too involved for our multiple-scattering purposes. The approach shows, however, that the t matrix depends on the Green's function G, which describes propagation in the medium without that scatterer. However, the Green's function will depend on further details of the scattering medium, such as the presence of walls or other scatterers. Generally, it cannot be taken from the literature but has to be calculated for the problem under consideration: *the t matrix describes scattering in a local environment*. The standard infinite-space t matrix found in the literature applies only to that specific situation.

D. Point scatterer in three dimensions

In three dimensions the Green's function reads

$$G(\mathbf{r},\mathbf{r}') = \frac{e^{ik|\mathbf{r}-\mathbf{r}'|}}{4\pi|\mathbf{r}-\mathbf{r}'|} \approx \frac{1}{4\pi|\mathbf{r}-\mathbf{r}'|} + \frac{ik}{4\pi} + O(|\mathbf{r}-\mathbf{r}'|), \tag{83}$$

which is closely related to the Yukawa potential for hadron-hadron interactions. The divergence at $r'=\mathbf{r}$ will cause some problems in taking the point limit.

1. Second-order born approximation

For weak scatterers one often truncates the Born series. A complication is that the Green's function in three dimensions diverges for $\mathbf{r}\to\mathbf{r}'$, which makes the Born series (80) ill defined for point scatterers. In reality these divergences are cut off by the physical size of the scatterer, so they play no role for weak scattering. One thus keeps the first-order term and the imaginary part of the second-order term; the regularized real part of the second-order Born term will be small compared to the first-order term. This leads to the second-order Born approximation

$$t = u + iu^2 \,\mathrm{Im}\, G(\mathbf{r},\mathbf{r}). \tag{84}$$

For the system under consideration this becomes

$$t = u + iu^2 \frac{k}{4\pi}. \tag{85}$$

The fact that $\mathrm{Im}\, t>0$ signifies that the t matrix still describes scattering [see Eq. (106)]. More detailed aspects of the scatterer, such as resonances, are not taken into account. For electrons the second-order Born approximation is often applied. Instead of working with point scatterers one usually considers a Gaussian random potential with average zero $\langle V(\mathbf{r})\rangle = 0$ and correlation $\langle V(\mathbf{r})V(\mathbf{r}')\rangle = u^2\delta(\mathbf{r}-\mathbf{r}')$. This leads exactly to $t = iu^2\,\mathrm{Im}\, G(\mathbf{r},\mathbf{r}) = iu^2k/4\pi$. For light, however, the second-order Born approximation is less applicable if resonances occur.

2. Regularization of the return Green's function

For finite-size scatterers the divergence of the Green's function at coinciding points is not a severe problem. The physical scatterer always has some finite radius $1/\Lambda$ that cuts off any divergency. When we wish to consider point scatterers, the divergence does cause a mathematical problem. In contrast to high-energy physics, cutoffs in condensed-matter physics represent physical param-

eters. Indeed, we shall identify Λ as an internal parameter of the point scatterer, which fixes the resonance frequency.

The return Green's function $G(\mathbf{r}\to\mathbf{r}')$ resulting from Eq. (83) diverges. It should be regularized as

$$G^{\rm reg}(\mathbf{r},\mathbf{r}) = \Lambda + \lim_{\mathbf{r}'\to\mathbf{r}}\left[G(r,\mathbf{r}') - \frac{1}{4\pi|\mathbf{r}-\mathbf{r}'|}\right] = \Lambda + \frac{ik}{4\pi}. \tag{86}$$

Another method, often used in quantum field theory, is to introduce a large-momentum cutoff,

$$G(\mathbf{r},\mathbf{r}) = \int \frac{d^3\mathbf{p}}{(2\pi)^3}\, G(\mathbf{p}) = \int \frac{d^3\mathbf{p}}{(2\pi)^3}\frac{1}{p^2} + \int \frac{d^3\mathbf{p}}{(2\pi)^3}\left\{ G(\mathbf{p}) - \frac{1}{p^2}\right\}$$

$$G^{\rm reg}(\mathbf{r},\mathbf{r}) = \Lambda + \int \frac{d^3\mathbf{p}}{(2\pi)^3}\left\{ G(\mathbf{p}) - \frac{1}{p^2}\right\} = \Lambda + \frac{ik}{4\pi}. \tag{87}$$

This subtraction is also possible if there are other scatterers or walls. Different regularization schemes define different point scatterers. The physical result is largely insensitive to such details.

3. Resonances

If we insert the regularized return Green's function in Eq. (79), we can write the t matrix in the same form as in the $d=1$ case, by introducing the effective scattering length $U_{\rm eff}$,

$$t = \frac{u}{1-uG^{\rm reg}(\mathbf{r},\mathbf{r})} = \frac{u}{1-u(\Lambda+ik/4\pi)} \equiv \frac{U_{\rm eff}}{1-U_{\rm eff}(ik/4\pi)}, \tag{88}$$

where

$$U_{\rm eff} \equiv \frac{u}{1-u\Lambda}. \tag{89}$$

For Schrödinger waves, the regularization brings only a shift in u as compared to the second-order Born approximation. This has no further consequences, since u and Λ are constants, and so is $U_{\rm eff}$. For scalar waves there is an important difference, since then u is frequency dependent [cf. Eq. (73)]: $u=\alpha k^2$. Let us call k_* the wave number at resonance. If we identify[1] $\Lambda \equiv 1/(\alpha k_*^2)$, we get

$$t = \frac{\alpha k^2 k_*^2}{k_*^2 - k^2 - i\nu k_*^2 k^3/4\pi}, \tag{90}$$

$$U_{\rm eff} = \frac{\alpha k^2}{1-k^2/k_*^2}. \tag{91}$$

One sees that $U_{\rm eff}\to\infty$ for $k\to k_*$. Then t becomes equal to $t_*=4\pi i/k=2i\lambda$. As $\lambda\gg 1/\Lambda$ this shows resonance with strong scattering: the effective scattering length $|t| = 2\lambda$ is much larger than the physical size of the scatterer $\sim 1/\Lambda$.

The resonance is an *internal* resonance of the scatterer, comparable with the s resonance of a Mie sphere. It is strongly influenced by the environment in which the sphere is embedded. For small frequencies $t\approx\alpha k^2$, leading to the Rayleigh law $\sigma\sim\omega^4$ for $\omega\to 0$.

4. Comparison with Mie scattering for scalar waves

We compare the above result of regularization with an exact result. The t matrix for scalar s-wave scattering reads [see, for example, Merzbacher (1970), p. 238]

$$t = \frac{4\pi e^{-2ika}}{mk\,\cot(mka) - ik} - \frac{4\pi e^{-ika}\sin ka}{k}, \tag{92}$$

where a is the radius of the sphere and m the ratio between refractive indices of the sphere and the outside. The first resonance occurs at wave number $k_* = \pi/(2ma)$. It becomes sharp if one takes small a, large m, such that k_* remains fixed. For k close to k_* one gets

$$t = 4\pi\left[\frac{\pi^4}{32m^2a^3}\left(\frac{1}{k^2}-\frac{1}{k_*^2}\right) - ik\right]^{-1}. \tag{93}$$

For our point scatterer (88) we have

$$t = \frac{U_{\rm eff}}{1-iU_{\rm eff}k/4\pi} = 4\pi\left[\frac{4\pi}{\alpha}\left(\frac{1}{k^2}-\frac{1}{k_*^2}\right) - ik\right]^{-1}, \tag{94}$$

where the scattering length is

$$\alpha = \int d^3r[\epsilon(r)-1] = \int_{r<a} d^3r[m^2-1] = \frac{4\pi a^3}{3}(m^2-1). \tag{95}$$

In the limit of small a this becomes $\alpha = 3\pi a^3 m^2/3$. Comparing Eq. (93) with Eq. (94) we find the prefactors $4\pi/\alpha$ and $\pi^4/32m^2a^3$. The difference is a factor $\pi^4/96 \approx 1.0147$, thus the results coincide within 2%. In Eq. (86) we called $1/\Lambda$ a measure of the radius of the scatterer. We find, if $m\gg 1$,

$$\frac{1}{\Lambda} = \frac{k_*^2(m^2-1)a^3}{3} \approx \frac{\pi^2}{12}a \approx 0.822a. \tag{96}$$

[1]That can be done provided $\alpha>0$, that is to say, when $\varepsilon_{\rm scatterer} > \varepsilon_{\rm medium}$.

Indeed $1/\Lambda$ is a good measure of the radius. We have thus found a simple expression for the t matrix which incorporates the essential physics near the s-wave resonance. Finally, we mention that Mie scatterers absorb radiation if the refractive index has a small imaginary part. For point scatterers absorption is described by giving u a small negative imaginary part.

E. Cross sections and the albedo

In the literature several cross sections are encountered. Here we discuss the three most important. Let a plane wave be incident in direction $\mathbf{n}'$. As mentioned above, the total wave scattered from one scatterer is

$$\Psi(\mathbf{r}) = e^{ik\mathbf{n}'\cdot r} + \int d^3\mathbf{r}'\, d^3\mathbf{r}''\, G(\mathbf{r},\mathbf{r}')\, t(\mathbf{r}',\mathbf{r}'')\, e^{ik\mathbf{n}'\cdot\mathbf{r}''}, \tag{97}$$

with a real-space representation of the t matrix [see Eq. (82)]. Its Fourier transform is called the off-shell t matrix,

$$t(\mathbf{p},\mathbf{p}') = \int d^3\mathbf{r}\, d^3\mathbf{r}'\, e^{-i\mathbf{p}\cdot\mathbf{r}+i\mathbf{p}'\cdot\mathbf{r}'} t(\mathbf{r},\mathbf{r}'). \tag{98}$$

Let us assume that the center of the scatterer is located at the origin. Far away it holds that

$$G(\mathbf{r},\mathbf{r}') \approx \frac{e^{ikr-ik\mathbf{n}\cdot\mathbf{r}'}}{4\pi r} \quad \left(\mathbf{n}\equiv\frac{\mathbf{r}}{r}\right). \tag{99}$$

We insert this in Eq. (97) and with Eq. (98) we find that the scattered wave has the form

$$\Psi_{\mathrm{sc}}(\mathbf{r}) \approx \frac{e^{ikr}}{4\pi r}\, t(k\mathbf{n},k\mathbf{n}'). \tag{100}$$

The *scattering cross section* is defined as the scattered intensity integrated over a sphere, normalized by the incoming intensity

$$\sigma_{\mathrm{sc}} = \int_{4\pi} r^2 d\mathbf{n} \left|\frac{t(k\mathbf{n},k\mathbf{n}')}{4\pi r}\right|^2 = \frac{1}{(4\pi)^2}\int_{4\pi} d\mathbf{n}\, |t(k\mathbf{n},k\mathbf{n}')|^2. \tag{101}$$

Notice that the t matrix is only needed for momenta $|\mathbf{p}|=k$ (''far field,'' ''on the mass shell,'' ''on-shell t matrix''). One often denotes it by $t(\mathbf{n},\mathbf{n}')$. An *isotropic point scatterer* thus has scattering cross section

$$\sigma_{\mathrm{sc}} = \frac{\overline{tt}}{4\pi}. \tag{102}$$

The second important quantity is the extinction cross section. It tells how much intensity is lost from the incoming beam. Let us assume that a plane wave is incident along the z axis from $z=-\infty$. We consider the intensity in a small solid angle around the z axis for large positive z. Because then $r \approx z + (x^2+y^2)/2z$, the total wave is given by

$$\Psi(\mathbf{r}) = e^{ikz} + t(\mathbf{n},\mathbf{n})\,\frac{e^{ikz}}{4\pi z}\, e^{ik(x^2+y^2)/2z}. \tag{103}$$

The intensity for large z is

$$\Psi^*\Psi = 1 + \mathrm{Re}\,\frac{t(\mathbf{n},\mathbf{n})}{2\pi z}\, e^{ik(x^2+y^2)/2z}. \tag{104}$$

We integrate this over x and y inside an area A perpendicular to the z axis. The condition that x and y be much smaller than z makes the integrals Gaussian, after which the z dependence disappears:

$$\int_A dx\, dy\, \Psi^*\Psi = A - \sigma_{\mathrm{ex}}. \tag{105}$$

The *extinction cross section* is the surface over which the incoming beam has to be integrated to collect an equal amount of intensity. It is equal to

$$\sigma_{\mathrm{ex}}(\mathbf{n}) = \frac{\mathrm{Im}\; t(\mathbf{n},\mathbf{n})}{k}. \tag{106}$$

For a point scatterer one has $t(\mathbf{n},\mathbf{n})=t$. The albedo of the scatterer is the ratio of scattered and extinct intensity,

$$a = \frac{\sigma_{\mathrm{sc}}}{\sigma_{\mathrm{ex}}} = \frac{k\overline{tt}}{4\pi\;\mathrm{Im}\; t}. \tag{107}$$

For pure scattering $a=1$; this is called the *optical theorem*. If absorption is present the absorption cross section can be defined as $\sigma_{\mathrm{abs}}=\sigma_{\mathrm{ex}}-\sigma_{\mathrm{sc}}$. The albedo then equals

$$a = \frac{\sigma_{\mathrm{sc}}}{\sigma_{\mathrm{sc}}+\sigma_{\mathrm{abs}}}. \tag{108}$$

For an extended spherical scatterer the extinction cross section is angle dependent. One defines the earlier encountered phase function in terms of the t matrix as

$$p(\cos\Theta) = p(\mathbf{n}\cdot\mathbf{n}') = \frac{k|t(\mathbf{n},\mathbf{n}')|^2}{4\pi\;\mathrm{Im}\; t}, \tag{109}$$

with

$$\int \frac{d\mathbf{n}}{4\pi}\, p(\mathbf{n},\mathbf{n}') = a. \tag{110}$$

Note that, because of the far-field construction, the optical theorem cannot be applied immediately in a system with many scatterers. Instead one has to impose the *Ward identity*, which is its generalization.

V. GREEN'S FUNCTIONS IN DISORDERED SYSTEMS

After our microscopic treatment of a single scatterer, we now consider scattering from many scatterers. The Green's function of a given sample depends on the realization of disorder: the location and the orientation of scatterers. Averaged over disorder it is called the *amplitude Green's function*. It describes, on the average, unscattered propagation, such as an incoming beam or the wave scattered from any given scatterer. It should be

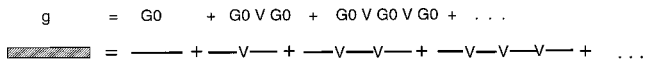

FIG. 3. The dressed Green's function contains all possible scattering paths with bare propagation between the scatterers.

contrasted with the *diffuse intensity*, which is the (multiple) scattered intensity that will be discussed below. For an introduction to Green's functions in disordered systems see Economou (1990).

A. Diagrammatic expansion of the self-energy

The amplitude Green's function is related to two important concepts: the density of states and the self-energy. Let us consider waves with frequency $\omega = ck_0$. It will be seen that the presence of many scatterers will change the "bare" wave number k_0 into the "effective wave number"

$$K = k + \frac{i}{2l_{\rm sc}}. \tag{111}$$

This describes a phase velocity $v_{\rm ph} = \omega/k = ck_0/k$.

For an electron in a random potential the definition of the amplitude Green's function is

$$G_{\mathbf{r},\mathbf{r}'} = \prod_{\mathbf{r}''} \int dV_{\mathbf{r}''} p(V_{\mathbf{r}''}) g_{\mathbf{r},\mathbf{r}'}, \tag{112}$$

with

$$g_{\mathbf{r},\mathbf{r}'} = \left(\frac{1}{p^2 - E + V} \right)_{\mathbf{r},\mathbf{r}'}. \tag{113}$$

The effect of the random potential is to introduce in the bare Green's function $g(p)$ the self-energy Σ,

$$G(p) = \frac{1}{p^2 - E - \Sigma(p)}. \tag{114}$$

Exact averaging over the disorder is only possible in particular cases in one dimension and cannot be done in general.[2] Therefore we employ a diagrammatic approximation to calculate the self-energy. Suppose that we have a system with randomly located strong scatterers (water drops in fog, lipid particles in milk, TiO_2 particles in a liquid or solid sample). In the limit of point scatterers the potential becomes $V(\mathbf{r}) = -\sum_{i=1}^{N} u\,\delta(\mathbf{r} - \mathbf{R}_i)$. The Green's function of this problem is represented diagrammatically in Fig. 3.

G_0 denotes a bare propagator, that is to say, the propagator in the medium without scatterers. The quantity needed is g, the Green's function of the random medium, also called the dressed propagator. To calculate all diagrams would amount to solving the problem

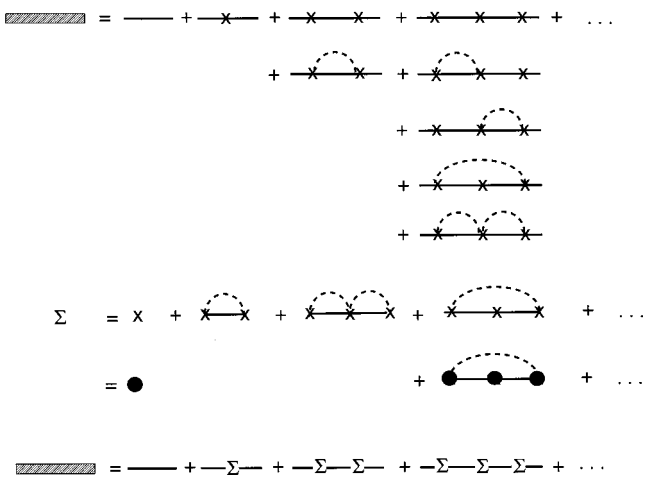
= + + +

which leads to the complex index of refraction

$$m=\frac{K}{k_0}\approx\sqrt{1+(nt/k_0^2)}. \tag{120}$$

B. Self-consistency

It is impossible to calculate all diagrams. Often, however, it is feasible to take into account without much extra effort, all higher-order contributions of a certain type. For the self-energy we can take $t=u/[1-uG(r,r)]$, instead of $t=u/[1-uG_0(r,r)]$. This is called a self-consistent approach. Now the last diagram in the series for Σ of Fig. 4 is included. Similar terms with any number of intermediate dots are also accounted for. (One has to be careful, however, to avoid overcounting of diagrams). Nevertheless, some two-scatterer diagrams have still been neglected at this self-consistent one-scatterer level.

Physically the self-consistent method is very natural: it describes that propagation from one scatterer to another does not happen in empty space, but in a space filled with other scatterers. Therefore self-consistency is a fundamental concept, and it will satisfy conservation laws (Ward identities). Indeed, without self-consistency there is no exact cancellation in the Ward identities. For instance, in the second-order Born approximation one will derive Eq. (128) with $1-a\sim u^3$, formally describing the absorption or even the creation of intensity, in situations in which intensity should be strictly conserved. In order to work with such approaches one must neglect u^3 terms. In the more physical self-consistent approach such *ad hoc* manipulations are not needed and not allowed.

The self-consistent t matrix in the independent-scatterer approximation,

$$t=\frac{u}{1-u\Lambda-(i/4\pi)u\sqrt{k_0^2+nt}}, \tag{121}$$

can lead to a real value of t. This amounts to a gap in the density of states (Polishchuk, Burin, and Maksimov, 1990). Probably there is no real gap, but rather a small density of states, which may lead to Anderson localization (Polishchuk *et al.*, 1990).

VI. TRANSPORT IN INFINITE MEDIA: ISOTROPIC SCATTERING

Just as the amplitude Green's function follows from solving the Dyson equation, the intensity follows from solving the Bethe-Salpeter equation. In this section we restrict ourselves to an approximate form of this equation, the so-called ladder approximation. It will be seen that this corresponds to the independent-scatterer approximation at the intensity level. The ladder approximation allows a microscopic derivation of the radiative transfer equation discussed in Sec. III.

In infinite media there are no boundaries, which simplifies the analysis. In practice this situation applies to cases in which the distance to boundaries is many mean free paths, so in the bulk of the multiple-scattering medium. We first consider this situation and derive the diffusion equation from microscopics. In doing so, we find expressions for the diffusion coefficient and the speed of transport.

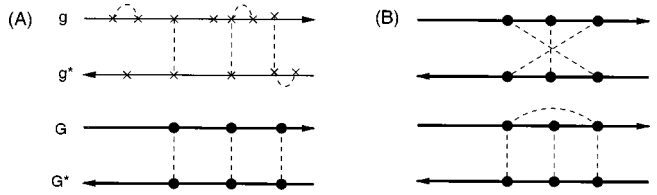

FIG. 5. Various intensity diagrams. (A) The ladder diagrams. Upper line: A typical ladder diagram before averaging. The crosses are scattering potentials, the Green's functions are bare. Lower line: Averaging over the possible scattering diagrams leads to the ladder diagrams, here a diagram with three common scatterers, in which the circles represent t matrices and the Green's functions are dressed. The ladder sum contains diagrams with an arbitrary number of common scatterers. (B) Some scattering diagrams that are not elements of the ladder diagrams. Upper portion is a maximally crossed diagram, responsible for the enhanced backscatter cone; lower diagram is of second order in the density.

A. Ladder approximation to the Bethe-Salpeter equation

For the transport of energy we must consider the intensity. We have to multiply the Green's function by its complex conjugate. In other words, we must multiply the retarded Green's function by the advanced one. This must be done before averaging over disorder. We indicate this in Fig. 5 by drawing the expansion for g (first line) and drawing the one for g^* below it.

When scattering from a certain scatterer occurs more than once, we indicate this again by dashed lines. Visits to scatterers are included in g or g^*, as before, but it may also happen that both g and g^* scatter from a common scatterer. This leads to the connection lines between the upper and lower propagators in the figure.

Of special importance are the ladder diagrams, depicted in Fig. 5(a), which describe the diffuse intensity in the independent-scatterer approximation. They lead to the classical picture of propagation of intensity from one common scatterer to another. As the intermediate propagation takes place in a medium with many other scatterers, each intermediate g or g^* line visits many new scatterers: they are the dressed propagators of the previous section.

Alternative names for the ladder diagrams are ladder sum, diffusion, and particle-hole channel. They are constructed in three steps: (i) Sum all immediate returns to the scatterers. As was explained in Sec. IV, this replaces the bare scattering potential u by the t matrix. (ii) Keep only those diagrams in which g and g^* visit a certain series of common scatterers once and only once and in the same sequence. The intensity g^*g propagates from one scatterer to another. (iii) Use the dressed Green's function as an intermediate propagator; in between the

common scatterers both g and g^* visit any number of other scatterers.

Let $I(\mathbf{r})=|\Psi(\mathbf{r})|^2$ denote the intensity arriving at point $\mathbf{r}$. According to Fig. 5 it can be decomposed into terms without scattering, terms with one common scattering, terms with two, etc.:

$$I(\mathbf{r})=|\Psi_{\rm in}(\mathbf{r})|^2+n\bar{t}t\int d^3\mathbf{r}'|G(\mathbf{r}-\mathbf{r}')|^2|\Psi_{\rm in}(\mathbf{r}')|^2 + (n\bar{t}t)2\int d^3\mathbf{r}'d^3\mathbf{r}''|G(\mathbf{r}-\mathbf{r}')|^2 \times|G(\mathbf{r}'-\mathbf{r}'')|^2|\Psi_{\rm in}(\mathbf{r}'')|^2+\cdots \quad (122)$$

which can be written as an integral equation,

$$\mathcal{L}(\mathbf{r})=n\bar{t}t|\Psi_{\rm in}(\mathbf{r})|^2+n\bar{t}t \times\int d^3\mathbf{r}'G(\mathbf{r}-\mathbf{r}')G^*(\mathbf{r}-\mathbf{r}')\mathcal{L}(\mathbf{r}'), \quad (123)$$

where $\mathcal{L}(\mathbf{r})=n\bar{t}tI(\mathbf{r})$. The ladder propagator $\mathcal{L}(\mathbf{r})$ is the intensity that leaves point $\mathbf{r}$ after being scattered.

In the second-order Born approximation the same scatterer is, at most, visited twice consecutively, with the result that the t matrices in the above ladder equations are replaced by the scattering potentials u.

B. Diffusion from the stationary ladder equation

In the bulk, that is to say, far from boundaries, the source term in the ladder equation vanishes. Equation (123) therefore takes the form

$$\mathcal{L}(\mathbf{r})=n\bar{t}t\int|G(\mathbf{r}')|^2\mathcal{L}(\mathbf{r}+\mathbf{r}')d^3\mathbf{r}'. \quad (124)$$

Now assume that $\mathcal{L}(\mathbf{r})$ varies slowly on the scale of one mean free path and expand

$$\mathcal{L}(\mathbf{r}'+\mathbf{r})=\mathcal{L}(\mathbf{r})+\mathbf{r}'\cdot\nabla\mathcal{L}(\mathbf{r})+\frac{1}{2}\mathbf{r}'\mathbf{r}':\nabla\nabla\mathcal{L}(\mathbf{r}), \quad (125)$$

where the colon denotes a tensor contraction. Inserting this in Eq. (124) yields three contributions. The first term is

$$n\bar{t}t\mathcal{L}(\mathbf{r})\int d^3\mathbf{r}'\,\frac{e^{-r'/l}}{(4\pi r')^2}=n\bar{t}t\,\frac{l}{4\pi}\,\mathcal{L}(\mathbf{r})=a\mathcal{L}(\mathbf{r}). \quad (126)$$

In the prefactor we have recognized the albedo a (see Sec. IV). The second term vanishes due to symmetry. The third term yields

$$\frac{1}{2}n\bar{t}t\int d^3\mathbf{r}'G^*(\mathbf{r}')G(\mathbf{r}')\mathbf{r}'\mathbf{r}':\nabla\nabla\mathcal{L}(\mathbf{r}) =\frac{1}{2}n\bar{t}t\times\frac{1}{3}\times2l^3\nabla^2\mathcal{L}(\mathbf{r}). \quad (127)$$

Inserting this in Eq. (124) yields the stationary diffusion equation

$$\nabla^2\mathcal{L}(\mathbf{r})=\frac{3(1-a)}{l^2}\,\mathcal{L}(\mathbf{r}), \quad (128)$$

in agreement with Eqs. (52) and (57), since for isotropic scattering it holds that $l_{\rm sc}=l_{\rm tr}$.

C. Diffusion coefficient and the speed of transport

Here we give a simple derivation of the nonstationary diffusion equation. In doing so, we automatically encounter the speed of transport. We again consider isotropic scatterers. In an infinite system it is useful to consider the Fourier-Laplace-transformed ladder equation

$$\mathcal{L}(\mathbf{q},\Omega)=S(\mathbf{q},\Omega)+n\bar{t}(\omega_-)t(\omega_+)\int\frac{d^3\mathbf{p}}{(2\pi)^3}\,G(p_+,\omega_+) \times G^*(p_-,\omega_-)\mathcal{L}(\mathbf{q},\Omega)$$

$$\equiv S(\mathbf{q},\Omega)+M(\mathbf{q},\Omega)\mathcal{L}(\mathbf{q},\Omega)$$

$$=\frac{S(\mathbf{q},\Omega)}{1-M(\mathbf{q},\Omega)}, \quad (129)$$

where S is the transformed source term; its precise form is of no interest here. We introduce

$$\mathbf{p}_\pm=\mathbf{p}\pm\frac{1}{2}\mathbf{q},\quad \omega_\pm=\omega\mp\frac{1}{2}\Omega. \quad (130)$$

The parameters $\mathbf{p}$ and ω are "internal" or "fast" variables, which involve one period of the wave. $\mathbf{q}$ and Ω are macroscopic or slowly varying parameters. They describe variations over distances much larger than the wavelength and times much larger than the oscillation period.

At $\Omega=0$, the bulk kernel has the property

$$M(\mathbf{q},\Omega=0)=n\bar{t}t\int\frac{d^3p}{(2\pi)^3}\,G(\mathbf{p}+\mathbf{q})G^*(\mathbf{p}) =\frac{\arctan(ql)}{ql}. \quad (131)$$

We want to know the behavior for large distances and times and therefore for small $\mathbf{q}$ and Ω. We expand to orders Ω and q^2. Denoting $G\equiv G(\mathbf{p},\omega)$, it holds that

$$G\left(\mathbf{p}+\frac{1}{2}\,\mathbf{q},\omega-\frac{1}{2}\,\Omega\right)\approx\left(p^2+\mathbf{p}\cdot\mathbf{q}+\frac{1}{4}\,q^2-\frac{\omega^2}{c^2}+\Omega\,\frac{\omega}{c^2}-nt+\Omega\,\frac{n}{2}\,\frac{dt}{d\omega}\right)^{-1}$$
$$\approx G+\left[-(\mathbf{p}\cdot\mathbf{q})-\frac{1}{4}\,q^2-\Omega\left(\frac{\omega}{c^2}+\frac{n}{2}\,\frac{dt}{d\omega}\right)\right]G^2+(\mathbf{p}\cdot\mathbf{q})^2G^3. \tag{132}$$

Inserting this in Eq. (129) implies for the kernel

$$M(\mathbf{q},\Omega)=n\bar{t}t\left\{1-\frac{1}{2}\,\Omega\left(\frac{d\,\log t}{d\omega}-\frac{d\,\log \bar{t}}{d\omega}\right)\right\}\left\{I_{11}-\Omega\left(\frac{\omega}{c^2}+\frac{n}{2}\,\frac{dt}{d\omega}\right)I_{21}+\Omega\left(\frac{\omega}{c^2}+\frac{n}{2}\,\frac{d\bar{t}}{d\omega}\right)I_{12}-\frac{q^2}{4}\,(I_{12}+I_{21})\right.$$
$$\left.+\frac{k_0^2q^2}{3}\,(I_{31}+I_{13}-I_{22})\right\}. \tag{133}$$

Here we have defined the integrals

$$I_{kl}=\int\frac{d^3\mathbf{p}}{(2\pi)^3}\,G^k(\mathbf{p})G^{*l}(\mathbf{p}). \tag{134}$$

They are calculated in the Appendix. Inserting their values yields

$$M(\mathbf{q},\Omega)=a-i\Omega\tau_{\rm sc}-\frac{1}{3}\,q^2l^2. \tag{135}$$

As discussed by Van Albada *et al.* (1991), τ has two contributions,

$$\tau=\frac{l}{c}+\tau_{\rm dw}\equiv\tau_{\rm sc}+\tau_{\rm dw}. \tag{136}$$

The first term is the "scattering time" or "time of travel" $\tau_{\rm sc}=l/c$. The explicit expression for the "dwell time" $\tau_{\rm dw}$ follows as

$$\tau_{\rm dw}={\rm Im}\,\frac{d\,\log t}{d\omega}+\frac{2\pi}{k_0\bar{t}t}\,{\rm Re}\,\frac{dt}{d\omega}. \tag{137}$$

We insert the t matrix of a point scatterer, Eq. (88), yielding

$$\tau_{\rm dw}=\bar{t}t\left(\frac{1}{4\pi cU_{\rm eff}}+\frac{k_0U'_{\rm eff}}{4\pi U_{\rm eff}^2}\right)$$
$$+\frac{2\pi(\bar{t}t)^2}{k_0\bar{t}t}\left(\frac{U'_{\rm eff}}{U_{\rm eff}^4}-\frac{k_0^2U'_{\rm eff}}{16\pi^2U_{\rm eff}^2}-\frac{k_0}{8\pi^2cU_{\rm eff}}\right)$$
$$=\frac{k_0\bar{t}t}{8\pi U_{\rm eff}^2}\left(1+\left[\frac{4\pi}{k_0U_{\rm eff}}\right]^2\right)\frac{dU_{\rm eff}}{d\omega}. \tag{138}$$

Notice that the terms without $U'_{\rm eff}$ have compensated for each other. This cancellation follows more generally from a Ward identity (Van Albada *et al.*, 1991). For electrons in a random potential, $\tau_{\rm dw}$ therefore vanishes.

For acoustic waves and light waves the situation is more interesting. Since $U_{\rm eff}$ depends explicitly on frequency, $U'_{\rm eff}$ does not vanish. Both terms are additive, leading to a finite dwell time $\tau_{\rm dw}$. Using Eq. (91) this yields at resonance

$$\tau_{\rm dw}=\frac{2\pi}{\omega}\cdot\frac{1}{\alpha k^3}=\frac{\text{period}}{\text{coupling}}. \tag{139}$$

This dwell time becomes longer when the coupling to the environment, that is, the normalized scattering strength $k^3\alpha=4\pi k^3a^3(m^2-1)/3$, becomes weaker. Therefore this is an important experimental effect. The speed of transport,

$$v=c\,\frac{\tau_{\rm sc}}{\tau_{\rm sc}+\tau_{\rm dw}}, \tag{140}$$

can be substantially smaller than the speed of light when realistic values of n are inserted in this formula.

For resonant atoms at fixed positions, the reduction of speed may be as large as 10^6 (Vdovin and Galitskii, 1967; Nieuwenhuizen, Burin, Kagan, and Shlyapnikov, 1994). As a final result the diffusion coefficient $D=vl/3$ reduces, as is observed experimentally. For the general situation and for more details, see Van Albada and Lagendijk (1985) and Lagendijk and Van Tiggelen (1996).

With this result for τ we find for the ladder propagator (129) at small $\mathbf{q}$, Ω

$$\mathcal{L}(\mathbf{q},\Omega)=\frac{3S(\mathbf{q}\approx0,t=0)}{l^2}\,\frac{1}{q^2+\kappa^2+i\tilde{\Omega}}, \tag{141}$$

involving the reduced external frequency

$$\tilde{\Omega}\equiv\frac{\Omega}{D}. \tag{142}$$

This is exactly the propagator of Sec. II with absorption length $L_{\rm abs}\equiv1/\kappa\equiv l/\sqrt{3(1-a)}$.

One often considers the Schwarzschild-Milne equation with a stationary δ source, $S(\mathbf{r},t)=n\bar{t}t\delta(\mathbf{r})=4\pi l^{-1}\delta(\mathbf{r})$. In the diffusion approximation this yields

$$\mathcal{L}(\mathbf{q},\Omega)=\frac{12\pi}{l^3}\,\frac{1}{q^2+\kappa^2+i\tilde{\Omega}}. \tag{143}$$

This form is commonly called the "diffuson."

VII. TRANSPORT IN A SEMI-INFINITE MEDIUM

In this section we consider in detail the transport equation for a very thick slab. We follow the approach of Nieuwenhuizen and Luck (1993). We shall also consider the case of a mismatch in refractive index between the medium and the outside.

A. Plane wave incident on a semi-infinite medium

In many situations the index of refraction of the scattering medium differs from that of its surroundings. An example is TiO_2 particles suspended in a liquid. The boundaries between media of different indexes act partly as mirrors. They cause a direct reflection of the incoming light and reinject part of the multiple-scattered light that tries to exit the system. As long as the system is optically thick, they lead to effects of order unity, no matter how small the ratio λ/l. Thus they are important in a quantitative analysis.

We shall calculate the angle-resolved intensity profile for a plane wave incident on a perfectly flat interface. This will create a specular reflection at the interface. The situation of nonspecular reflections from nonideal interfaces also has some practical relevance.

Consider a semi-infinite medium. For $z>0$ there is a scattering medium with refractive index n_0. For $z<0$ there is a dielectric with index $n_1 \equiv n_0/m$. Our notation is indicated in Fig. 1. The system is governed by Eq. (73). We first determine the incoming wave in the scattering medium. We consider a system with scatterers in the half-space $z>0$. We replace the action of the scatterers by a self-energy term. The average wave equation reads, after Fourier transformation of the transverse vector to $\mathbf{q}_\perp=(q_x,q_y)$,

$$\frac{d^2}{dz^2}\Psi(z)+P^2\Psi(z)=0, \quad z>0, \tag{144}$$

$$\frac{d^2}{dz^2}\Psi(z)+\mathbf{p}^2\Psi(z)=0, \quad z<0, \tag{145}$$

$$P^2=k_0^2-\mathbf{q}_\perp{}^2+nt, \quad p^2=k_1^2-\mathbf{q}_\perp{}^2. \tag{146}$$

A plane wave of unit amplitude, incident from $z<0$, causes a reflected wave for $z<0$ and a refracted wave for $z>0$:

$$\Psi_{\rm in}(\mathbf{r})=e^{i\mathbf{k}_\perp^a\cdot\rho+ip_a z}-\frac{P_a-p_a}{P_a+p_a}\,e^{i\mathbf{k}_\perp^a\cdot\rho-ip_a z} \quad (z<0)$$

$$=\frac{2p_a}{P_a+p_a}\,e^{i\mathbf{k}_\perp^a\cdot\rho+iP_a z} \quad (z>0). \tag{147}$$

The prefactors in Eq. (147) follow from the requirement of continuity of Ψ and its derivative. To lowest order in the density we find for the real and imaginary parts of P

$$P=k_0\cos\theta'+i\,\frac{1}{2l\cos\theta'}, \tag{148}$$

where θ' is the angle of the refracted incoming wave with respect to the z axis.

The source term in the scattering medium, the unscattered incoming intensity, can be written as

$$I_{\rm in}=|\Psi_{\rm in}|^2=\left|\frac{2p_a}{P_a+p_a}\right|^2 e^{-z/l\cos\theta_a}=\frac{p_a}{P_a}\,T_a e^{-z/l\mu_a}. \tag{149}$$

Inside the random medium the unscattered intensity is damped exponentially (the Lambert-Beer law). To leading order in $1/kl$,

$$T_a=\frac{4p_aP_a}{(P_a+p_a)^2}=1-R(\mu_a),$$

$$R(\mu)=\left|\frac{\mu-\sqrt{\mu^2-1+1/m^2}}{\mu+\sqrt{\mu^2-1+1/m^2}}\right|^2, \tag{150}$$

where $R(\mu)$ is the angular reflection coefficient for scalar waves, and $R=1$ for total reflection, which occurs when $m>1/\sqrt{1-\mu^2}$. For vector waves the same equation applies in the *s*-wave channel (Amic *et al.*, 1997). In this expression for $R(\mu)$ the imaginary part of P_a, of order $1/kl$, has been neglected. It has been shown by Nieuwenhuizen and Luck (1993) that we must neglect this to ensure flux conservation.

We use the optical depth $\tau=z/l$ (not to be confused with the average time per scattering $\tau=\tau_{\rm sc}+\tau_{\rm dw}$) and introduce $\Gamma(\tau)$ as

$$I(z)=\frac{l}{4\pi}\,\mathcal{L}(z=\tau l)=\frac{p_a}{P_a}\,T_a\Gamma(\tau). \tag{151}$$

Γ is the diffuse intensity per unit of intensity entering inside the medium. In terms of Γ the ladder equation becomes dimensionless:

$$\Gamma(\tau)=e^{-\tau/\mu_a}+\int_0^\infty d\tau' M(\tau,\tau')\Gamma(\tau'), \tag{152}$$

where $M(\tau,\tau')$ follows from the square of the amplitude Green's function. In contrast to Eq. (36) G now consists of two terms for $z,z'>0$: a direct term and a term involving reflection for the boundary $z=0$:

$$G(z,z',\mathbf{q}_\perp)=\frac{i}{2P}\left\{e^{iP|z-z'|}+\frac{P-p}{P+p}\,e^{iP(z+z')}\right\}. \tag{153}$$

We shall later need G for $z<0$, $z'>0$ for which

$$G(z,z',\mathbf{q}_\perp)=\frac{i}{P+p}\,e^{-ipz+iPz'}. \tag{154}$$

Thus inside the random medium, $|G|^2$ has four terms. The cross terms oscillate quickly and can be omitted. We keep the previous bulk contribution to the kernel M_B and the new layer kernel M_L, $M=M_B+M_L$. For the bulk kernel we find

$$M_B(z,z')=4\pi\int d^2\rho|G(z,\rho;z',\rho')|^2. \tag{155}$$

It holds that

$$M_B(z,0)=\int dx\,dy\,\frac{1}{4\pi}\,\frac{e^{-\sqrt{x^2+y^2+z^2}/l}}{x^2+y^2+z^2}. \tag{156}$$

Since

$$r^2=z^2+\rho^2=z^2/\mu^2 \Rightarrow \rho\, d\rho=-z^2 d\mu/\mu^3, \tag{157}$$

one gets

$$\begin{aligned} M_B(z,0)&=4\pi\int dx\,dy\,\frac{1}{(4\pi r)^2}\,e^{-z/l\mu}\\ &=\int_0^\infty \frac{\rho\,d\rho}{2r^2}\,e^{-z/l\mu}\\ &=\int_0^1 \frac{d\mu}{2\mu}\,e^{-z/l\mu}, \end{aligned} \tag{158}$$

yielding for the bulk kernel [cf. Eq. (36)]

$$\begin{aligned} M_B(\tau,\tau')&=\int_0^1 \frac{d\mu}{2\mu}\,e^{-|\tau-\tau'|/\mu}\\ &=\frac{1}{2}\,E_1(|\tau-\tau'|), \end{aligned} \tag{159}$$

where E_1 is an exponential integral. In the same fashion the layer term is

$$\begin{aligned} M_L(\tau,\tau')&=4\pi\int dx\,dy\left|\frac{i}{2P}\,\frac{P-p}{P+p}\,e^{iP(z+z')}\right|^2\\ &=\int_0^1 \frac{d\mu}{2\mu}\,e^{-(\tau+\tau')/\mu}R(\mu). \end{aligned} \tag{160}$$

It consists of three effects: an exponential decay of intensity that goes from the point $\mathbf{r}'$ with angle θ towards the wall having an optical path length τ'/μ; a reflection factor $R(\mu)$; a further decay over an optical path length τ/μ between the wall and the observation point $\mathbf{r}$.

We now calculate the angle-resolved reflection. For a plane-wave incidence the solution of Eq. (123) is $\mathcal{L}(z,\rho)=\mathcal{L}(z)$. We can write for the reflected intensity at point (z',ρ'), with $z'>0$,

$$I_R(z',\rho')=\int dz\,d^2\rho\mathcal{L}(z,\rho)|G(z,\rho;z',\rho')|^2. \tag{161}$$

Here $\mathcal{L}(z)$ is related to $\Gamma(\tau)$ via $z=l\tau$ and Eq. (151).

It is useful to consider first a finite area A and to continue this area periodically. We can then integrate out the ρ dependence; later we shall take the limit $A\to\infty$. Using the periodicity of the surface one can express the Green's function as

$$G(z,\rho;z',\rho')=\frac{1}{A}\sum_{\mathbf{q}_\perp} G(z;z';\mathbf{q}_\perp)e^{i\mathbf{q}_\perp\cdot(\rho-\rho')}. \tag{162}$$

Since the incoming plane wave is infinitely broad, the diffuse intensity I does not depend on ρ. The integration over ρ is simple:

$$\begin{aligned} \int d^2\rho|G(z,\rho;z',\rho')|^2&=\frac{1}{A}\sum_{\mathbf{q}_\perp} GG^*\\ &\approx\int \frac{d^2\mathbf{q}_\perp}{(2\pi)^2}\,|G(z,z',\mathbf{q}_\perp)|^2. \end{aligned} \tag{163}$$

The last step holds in the limit $A\to\infty$. If we denote the outgoing $\mathbf{q}_\perp$ by $\mathbf{q}_\perp^b$, we can express $d^2\mathbf{q}_\perp$ as

$$\begin{aligned} d^2\mathbf{q}_\perp^b&=q_\perp^b dq_\perp^b d\phi_b=k_1^2\sin\theta_b\cos\theta_b d\theta_b d\phi_b\\ &=k_1^2\cos\theta_b d\Omega_b. \end{aligned} \tag{164}$$

Inserting Eqs. (164) and (163) in Eq. (161) yields a result that is independent of the observation point (z',ρ'):

$$\begin{aligned} &I_R(z',\rho')\\ &=\int dz\int \frac{k_1^2\cos\theta_b}{4\pi^2}\,d\Omega_b\,\frac{1}{|P_b+p_b|^2}\,\mathcal{L}(z)e^{-z/l\cos\theta_b'}, \end{aligned} \tag{165}$$

where θ_b' is the direction of the radiation in the medium, which is refracted into the outgoing direction θ_b (see Fig. 1); we also recall that $\mu_b=\cos\theta_b'$. We finally find for the angle-resolved reflected diffuse intensity.

$$\begin{aligned} A_R&\equiv\frac{dR(a\to b)}{d\Omega_b}=\frac{dI_R}{d\Omega_b}\\ &=\frac{k_1^2\cos\theta_b}{4\pi^2}\,\frac{T_b}{p_bP_b}\int dz\,\mathcal{L}(z)e^{-z/l\cos\theta_b'}. \end{aligned} \tag{166}$$

Using Eqs. (151) and (146) at $nt\to 0$, one can express the numerical prefactor of the integral

$$\begin{aligned} \frac{T_b}{4P_bp_b}&=\frac{k_1^2}{(2\pi)^2}\cos\theta_b 4\pi\,\frac{p_aT_a}{P_a}\\ &=\frac{k_1^2p_a}{4\pi p_b}\cos\theta_b\,\frac{T_aT_b}{P_aP_b}\\ &=\frac{k_1^2}{4\pi}\,\frac{\cos\theta_a}{\cos\theta_b}\cos\theta_b\,\frac{T_aT_b}{k_0\mu_ak_0\mu_b}\\ &=\frac{\cos\theta_a}{4\pi m^2}\,\frac{T_aT_b}{\mu_a\mu_b}. \end{aligned} \tag{167}$$

For the angle-resolved diffuse reflection of a semi-infinite medium we thus find

$$A_R(\theta_a,\theta_b)=\frac{\cos\theta_a}{4\pi m^2}\,\frac{T_aT_b}{\mu_a\mu_b}\,\gamma(\mu_a,\mu_b), \tag{168}$$

with the generalized *bistatic coefficient*.

$$\begin{aligned} \gamma(\mu_a,\mu_b)&=\int_0^\infty d\tau\,\Gamma_S(\mu_a,\tau)e^{-\tau/\mu_b}\\ &=\int_0^\infty d\tau\,d\tau'\,G_S(\tau,\tau')e^{-\tau/\mu_a}e^{-\tau'/\mu_b}. \end{aligned} \tag{169}$$

In the absence of index mismatch ($m=1$) one has $T_{a,b}=1$, $\mu_{a,b}=\cos\theta_{a,b}$, so the prefactor in Eq. (168) becomes $1/(4\pi\cos\theta_b)$. Figure 6 shows numerical results for A_R for perpendicular incidence ($\theta_a=0$); see Nieuwenhuizen and Luck (1993).

B. Air-glass-medium interface

We now consider a semi-infinite scattering medium, separated from the air by another dielectric, such as

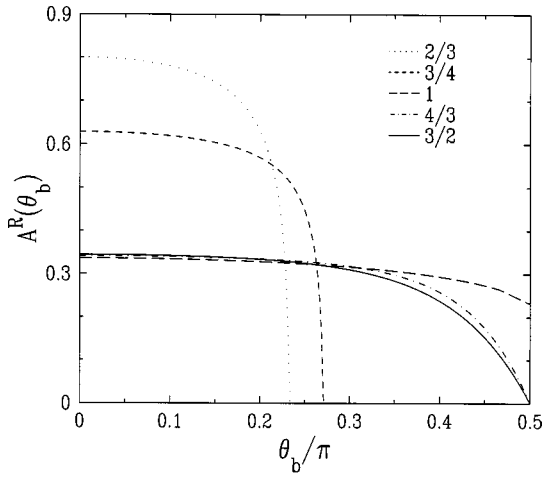

FIG. 6. Angle-resolved reflection coefficient for perpendicular incidence on a semi-infinite medium, for different values of the index ratio m. For $m<1$ no radiation can exit the random medium at an angle exceeding the Brewster angle.

glass, of thickness d. For $z<-d$ there is air, for $-d<z<0$ glass, and for $z>0$ the scattering medium. A plane wave of unit amplitude comes in from $z=-\infty$ with wave vector $(\mathbf{q}_\perp, k_z)$. The perpendicular component $\mathbf{q}_\perp$ is conserved at the interfaces. We denote by p_i the z component of the wave vectors in the three sectors $i=0,1,2$, where $i=0$ corresponds to the scattering medium, $i=1$ to air, and $i=2$ to glass. The wave numbers in the three media are $k_0=\omega/c_0$, $k_1=\omega/c_1$, and $k_2=\omega/c_2$, respectively, where c_i is the speed of propagation in the medium i. The incoming, refracted, and specularly reflected waves are given by

$$\Psi(r)=\begin{cases} e^{i\mathbf{q}_\perp\cdot\rho+ip_1z}+re^{i\mathbf{q}_\perp\cdot\rho-ip_1z} & (z<-d) \\ t_1e^{i\mathbf{q}_\perp\cdot\rho+ip_2z}+r_1e^{i\mathbf{q}_\perp\cdot\rho-ip_2z} & (-d<z<0) \\ te^{i\mathbf{q}_\perp\cdot\rho+ip_0z} & (z>0). \end{cases}$$

Here r is the reflection amplitude of the system, t the transmission amplitude, and $p_i=\sqrt{k_i^2-\mathbf{q}_\perp^2}$. Continuity requirements at $z=-d$ and $z=0$ yield r, r_1 and t, t_1:

$$r=\frac{(p_0+p_2)(p_1-p_2)-(p_0-p_2)(p_1+p_2)e^{2ip_2d}}{(p_0+p_2)(p_1+p_2)-(p_0-p_2)(p_1-p_2)e^{2ip_2d}},$$

$$t=\frac{4p_1p_2e^{i(p_2-p_1)d}}{(p_0+p_2)(p_1+p_2)-(p_0-p_2)(p_1-p_2)e^{2ip_2d}}. \tag{170}$$

The reflection and transmission coefficients of the double interface are

$$|r|^2; \quad \frac{p_0}{p_1}|t|^2, \tag{171}$$

respectively. As we assume the thickness of the glass plate is not smooth within one wavelength, these expressions must be averaged over the spread in thickness. This amounts to averaging over the phase $2p_2d\equiv\varphi$ and leads to the average transmission and reflection coefficients

$$T_3=1-R_3=\frac{p_0}{p_1}\int_{-\pi}^{\pi}\frac{d\varphi}{2\pi}|t|^2. \tag{172}$$

The integrand is of the form $A/(B-C\cos\phi)$. The final result is

$$T_3=1-R_3=\frac{4p_0p_1p_2}{(p_0+p_1)(p_0p_1+p_2^2)}. \tag{173}$$

We can check this in special cases. Inserting $p_2=p_1=p$ and $p_0=P$ indeed reduces to the previous result for two media.

We can describe this system by replacing $T(\mu)$ in previous equations by $T_3(\mu)$ and replacing the reflection coefficient $R(\mu)$ in the Milne kernel by $R_3(\mu)$. As before, $\mu\equiv p_0/k_0$ is the cosine of the angle θ' between the radiation and the z axis.

The specular reflections in the glass have now been taken into account. For a not too narrow beam this is useful for thin glass plates. For a not so broad beam impinging on a medium with thick plates, multiple reflections from the glass interfaces can result in components that fall outside the incoming beam and even outside the medium (Ospeck and Fraden, 1994).

C. Solutions of the Schwarzschild-Milne equation

We consider properties of the transport equation in a semi-infinite space (Nieuwenhuizen and Luck, 1993). The Milne equation (152) has a special solution $\Gamma_S(\mu_a;\tau)$, while the associated homogeneous equation without source term has a solution $\Gamma_H(\tau)$. We are interested in the asymptotic behavior of $\Gamma_S(\mu_a;\tau)$ and $\Gamma_H(\tau)$. Deep in the bulk ($\tau\gg1$) one expects a slow variation of $\Gamma(\tau')$ at the scale of one mean free path [$|\tau-\tau'|=\mathcal{O}(1)$] and one can expand

$$\Gamma(\tau')=\Gamma(\tau)+(\tau'-\tau)\Gamma'(\tau)+\frac{1}{2}(\tau'-\tau)^2\Gamma''(\tau)+\cdots. \tag{174}$$

When this is inserted in Eq. (152), one finds for $\tau\gg1$

$$\Gamma(\tau)\approx\Gamma(\tau)+\frac{1}{3}\Gamma''(\tau)+\cdots \tag{175}$$

where for large τ

$$\frac{1}{2}\int_0^1\frac{d\mu}{2\mu}\int_0^\infty d\tau' e^{-|\tau-\tau'|/\mu}(\tau-\tau')^2\approx\frac{1}{3}. \tag{176}$$

The term $\mathcal{O}(\Gamma')$ vanishes due to symmetry of the $(\tau'-\tau)$ integral. Equation (175) thus yields again the diffusion behavior $\Gamma''(\tau)\approx0$. We therefore consider the homogeneous solution Γ_H and the special solution Γ_S with the asymptotic behaviors

$$\begin{cases}\Gamma_H(\tau)\approx\tau+\tau_0 \\ \Gamma_S(\tau;\mu_a)\approx\tau_1(\mu_a)\end{cases} \quad (\tau\to\infty). \tag{177}$$

Corrections occur due to the interface and decay exponentially in τ. For a numerical solution one may introduce $\delta\Gamma_S(\tau)=\Gamma_S(\tau)-\tau_1(\mu_a)$ and $\delta\Gamma_H(\tau)=\Gamma_H(\tau)-\tau-\tau_0$ and integrate them from $\tau=\infty$. The requirement

TABLE I. Numerical values of several fundamental quantities in radiative transfer theory for typical values of the index ratio n.

m	τ_0	$\tau_1(1)$	$\gamma(1,1)$	ΔQl
2	6.08	21.7	21.5	0.136
3/2	2.50	10.8	10.6	0.269
4/3	1.69	8.34	7.94	0.343
1	0.710 446	5.036 48	4.227 68	1/2
3/4	0.815	5.39	4.63	0.479
2/3	0.881	5.60	4.85	0.465
1/2	1.09	6.25	5.55	0.427

that they vanish there determines τ_0 and τ_1. The constant τ_0 depends only on the index ratio m, while $\tau_1(\mu_a)$ also depends on the direction of the incoming beam.

We define the Green's function $G_S(\tau,\tau')$ as the solution of the inhomogeneous equation

$$G_S(\tau,\tau')=\delta(\tau-\tau')+\int_0^\infty d\tau''\{M_B(\tau,\tau'')+M_L(\tau,\tau'')\}G_S(\tau'',\tau'), \tag{178}$$

subject to the boundary condition $G_S(\infty,\tau')<\infty$. This function is symmetric, $G_S(\tau,\tau')=G_S(\tau',\tau)$, and has the limit

$$\lim_{\tau'\to\infty} G_S(\tau,\tau')=\frac{1}{D}\Gamma_H(\tau). \tag{179}$$

The latter equality can be proven by taking the limit $\tau'\to\infty$ in Eq. (178). The delta function vanishes and the remaining equation is the same as the one for $\Gamma_H(\tau)$. Therefore $G_S(\tau,\tau'\to\infty)$ is proportional to $\Gamma_H(\tau)$. The multiplicative prefactor can be fixed by expanding $G_S(\tau,\tau')$ in $\tau'-\tau$ and inserting this in the right-hand side of Eq. (178). Using Eq. (176) again, one finds for $\tau,\tau'\gg 1$

$$0=\delta(\tau-\tau')+\frac{1}{3}\frac{d^2}{d\tau^2}G_S(\tau,\tau'). \tag{180}$$

The solution is $G_S(\tau,\tau')=3\min(\tau,\tau')$ in the regime $(\tau,\tau',|\tau-\tau'|\gg 1)$. The diffusion coefficient D in Eq. (179) reads 1/3 in reduced units, that is to say, $D=vl/3$ in physical units.

From Eq. (178) it follows that

$$\Gamma_S(\tau;\mu)=\int_0^\infty d\tau' G_S(\tau,\tau')e^{-\tau'/\mu} \tag{181}$$

and, in particular, using Eqs. (177) and (179),

$$\tau_1(\mu)=\lim_{\tau\to\infty}\Gamma_S(\tau;\mu)=\frac{1}{D}\int_0^\infty \Gamma_H(\tau)e^{-\tau/\mu}d\tau. \tag{182}$$

The physical interpretation of $\tau_1(\mu)$ is the limit intensity $(z=\tau l\to\infty)$ of a semi-infinite medium.

Numerical values of the injection depth τ_0, the normalized limit intensity $\tau_1(1)$, and the normalized bistatic coefficient $\gamma(1,1)$ can be found in Table I for various values of the index ratio m.

Nieuwenhuizen and Luck (1993) verified explicitly that in this approach flux is conserved. This derivation will not be reproduced here. We refer the interested reader to the original paper.

VIII. TRANSPORT THROUGH A SLAB

We now discuss the transmission properties of an optically thick slab with isotropic scatterers. We derive the "ohmic" or diffusive scaling behavior $T\sim l/L$ mentioned in Sec. II and give the full angular dependence of the transmission and reflection. This result is then used to calculate the resistance of an idealized conductor, see also Sec. XVI.A.

A. Diffuse transmission

We consider a medium with finite thickness $L\gg l$. The medium has optical thickness $b=L/l\gg 1$. For the moment we wish to neglect boundary effects. Therefore we are restricted to positions not too close to the boundary (10 mean free paths is a good measure, as the corrections decay exponentially). The solution for $\Gamma(\tau)$ is a linear combination of the special and the homogeneous solutions,

$$\begin{aligned}\Gamma(\tau)&=\Gamma_S(\tau)-\alpha\Gamma_H(\tau)\ \text{ for }\ 0\leqslant\tau\leqslant 10\\ &=\tau_1(\mu)-\alpha(\tau+\tau_0)\ \text{ for }\ \tau>10.\end{aligned} \tag{183}$$

Near the other boundary it holds similarly that

$$\begin{aligned}\Gamma(\tau)&=\alpha'\Gamma_H(b-\tau)\ \text{ for }\ 0\leqslant b-\tau\leqslant 10\\ &=\alpha'(b-\tau+\tau_0)\ \text{ for }\ b-\tau>10.\end{aligned} \tag{184}$$

As they have the same functional form, both shapes can be matched in the bulk of the sample. This yields

$$\alpha=\alpha'=\frac{\tau_1(\mu)}{b+2\tau_0}. \tag{185}$$

Inserting this value in Eqs. (183) and (184) gives the intensity anywhere in the slab, expressed in terms of Γ_S and Γ_H of the semi-infinite problem. Notice the important role played by the diffusive behavior in the bulk. The Schwarzschild-Milne equation has brought the precise behavior at scales of one mean free path from the boundaries.

To calculate the angular transmission profile, we follow the derivation for the diffuse reflection [see Eq. (168)]. The expression for the differential transmission coefficient per unit solid angle $d\Omega_b$ of a beam incident under angle θ_a is given analogously as

$$\frac{dT(a\to b)}{d\Omega_b}=\frac{\cos\theta_a T_a T_b}{4\pi m^2\mu_a\mu_b}\int_0^b d\tau\Gamma(\tau)e^{-(b-\tau)/\mu_b}. \tag{186}$$

Using the solution for $\Gamma(\tau)$ we rewrite the integral

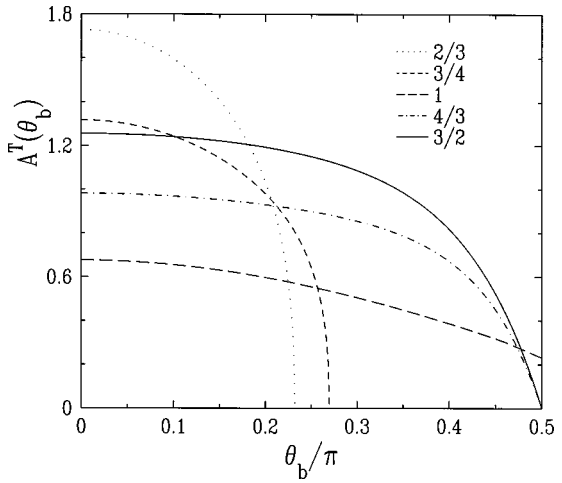

FIG. 7. Angle-resolved transmission coefficient for perpendicular incidence on a thick slab. The ratio of refractive indices, m, has been indicated.

$$\int_0^b d\tau\Gamma(\tau)e^{-(b-\tau)/\mu_b}\approx\alpha\int_{-\infty}^b d\tau\Gamma_H(b-\tau)e^{-(b-\tau)/\mu_b}$$
$$=\alpha\int_0^\infty d\tau\Gamma_H(\tau)e^{-\tau/\mu_b}$$
$$=\frac{\tau_1(\mu_a)}{b+2\tau_0}\,\tau_1(\mu_b)D, \tag{187}$$

where we used Eq. (182). We have derived the angle-dependent differential transmission coefficient for a slab of optical thickness $b=L/l$,

$$\frac{dT(a\to b)}{d\Omega_b}\equiv\frac{A^T(\theta_a,\theta_b)}{b+2\tau_0}$$
$$\equiv\frac{\cos\,\theta_a T_a T_b}{12\pi m^2\mu_a\mu_b(b+2\tau_0)}\,\tau_1(\mu_a)\tau_1(\mu_b). \tag{188}$$

As the intensity at the side of incidence ($z=0$) equals $\Gamma(\tau)=\Gamma_S(\tau)-\alpha\Gamma_H(\tau)$, it is clear that the transmission term $\alpha\Gamma_H(b-\tau)$ arises at the cost of the reflection. Therefore flux conservation is also satisfied for an optically thick slab.

In Fig. 7 we show $A^T(\theta_a,\theta_b)$, the normalized angle-resolved transmission for perpendicular incidence ($\theta_a=0$), for several values of the index ratio m.

B. Electrical conductance and contact resistance

For metallic conductors in the mesoscopic regime the conductance is given by the Landauer formula (Landauer, 1975):

$$G=\frac{2e^2}{h}\sum_{a,b}T_{ab}^{\rm flux}, \tag{189}$$

where $h/e^2\approx 25k\Omega$ is the quantum unit of resistance. This equation simply counts the weight of the channels that contribute to transmission. In the above description the wave number k_0 can be replaced by the Fermi wave-number vector k_F. The analog of the contrast in refractive index is now the potential difference between the conductor and the contact regions ($V_1\neq V_0$). In our formalism the conductance is given by

$$G=\frac{2e^2}{h}\sum_{a,b}T_{ab}^{\rm flux}=\frac{2e^2}{h}\sum_{a,b}T_{ab}\,\frac{\cos\,\theta_b}{\cos\,\theta_a}$$
$$=\frac{2e^2}{h}\,\frac{k_F^2A}{3\pi(b+2\tau_0)}, \tag{190}$$

with $T_{ab}=A^T(\theta_a,\theta_b)/(b+2\tau_0)$. From this one gets

$$G=\frac{A\sigma_B}{L+2z_0},\quad \sigma_B=\frac{2e^2k_F^2l}{3\pi h}, \tag{191}$$

where $z_0=\tau_0 l$ and σ_B is the "Boltzmann" value for the bulk conductivity. We distinguish a bulk resistance and a contact resistance R_c,

$$R=\frac{1}{G}=\frac{L}{A\sigma_B}+2R_c,\quad R_c=\frac{3\pi\hbar}{2e^2Ak_F^2}\,\tau_0. \tag{192}$$

The number of modes can be estimated as $N\approx Ak_F^2$. The above expression shows that R_c is proportional to the dimensionless thickness τ_0 and inversely proportional to the number of channels. The nontrivial part is coded in τ_0. It depends on the potential drop $V-V_1$, but not on the density of scatterers. Because

$$k_F^2-V_1=k_1^2,\quad k_F^2-V_0=k_0^2, \tag{193}$$

we can make an analogy with light scattering by putting $k_0^2=m^2k_1^2$:

$$m^2\Rightarrow\frac{k_F^2-V_0}{k_F^2-V_1}. \tag{194}$$

IX. THE ENHANCED BACKSCATTER CONE

So far we have seen effects that are largely diffusive and that could to some extent also be derived from particle diffusion. The enhanced backscatter cone is the clearest manifestation of interference due to the wave nature of light. The wave character manifests itself most clearly in loop processes. The advanced and retarded waves can go around in two ways, in the same direction and in opposite directions. This leads to an enhanced return to the origin, which is the basic mechanism for Anderson localization (Sec. I).

The optically enhanced backscatter in the exact backscatter direction has the same characteristics as a closed loop. It brings two possibilities, thus a factor of 2, for all scattering series involved. For Faraday-active media it will be suppressed in a magnetic field. Away from the backscatter direction there is partial extinction.

A. Milne kernel at nonzero transverse momentum

We follow the discussion of Nieuwenhuizen and Luck (1993). The backscatter diagrams are closely related to the standard ladder diagrams. The only difference is the

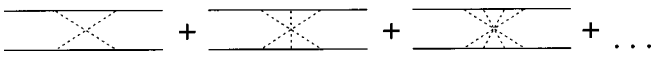

FIG. 8. Maximally crossed diagrams.

crossed attachment of the incoming and outgoing lines to the first and last scatterers. These diagrams are called maximally crossed diagrams (Fig. 8).

Let the incoming wave be denoted by a and the outgoing wave by b. Their wave vectors have components $(\mathbf{k}_\perp^a, p_a)$, $(\mathbf{k}_\perp^b, p_b)$. The product of incoming and outgoing waves at the first scatterer is

$$\Psi^*\Psi = \frac{p_a T_a}{P_a}\, e^{i(\mathbf{k}_\perp^a - \mathbf{k}_\perp^b)\cdot\rho + i(p_a - p_a^*)z}, \tag{195}$$

with $\rho=(x,y)$. We define the transverse wave vector

$$\mathbf{Q} \equiv (\mathbf{k}_\perp^a - \mathbf{k}_\perp^b). \tag{196}$$

For perpendicular incidence one has $(\theta_a=0;\ \mathbf{k}_\perp^a=0)$. We consider the regime of angles close to the backscatter direction $(\theta_b \simeq 0)$. Then it holds that $|\mathbf{Q}| \simeq k_1\theta_b$ so that

$$\Psi^*\Psi = \frac{T(1)}{m}\, e^{i\mathbf{Q}\cdot\rho} e^{-z/l}. \tag{197}$$

Consider the diffuse intensity I in the backscatter cone. It is given by

$$I(\mathbf{r}) = \frac{T(1)}{m}\, e^{i\mathbf{Q}\cdot\rho} e^{-z/l} + \frac{4\pi}{l}\int d\mathbf{r}' |G(\mathbf{r}-\mathbf{r}')|^2 I(\mathbf{r}'). \tag{198}$$

Notice that dependence occurs only in the source term of this integral equation. Inserting $I(\mathbf{r}) = e^{iQ\cdot\rho} I(z,Q)$ yields the Milne equation for $I(z,Q)$,

$$I(z,Q) = \frac{T(1)}{m}\, e^{-z/l} + \int \frac{dz'}{l}\, M_C(z,z',Q) I(z',Q), \tag{199}$$

with the Q-dependent Milne-cone kernel

$$M_C(z,z',Q) = 4\pi \int d^2\rho' e^{i\mathbf{Q}\cdot(\rho'-\rho)} |G(\mathbf{r},\mathbf{r}')|^2. \tag{200}$$

The normalized intensity of the maximally crossed diagrams satisfies

$$\Gamma_C(\tau,Q) = \frac{m I(z,Q)}{T(1)},$$

$$\Gamma_C(\tau,Q) = e^{-\tau} + \int d\tau' M_C(\tau,\tau',Q)\Gamma_C(\tau',Q). \tag{201}$$

The Milne kernel again has a bulk and a layer term,

$$M_C(\tau,\tau',Q) = M_B(\tau,\tau',Q) + M_L(\tau,\tau',Q). \tag{202}$$

Inserting $|G(\mathbf{r})|^2 = e^{-r/l}/(4\pi r)^2$ yields

$$M_B(z,z',Q) = 4\pi \int \rho\, d\rho\, d\phi\, \frac{1}{(4\pi)^2[(z-z')^2+\rho^2]} \times e^{iQ\rho\cos\phi} e^{-\sqrt{(z-z')^2+\rho^2}/l}. \tag{203}$$

In terms of the variables $\tau = z/l$ and $\mu = \cos\theta'$, where θ' is the angle between ρ and the z axis, we find that

$$\frac{\sqrt{(z-z')^2+\rho^2}}{l} = \frac{|\tau-\tau'|}{\mu}, \quad \frac{\rho\, d\rho}{l^2} = -\frac{|\tau-\tau'|^2}{\mu^3}\, d\mu.$$

Inserting this in Eq. (203) yields

$$M_B(|\tau-\tau'|,Q) = \int_0^1 \frac{d\mu}{2\mu} \int_{-\pi}^{\pi} \frac{d\phi}{2\pi}\, e^{iQl\cos\phi|\tau-\tau'|\sqrt{\mu^{-2}-1}} e^{-|\tau-\tau'|/\mu} = \int_0^1 \frac{d\mu}{2\mu} J_0(Ql|\tau-\tau'|\sqrt{\mu^{-2}-1}) e^{-|\tau-\tau'|/\mu}, \tag{204}$$

where J_0 is the zero-order Bessel function. A similar analysis yields for the layer term

$$M_L(\tau+\tau',Q) = \int_0^1 \frac{d\mu}{2\mu} R(\mu) J_0(Ql(\tau+\tau') \times \sqrt{\mu^{-2}-1}) e^{-(\tau+\tau')/\mu}. \tag{205}$$

This form is useful at small and large Q.

B. Shape of the backscatter cone

The intensity in the backscatter direction consists of two parts: a diffuse background A^R, discussed in Sec. VII, and a contribution A^C from the maximally crossed diagrams. In the case of perpendicular incidence we have found for the background contribution Eq. (168)

$$A^R(0,0) = \frac{T(1)^2\gamma(1,1)}{4\pi m^2}, \tag{206}$$

where the normalized bistatic coefficient γ is given by

$$\gamma(\mu_a,\mu_b) = \int_0^\infty d\tau\, e^{-\tau/\mu_b} \Gamma_S(\tau,\mu_a) \tag{207}$$

$$= \int_0^\infty d\tau \int_0^\infty d\tau'\, e^{-\tau/\mu_b - \tau'/\mu_a} G_S(\tau,\tau'). \tag{208}$$

The contribution of the maximally crossed diagrams, normalized by the diffuse background, is given by

$$A^C(Q) = \frac{\gamma_C(Q) - \gamma_{\mathrm{TR}}}{\gamma(1,1)}, \tag{209}$$

where γ_{TR} is the amplitude of the paths that are identical to their time-reversed analogs. Such paths do not yield a time-reversed contribution, and this should thus be subtracted from the first term. For low scatterer density, γ_{TR} consists of the single scattering event (in, scatter, out). This process yields [cf. Eq. (169)]

$$\gamma_{\mathrm{TR}} = \int_0^\infty d\tau \int_0^\infty d\tau'\, e^{-\tau-\tau'}\, \delta(\tau-\tau') = \frac{1}{2}. \tag{210}$$

The nontrivial term is defined as

$$\gamma_C(Q)=\int_0^\infty d\tau e^{-\tau}\Gamma_C(\tau,Q)$$
$$=\int_0^\infty d\tau\int_0^\infty d\tau' e^{-\tau-\tau'}G_C(\tau,\tau',Q), \qquad (211)$$

where G_C is the solution of Eq. (201) with source $\delta(\tau-\tau')$ instead of $e^{-\tau}$ and vanishing for $\tau\to\infty$. In Fig. 9 we present the numerical results for $A^C(Q)$ for several values of the index ratio m.

C. Decay at large angles

From Eqs. (204) and (205) it follows that M_B and M_L decay quickly as functions of τ when Q is large. Physically this happens because the enhanced backscatter is suppressed at large angles due to dephasing. For large angles we can therefore restrict Eq. (211) to low-order scattering. To second order we have $G_C(\tau,\tau';Q)=\delta(\tau-\tau')+M_C(\tau,\tau';Q)$. This yields

$$\gamma_C(Q)=\frac{1}{2}+\int_0^\infty d\tau d\tau' e^{-\tau-\tau'}[M_B(|\tau-\tau'|;Q)+M_L(\tau+\tau';Q)]. \qquad (212)$$

For the bulk term

$$\int_0^\infty d\tau d\tau' e^{-\tau-\tau'}M_B(|\tau-\tau'|;Q)\overset{(204)}{=}\int_0^1\frac{d\mu}{2\mu}\int_{-\pi}^{\pi}\frac{d\phi}{1+1/\mu-iQl\cos\phi\sqrt{1/\mu^2-1}}$$
$$=\int_0^1\frac{d\mu}{2}\frac{1}{\sqrt{(\mu+1)^2+Q^2l^2(1-\mu^2)}}\overset{Q_{\text{large}}}{\approx}\frac{\pi}{4Ql}. \qquad (213)$$

Inserting Eq. (205) yields for the layer term in Eq. (212)

$$\int_0^\infty d\tau d\tau' e^{-\tau-\tau'}M_L(\tau+\tau';Q)=\int_0^1\frac{d\mu}{2}\int_{-\pi}^{\pi}\frac{d\phi}{2\pi}R(\mu)\frac{\mu}{(\mu+1-iQl\cos\phi\sqrt{1-\mu^2})^2}$$
$$=\frac{1}{2}\int_0^1 d\mu\,\mu R(\mu)\frac{\mu+1}{[(\mu+1)^2+Q^2l^2(1-\mu^2)]^{3/2}}. \qquad (214)$$

The integrand decays quickly for large values of $Q^2l^2(1-\mu^2)$. Setting $\mu=1-x/(Q^2l^2)$ we obtain for the layer term

$$\frac{R(1)}{Q^2l^2}\int_0^\infty\frac{dx}{(4+2x)^{3/2}}=\frac{R(1)}{2Q^2l^2}. \qquad (215)$$

This yields

$$A^C(Q)\simeq\frac{T(1)^2}{4\pi m^2}\left(\frac{\pi}{4Ql}+\frac{R(1)}{2Q^2l^2}\right) \qquad (216)$$

for large Q. The effect of the layer term is essentially the square of the bulk term. This is because the paths involved are essentially twice as long (Fig. 10).

D. Behavior at small angles

Assuming a linear Q dependence, we expand Γ_C around $Q=0$,

$$\Gamma_C(\tau;Q)\simeq\Gamma_C(\tau;Q=0)-Q\tilde{\Gamma}_C(\tau;Q). \qquad (217)$$

Inserting this in Eq. (201) and subtracting the $Q=0$ terms yields, to leading order in Q,

$$\tilde{\Gamma}_C(\tau;Q)=\int_0^\infty d\tau' M_C(\tau,\tau';Q)\tilde{\Gamma}_C(\tau';Q). \qquad (218)$$

As this is a homogeneous equation, it holds that $\tilde{\Gamma}_C(\tau;Q)=\alpha\Gamma_H(\tau;Q)$, so that Eq. (217) becomes

$$\Gamma_C(\tau;Q)=\Gamma_S(\tau)-\alpha Q\Gamma_H(\tau)\overset{\tau\gg1}{\approx}\tau_1(1)-\alpha Ql\tau. \qquad (219)$$

Deep inside the scattering medium ($\tau\gg1$) the diffusion approximation holds, implying

$$\Gamma_C''(\tau;Q)=Q^2l^2\Gamma_C(\tau;Q)\Rightarrow\Gamma_C(\tau;Q)=\tilde{\alpha}e^{-Ql\tau}. \qquad (220)$$

Matching this for small $Ql\tau$ with Eq. (219) one finds $\tilde{\alpha}=\alpha=\tau_1(1)$. Using Eq. (207) this yields

$$\gamma_C(Q)=\gamma_C(0)-3Ql\tau_1^2(1)$$
$$=\gamma_C(0)\left(1-\frac{Q}{\Delta Q}\right), \qquad (221)$$

where we used Eq. (182) with $D=\frac{1}{3}$. The normalized opening angle ΔQ is

$$\Delta Q=3\frac{\gamma_C(0)}{l\tau_1^2(1)}. \qquad (222)$$

Note that $\gamma_C(0)\equiv\gamma(Q=0;\mu_a=\mu_b=1)$. The linearity of the peak of the cone is a result of diffusion, that is to say, of long light paths. The complicated expression for the opening angle shows that the skin layer plays an important quantitative role. The reason for this is obvious: the light has to traverse it.

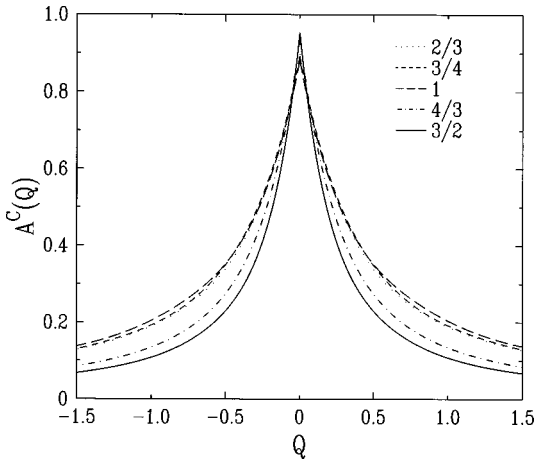

FIG. 9. Backscatter cone of a semi-infinite medium at normal incidence for several values of m. The diffusive background was subtracted.

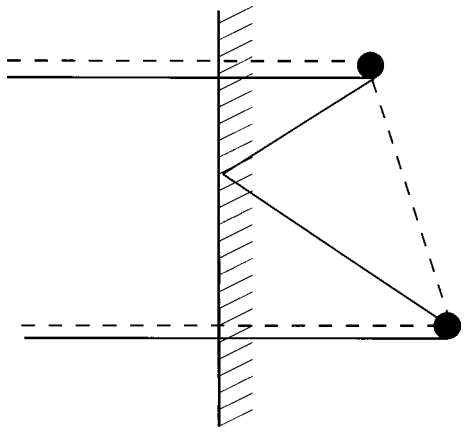

FIG. 10. The effect of internal reflection on the backscatter cone. At large angles the backscatter cone is mainly determined by second-order scattering. The term with internal reflection has a larger optical path and therefore decays faster.

X. EXACT SOLUTION OF THE SCHWARZSCHILD-MILNE EQUATION

Some useful formulas were given in previous sections for calculation of the diffuse intensity. However, the Schwarzschild-Milne equation can be solved exactly in the absence of internal reflections (Chandrasekhar, 1960). We summarize the approach of Nieuwenhuizen and Luck (1993) here and generalize the Schwarzschild-Milne equation to include internal reflections.

A. The Homogeneous Milne equation

The starting point of this analysis is the integral form of the radiative transfer equation, i.e., the Schwarzschild-Milne equation, Eq. (152). In the absence of internal reflections, $M_L=0$, the remaining kernel M_B depends only on the difference $(\tau-\tau')$, giving the Milne equation the structure of a convolution equation. Because of its half-space geometry the problem is still nontrivial.

We consider first the homogeneous Milne equation. Its solution $\Gamma_H(\tau)$ has the asymptotic behavior $\Gamma_H(\tau)=\tau+\tau_0$ [Eq. (177)]. We define the Laplace transforms of $M_B(\tau,0)$ and of $\Gamma_H(\tau)$ as

$$m(s)=\int_{-\infty}^{\infty} M_B(\tau,0)e^{s\tau}d\tau \quad (-1<\mathrm{Re}\ s<1) \tag{223}$$

$$g_H(s)=\int_0^{\infty}\Gamma_H(\tau)e^{s\tau}d\tau=D\tau_1(\mu=-1/s) \quad (\mathrm{Re}\ s<0). \tag{224}$$

In the case of isotropic scattering the Milne kernel equation (158) leads to

$$m(s)=\frac{1}{2s}\ln\frac{1+s}{1-s}. \tag{225}$$

The small-s behavior of $m(s)$

$$m(s)=1+Ds^2+\mathcal{O}(s^4) \quad (s\to 0) \tag{226}$$

determines the dimensionless diffusion constant $D=1/3$.

It turns out that the problem can be solved for any symmetric Milne kernel. The homogeneous Milne integral equation is equivalent to

$$\phi(s)g_H(s)=\int_{-i\infty}^{i\infty}\frac{dt}{2\pi i}\frac{m(t)g_H(t)}{t-s} \tag{227}$$

$$(-1<\mathrm{Re}\ t<\mathrm{Re}\ s<0),$$

with $\phi(s)=1-m(s)$, and the asymptotic behavior Eq. (177) is equivalent to

$$s^2g_H(s)=1-\tau_0 s+\mathcal{O}(s^2) \quad (s\to 0). \tag{228}$$

Equation (227) can be solved in closed form, for an arbitrary bulk kernel. Let us consider first the following "rational case," in which $M_B(\tau,0)$ is a finite superposition of N decaying exponentials, namely,

$$M_B(\tau,0)=\sum_{a=1}^{N}\frac{w_a p_a}{2}e^{-p_a|\tau|}, \tag{229}$$

with weights $w_a>0$ and decay rates (inverse decay lengths) $p_a>0$. We then have

$$m(s)=\sum_{a=1}^{N}\frac{w_a p_a^2}{p_a^2-s^2},$$
$$\phi(s)=-s^2\sum_{a=1}^{N}\frac{w_a}{p_a^2-s^2}. \tag{230}$$

By comparing with Eq. (226), we obtain the normalization conditions $\Sigma_a w_a=1$, $\Sigma_a w_a/p_a^2=D$. Equation (227) can be evaluated by means of residue calculus. It loses its integral nature and becomes

$$\phi(s)g_H(s)=-\sum_{a=1}^{N}\frac{w_a p_a g_H(-p_a)}{2(p_a+s)}. \tag{231}$$

In order to solve Eq. (231), we first write the rational function $\phi(s)$ in factorized form,

$$\phi(s)=\frac{\Pi_{\alpha=1}^{N-1}(1-z_\alpha^2/s^2)}{\Pi_{a=1}^{N}(1-p_a^2/s^2)}. \tag{232}$$

The $(N-1)$ zeros of $[\phi(s)/s^2]$ in the variable s^2 have been denoted by z_α^2, with $\mathrm{Re}\, z_\alpha>0$, for $1\leqslant\alpha\leqslant N-1$. The normalization of Eq. (232) has been fixed by using $\phi(\infty)=1$.

An alternative expression for the diffusion constant D is derived by setting s equal to zero in Eq. (232) and comparing with Eqs. (226) and (230). We get

$$D=\frac{\Pi_{\alpha=1}^{N-1}z_\alpha^2}{\Pi_{a=1}^{N}p_a^2}. \tag{233}$$

The solution of Eq. (231) is of the form

$$\phi(s)g_H(s)=\frac{\mathcal{N}_0(s)}{\Pi_{a=1}^{N}(p_a+s)} \tag{234}$$

with $\mathcal{N}_0(s)$ a polynomial of degree $(N-1)$, which can be determined as follows. Consider the value $s=-z_\alpha$: we have $\phi(-z_\alpha)=0$, whereas $g_H(-z_\alpha)$ is finite. Equation (234) shows therefore that $s=-z_\alpha$ is a zero of the polynomial $\mathcal{N}_0(s)$. Since there are exactly $(N-1)$ such values, the solution Eq. (234) is determined up to a normalization, which can be fixed by using Eq. (228). We thus obtain

$$s^2g_H(s)=\frac{\Pi_{a=1}^{N}(1-s/p_a)}{\Pi_{\alpha=1}^{N-1}(1-s/z_\alpha)}. \tag{235}$$

This equation can be recast for $\mathrm{Re}\, s<0$ as

$$s^2g_H(s)=\exp\left\{\sum_{a=1}^{N}\ln(1-s/p_a)-\sum_{\alpha=1}^{N-1}\ln(1-s/z_\alpha)\right\}. \tag{236}$$

The sum over the poles and zeros of the function $[\phi(s)/s^2]$, with positive real parts, can be rewritten as the following complex integrals:

$$\begin{aligned}s^2g_H(s)&=\exp\left\{\int_{-i\infty}^{+i\infty}\frac{dz}{2\pi i}\left[\frac{\phi'(z)}{\phi(z)}-\frac{2}{z}\right]\ln(1-s/z)\right\}\\&=\exp\left\{-s\int_{-i\infty}^{+i\infty}\frac{dz}{2\pi iz(z-s)}\ln\left[-\frac{\phi(z)}{Dz^2}\right]\right\}.\end{aligned} \tag{237}$$

This result gives the solution of the problem for an arbitrary bulk Milne kernel.

The thickness τ_0 of the skin layer can be evaluated by comparing the results of Eqs. (235) and (237) with the expansion (228). We get

$$\begin{aligned}\tau_0&=\sum_{a=1}^{N}\frac{1}{p_a}-\sum_{\alpha=1}^{N-1}\frac{1}{z_\alpha}\\&=\int_{-i\infty}^{+i\infty}\frac{dz}{2\pi iz^2}\ln\left[-\frac{\phi(z)}{Dz^2}\right].\end{aligned} \tag{238}$$

The value for the case of point scattering is obtained by inserting into Eq. (238) the expression for $\phi(z)$ coming from Eq. (225). By making the change of variable $z=i\tan\beta$, we get

$$\begin{aligned}\tau_0&=\frac{1}{\pi}\int_0^{\pi/2}\frac{d\beta}{\sin^2\beta}\ln\frac{\tan^2\beta}{3(1-\beta\cot\beta)}\\&=0.710\,446\,090\ldots.\end{aligned} \tag{239}$$

We recover a well-known numerical value (Chandrasekhar, 1960; Van de Hulst, 1980; Van de Hulst and Stark, 1990).

B. The inhomogeneous Milne equation

The above method can be generalized to the inhomogeneous situation (Nieuwenhuizen and Luck, 1993). For point scattering one obtains the result

$$\tau_1(\mu)=\mu\sqrt{3}\,\exp\left\{-\frac{\mu}{\pi}\int_0^{\pi/2}d\beta\,\frac{\ln(1-\beta\cot\beta)}{\cos^2\beta+\mu^2\sin^2\beta}\right\}. \tag{240}$$

This quantity is maximal at normal incidence $(\mu=1)$, where it assumes the somewhat simpler form

$$\begin{aligned}\tau_1(1)&=\sqrt{3}\,\exp\left\{-\frac{1}{\pi}\int_0^{\pi/2}d\beta\,\ln(1-\beta\cot\beta)\right\}\\&=5.036\,475\,57\ldots.\end{aligned} \tag{241}$$

Finally, it is worth noticing that Eq. (236) also implies the following remarkably simple result:

$$\gamma(\mu_a,\mu_b)=\frac{\tau_1(\mu_a)\tau_1(\mu_b)}{3(\mu_a+\mu_b)}, \tag{242}$$

which is particular to the situation in which there are no internal reflections. In the presence of mismatch the functional form changes. See Eq. (286) for the limit of strong mismatch.

C. Enhanced backscatter cone

Exact results can also be derived for the backscatter cone in the absence of internal reflections. Consider, for the sake of simplicity, the enhanced backscatter of a normally incident beam $(\mu_a=1)$. The Q-dependent Milne equation (201) can be solved by means of the Laplace transformation.

In the case of point scattering, one gets for the backscatter amplitude (Gorodnichev, Dudarev, and Rogozkin, 1990)

$$\gamma_C(Q)=\frac{1}{2}\exp\left\{-\frac{2}{\pi}\int_0^{\pi/2}d\beta\ln\times\left(1-\frac{\arctan\sqrt{Q^2l^2+\tan^2\beta}}{\sqrt{Q^2l^2+\tan^2\beta}}\right)\right\}. \tag{243}$$

For small values of the reduced wave vector Q, the result Eq. (243) assumes the general form Eq. (221), cor-

responding to the triangular shape of the backscatter cone. The value for $Q=0$ reads

$$\gamma(1,1)=\frac{[\tau_1(1)]^2}{6}=4.227\,681\,04, \tag{244}$$

in agreement with Eq. (242). In agreement with Table I, one has $\Delta Q=1/2l$ [see Eq. (221)].

We end this section by mentioning the expression for the backscatter cone amplitude for isotropic scattering by point scatterers with an arbitrary albedo,

$$\gamma_C(a;Q)=\frac{a}{2}\exp\left\{-\frac{2}{\pi}\int_0^{\pi/2}d\beta \times\ln\left(1-a\,\frac{\arctan\sqrt{Q^2l^2+\tan^2\beta}}{\sqrt{Q^2l^2+\tan^2\beta}}\right)\right\}. \tag{245}$$

This result shows that, as soon as the scattering albedo a is smaller than unity the backscatter amplitude is an analytic function of Q^2, i.e., the cusp at $Q=0$ disappears. This confirms the physical intuition that the triangular shape of the cone is due to the existence of arbitrarily long diffusive paths. It is therefore a characteristic of the problem with unit albedo, i.e., with no absorption, in a half-space geometry. When the reduced wave vector Q and the strength of absorption $(1-a)$ are both small, we observe the following scaling behavior:

$$\gamma_C(a;Q)\approx\frac{\gamma_C(1;0)}{1+2\sqrt{Q^2l^2+3(1-a)}}. \tag{246}$$

The denominator of this expression is not reproduced quantitatively by the diffusion approximation [see, for example, Eq. (71) of Van der Mark, Van Albada, and Lagendijk (1988)], although it pertains to the long-distance physics of the problem. We also notice that the prefactor of the square root is nothing but the reciprocal of the value (222) of $l\Delta Q$. Indeed, Eq. (242) yields $\gamma_C(0)\equiv\gamma(1,1)=\tau(1)^2/6$, by which Eq. (222) reduces to $\Delta Q=1/(2l)$.

D. Exact solution for internal reflections in diffusive media

The solution for internal reflections, $m\neq1$, can be simply expressed in the solution without internal reflections, $m=1$. Let us look at $\Gamma_H^{(m)}$, the homogeneous solution for the situation with index ratio m. If we define

$$g_H(\mu)=\frac{R(\mu)}{2\mu}\int_0^\infty d\tau' e^{-\tau'/\mu}\Gamma_H^{(m)}(\tau'), \tag{247}$$

then we get from the homogeneous version of Eq. (152)

$$\Gamma_H^{(m)}(\tau)=M_B*\Gamma_H^{(m)}(\tau)+\int_0^1 d\mu\, g_H(\mu)e^{-\tau/\mu}. \tag{248}$$

We observe that comparison with Eq. (152) immediately gives the solution

$$\Gamma_H^{(m)}(\tau)=\Gamma_H^{(1)}(\tau)+\int_0^1 d\mu\, g_H(\mu)\Gamma_S^{(1)}(\tau;\mu). \tag{249}$$

Using the definition Eq. (247) we have to solve the inhomogeneous equation

$$g_H(\mu)=\frac{R(\mu)\tau_1^{(1)}(\mu)}{6\mu}+\frac{R(\mu)}{2\mu}\int_0^1 d\mu'\,\gamma^{(1)}(\mu,\mu')g_H(\mu'), \tag{250}$$

where we used the identities (Nieuwenhuizen and Luck, 1993)

$$\int_0^\infty d\tau\,\Gamma_H^{(1)}(\tau)e^{-\tau/\mu}=\frac{1}{3}\,\tau_1(\mu), \tag{251}$$

$$\gamma^{(m)}(\mu_b,\mu_a)=\int_0^\infty d\tau\,\Gamma_S^{(m)}(\tau,\mu_a)e^{-\tau/\mu_b}. \tag{252}$$

In a similar fashion we find for the special solution

$$\Gamma_S^{(m)}(\tau;\mu_a)=\Gamma_S^{(1)}(\tau;\mu_a)+\int_0^1 d\mu\, g_S(\mu,\phi,\mu_a)\Gamma_S^{(1)}(\tau;\mu) \tag{253}$$

with

$$g_S(\mu;\mu_a)=\frac{R(\mu)}{2\mu}\,\gamma^{(1)}(\mu;\mu_a)+\frac{R(\mu)}{2\mu}\times\int_0^1 d\mu'\,\gamma^{(1)}(\mu,\mu')g_S(\mu';\mu_a). \tag{254}$$

Following the same steps we obtain the enhanced backscatter intensity. We must solve

$$g(\mu,\phi;\mu_a,Q)=\frac{R(\mu)}{2\mu}\,\gamma^{(1)}\left(\frac{\mu}{1+iQl\sqrt{1-\mu^2}\cos\phi},\mu_a;Q\right)+\frac{R(\mu)}{2\mu}\int_0^1 d\mu'\int_{-\pi}^{\pi}\frac{d\phi'}{2\pi} \times\gamma^{(1)}\left(\frac{\mu}{1+iQl\sqrt{1-\mu^2}\cos\phi},\frac{\mu'}{1+iQl\sqrt{1-\mu'^2}\cos\phi'};Q\right)g(\mu',\phi';\mu_a,Q), \tag{255}$$

where (Luck, 1997)

$$\gamma^{(1)}(\mu_a,\mu_b,Q)=\frac{\tau_1^{(1)}(\mu_a,Q)\tau_1^{(1)}(\mu_b,Q)}{3(\mu_a+\mu_b)} \tag{256}$$

involves

$$\tau_1^{(1)}(\mu;Q)=\mu\sqrt{3}\,\exp\left\{-\frac{\mu}{\pi}\int_0^{\pi/2}\frac{d\beta}{\cos^2\beta+\mu^2\sin^2\beta}\times\ln\left(1-\frac{\arctan\sqrt{Q^2l^2+\tan^2\beta}}{\sqrt{Q^2l^2+\tan^2\beta}}\right)\right\}. \tag{257}$$

We find the following expressions for the dimensionless injection depth τ_0, the limit intensity τ_1, the differential reflection $dR/d\Omega$, and $B(Q)$, the intensity of the backscatter cone normalized to the diffuse background, at outgoing angle θ_b coded in $Q=kl(\theta_a-\theta_b)$:

$$\tau_0^{(m)}=\tau_0^{(1)}+\int_0^1 d\mu\, g_H(\mu)\tau_1^{(1)}(\mu), \tag{258}$$

$$\tau_1^{(m)}(\mu_a)=\tau_1^{(1)}(\mu_a)+\int_0^1 d\mu\, g_S(\mu;\mu_a)\tau_1^{(1)}(\mu), \tag{259}$$

$$\frac{dR}{d\Omega_b}(\theta_b;\theta_a)=\frac{\cos\theta_a}{4\pi m^2}\frac{T(\mu_a)T(\mu_b)}{\mu_a\mu_b}\gamma^{(m)}(\mu_a,\mu_b),$$

$$\gamma^{(m)}(\mu_a,\mu_b)=\gamma^{(1)}(\mu_a,\mu_b)+\int_0^1 d\mu\, g_S(\mu;\mu_a)\gamma^{(1)}(\mu,\mu_b), \tag{260}$$

$$B(\mu_a,Q)=\frac{1}{\gamma^{(m)}(\mu_a,\mu_a)}\left\{\gamma^{(1)}(\mu_a,\mu_a;Q)-\frac{\mu_a}{2}+\int_0^1 d\mu\int_{-\pi}^{\pi}\frac{d\phi}{2\pi}\times\gamma^{(1)}\left(\frac{\mu}{1+iQl\sqrt{1-\mu^2}\cos\phi},\mu_a;Q\right)\times g(\mu,\phi;\mu_a,Q)\right\}, \tag{261}$$

respectively. The subtracted term in $B(Q)$ comes from single scattering, which does not contribute to enhanced backscatter.

Equations (250), (254), and (255) can be solved numerically. In many cases only a few iterations are needed. For m close to unity the leading corrections for τ_0 and $\tau_1(\mu)$ are given by the first term in the equation for the g's.

Explicit results can be obtained in the limit of large index mismatch (Nieuwenhuizen and Luck, 1993). The point is that for $R(\mu)=1$ the integral kernel becomes $(1/2\mu)\gamma^{(1)}(\mu,\mu')$, which has a unit eigenvalue with right eigenfunction $g(\mu')=1$ and left eigenfunction $g(\mu)=2\mu$. For a large index mismatch this eigenvalue will bring the leading effects. The results will be discussed in the next section.

E. Exact solution for very anisotropic scattering

As discussed in Sec. III the main effect of anisotropic scattering is that the scattering mean free path $l=1/n\sigma$ is replaced by the transport mean free path $l_{\rm tr}=l/(1-\langle\cos\Theta\rangle)=l\tau_{\rm tr}$. As a result, the injection depth decomposes as $z_0=\tau_0 l_{\rm tr}$; likewise the opening angle of the backscatter cone is proportional to $1/l_{\rm tr}$.

For anisotropic scattering the transport equation cannot be solved exactly in general. Several special cases were discussed by Van de Hulst (1980). He found that in the absence of index mismatch the effects of anisotropy are typically not very large. Amic *et al.* (1996) showed that the limit of strongly forward scattering can be solved exactly. This extremely anisotropic case is expected to set bounds for more realistic anisotropic scattering kernels. The approach of Amic *et al.* (1996) goes along the lines of previous sections. However, certain constants occurring there are replaced by functions of an angle, which are only partly known. For details of the lengthy derivation we refer the reader to the original paper. The main results are presented in Table II, compared with the case of isotropic scattering.

We can compare the universal results in the very anisotropic scattering regime, for some of the quantities listed in Table II, with the outcomes of numerical approaches. Van de Hulst (1980) has investigated the dependence of various quantities on anisotropy for several commonly used phenomenological phase functions, including the Henyey-Greenstein phase function

$$p(\Theta)=\frac{1-g^2}{(1-2g\cos\Theta+g^2)^{3/2}}. \tag{262}$$

The data on the skin layer thickness show that, as a function of anisotropy, τ_0 varies from 0.7104 (isotropic scattering) to 0.7150 (moderate anisotropy), passing a minimum of 0.7092 (weak anisotropy); see Van de Hulst (1980). The trend shown by these data suggests that the universal value 0.718211 is actually an absolute upper bound for τ_0. Numerical data concerning $\tau_1(1)$ are also available. Van de Hulst (1997) has extrapolated two series of data concerning the Henyey-Greenstein phase function, which admit a common limit for very anisotropic scattering ($g\to 1$). This limit reads in our notation $\tau_1(1)/4=1.284\,645$, whereas Van de Hulst (1997) gives the two slightly different estimates 1.273 ± 0.002 and 1.274 ± 0.007. The agreement is satisfactory, although one cannot entirely exclude the possibility that the observed 0.8% relative difference is a small but genuine nonuniversality effect. Indeed, the Henyey-Greenstein phase function might belong to another universality class that is inappropriate for the approach of Amic *et al.* (1996). The same remark applies to a less complete set of data (Van de Hulst, 1997) concerning the intensity $\gamma(1,1)$ of reflected light at normal incidence.

In the presence of index mismatch the very anisotropic scattering limit can be solved exactly along the same lines as for isotropic scattering. The formalism becomes very cumbersome, however. In the limit of a large index mismatch the leading behaviors are expected to be

TABLE II. Anisotropic vs isotropic scattering. $\tau_0 l_{tr}$ is the thickness of a skin layer; $\tau_1(1)$ and $\gamma(1,1)$ yield the transmitted and reflected intensities, respectively, in the normal direction; $B(0)$ is the peak value of the enhancement factor at the top of the backscatterer cone; $\tau_{tr}\Delta Q = k_1 l_{tr}\Delta\theta$ is the dimensionless width of this backscatter cone. The third row gives the relative difference in the two cases.

	τ_0	$\tau_1(1)$	$\gamma(1,1)$	$B(0)$	$\tau_{tr}\Delta Q$
Isotropic ($\tau_{tr}=1$)	0.710 446	5.036 475	4.227 681	1.881 732	1/2
Very anisotropic ($\tau_{tr}\gg 1$)	0.718 211	5.138 580	4.889 703	2	0.555 543
Difference (%)	1.1	2.0	15.7	6.3	11.1

the same as for isotropic scattering. The reason is that a large mismatch implies that the radiation that has entered the scattering medium will often be reflected internally before it can exit the medium. Therefore it undergoes many scatterings, so it loses the nature (anisotropic or not) of the individual events. This was verified explicitly by Amic *et al.* (1996).

XI. LARGE INDEX MISMATCH

We have seen that the occurrence of internal reflections complicates the solution of the Schwarzschild-Milne equation. Yet in the limit of a large index mismatch the boundaries will act as good mirrors. They reinject the radiation so often that it is also diffusive close to the boundaries. It turns out that, to leading order, the radiative transfer problem is greatly simplified.

Following Nieuwenhuizen and Luck (1993) we consider the Schwarzschild-Milne equation in the regime of large index mismatch ($m\to 0$, or $m\to\infty$). In both cases the reflection coefficient $R(\mu)$ is close to unity and the effect of $T(\mu)=1-R(\mu)$ is small. We can thus expand in powers of T. We first consider the Green's function of the Schwarzschild-Milne equation, Eq. (178), and write the kernel as

$$M(\tau,\tau') = M_B(\tau-\tau') + M_L(\tau+\tau') \tag{263}$$

$$= M_B(\tau-\tau') + M_B(\tau+\tau') - N(\tau+\tau') \tag{264}$$

$$N(\tau+\tau') = \int_0^1 \frac{d\mu}{2\mu}\, e^{-(\tau+\tau')/\mu} T(\mu), \tag{265}$$

where N is of order $\int d\mu\, T(\mu) \ll 1$. This allows an expansion of Eq. (178) in powers of N. If $N=0$ (which happens for $m\to 0$ or $m\to\infty$), the kernel M has unit eigenvalue, and Eq. (178) has eigenfunction $G_S(\tau)=C_S=\text{const.}$, showing that for a medium with perfect mirrors the intensity inside is independent of the conditions outside. For small N the value of C_S will depend sensitively on N. Let us write the Green's function for $N\ll 1$ as

$$G_S(\tau,\tau') = C_S + G_0(\tau,\tau') + G_1(\tau,\tau'),$$

$$C_S \gg 1, \quad G_0 \approx 1, \quad G_1 \ll 1. \tag{266}$$

We insert this in Eq. (178):

$$C_S + G_0 + G_1 = \delta(\tau-\tau') + C_S + \int_0^\infty d\tau''\{M_B(\tau-\tau'') + M_B(\tau+\tau'')\}(G_0+G_1) - \int_0^\infty d\tau'' N(\tau+\tau'')(C_S+G_0+G_1). \tag{267}$$

Comparing terms of equal order yields

$$C_S = C_S, \tag{268}$$

$$G_0(\tau,\tau') = \delta(\tau-\tau') + \int_0^\infty d\tau''\{M_B(\tau-\tau'') + M_B(\tau+\tau'')\} \times G_0(\tau'',\tau') - C_S\int_0^\infty d\tau'' N(\tau+\tau''), \tag{269}$$

$$G_1(\tau,\tau') = \int_0^\infty d\tau''\{M_B(\tau-\tau'') + M_B(\tau+\tau'')\} \times G_1(\tau'',\tau') - \int_0^\infty d\tau'' N(\tau+\tau'') G_0(\tau'',\tau'), \tag{270}$$

where we have neglected terms of order $NG_1 \sim \mathcal{T}^2$. Integrating these results over τ yields an expression for C_S and a compatibility condition to ensure that G_0 has a unique solution:

$$C_S = \left\{ \int_0^\infty \int_0^\infty d\tau\, d\tau'' N(\tau+\tau'') \right\}^{-1}, \tag{271}$$

$$\int_0^\infty d\tau\, d\tau'' N(\tau+\tau'') G_0(\tau'',\tau') = 0 \quad \text{for all} \quad \tau'. \tag{272}$$

We can simplify the expression for C_S by introducing the angle-averaged flux-transmission coefficient $\mathcal{T}$:

$$C_S = \left\{ \int_0^\infty \int_0^\infty d\tau\, d\tau' \int_0^1 \frac{d\mu}{2\mu}\, e^{-(\tau+\tau')/\mu} T(\mu) \right\}^{-1} = 2\left\{ \int_0^1 \mu\, d\mu\, T(\mu) \right\}^{-1} \equiv \frac{4}{\mathcal{T}}, \tag{273}$$

where

$$\mathcal{T} \equiv 2\int_0^1 \mu\, d\mu\, T(\mu) = 2\int_0^{\pi/2} \cos\theta \sin\theta\, d\theta\, T(\cos\theta). \tag{274}$$

Note that $\mu=\cos\theta$ stands for the projection factor of flux in the z direction. The expression for $\mathcal{T}$ can be worked out explicitly using

$$T(\mu)=\frac{4\mu\sqrt{\mu^2-1+m^{-2}}}{(\mu+\sqrt{\mu^2-1+m^{-2}})^2}. \tag{275}$$

For $m<1$ we introduce $\epsilon^2=m^{-2}-1$,

$$\mathcal{T}=2\int_0^1 \mu\, d\mu\, \frac{4\mu\sqrt{\mu^2+\epsilon^2}}{(\mu+\sqrt{\mu^2+\epsilon^2})^2}. \tag{276}$$

When we substitute $\phi=\sinh^{-1}(\mu/\epsilon)$ this becomes

$$\mathcal{T}=8\epsilon^2\int_0^{\phi_+} d\phi\, \frac{\sinh^2\phi\,\cosh^2\phi}{e^{2\phi}} \tag{277}$$

$$=2\epsilon^2\int_0^{\phi_+} d\phi\, \sinh^2 2\phi e^{-2\phi}$$

$$=\frac{\epsilon^2}{2}\int_0^{\phi_+} d\phi[e^{2\phi}-2e^{-2\phi}+e^{-6\phi}] \tag{278}$$

$$=\frac{\epsilon^2}{2}\left\{\frac{e^{2\phi_+}}{2}+e^{-2\phi_+}-\frac{e^{-6\phi_+}}{6}-\frac{4}{3}\right\}. \tag{279}$$

Using

$$\sinh\phi_+=\frac{1}{\epsilon}=\frac{m}{\sqrt{1-m^2}},\quad \cosh\phi_+=\frac{1}{\sqrt{1-m^2}}, \tag{280}$$

we find $\exp(2\phi_+)=(1+m)/(1-m)$. This yields

$$\mathcal{T}=\frac{4m(m+2)}{3(m+1)^2}\quad (m\leqslant 1). \tag{281}$$

The leading behavior for $m\to 0$ could have been found more quickly by taking the leading behavior of the numerator and denominator of Eq. (276),

$$\mathcal{T}\approx 2\int_0^1 \mu\, d\mu\, \frac{4\mu\epsilon}{\epsilon^2}=\frac{8}{3}m\quad (m\to 0). \tag{282}$$

Now we do the same for $m>1$. We must not forget the Brewster angle: for $\mu<\sqrt{1-m^{-2}}$ there occurs total reflection. We now introduce $\epsilon^2=1-m^{-2}$ and carry out the integration from ϵ to 1:

$$\mathcal{T}=8\int_\epsilon^1 \mu^2 d\mu\, \frac{\sqrt{\mu^2-\epsilon^2}}{(\mu+\sqrt{\mu^2-\epsilon^2})^2} \tag{283}$$

$$=\frac{4(2m+1)}{3m^2(1+m)^2}\quad (m\geqslant 1). \tag{284}$$

The leading behavior for large m could again have been found by keeping leading terms:

$$\mathcal{T}\approx\frac{8}{3m^3}\quad (m\to\infty). \tag{285}$$

Further we notice that $\mathcal{T}=1$ for $m=1$, as it should be.

A. Diffuse reflected intensity

We can now derive simply the leading behavior of the generalized bistatic coefficient:

$$\gamma(\mu_a,\mu_b)=\int_0^\infty d\tau\, d\tau'\, G_S(\tau,\tau')e^{-\tau/\mu_b}e^{-\tau'/\mu_a} \tag{286}$$

$$=\int_0^\infty d\tau\, d\tau'\, C_S e^{-\tau/\mu_b}e^{-\tau'/\mu_a}+\mathcal{O}(\mathcal{T}^0) \tag{287}$$

$$=\frac{4\mu_a\mu_b}{\mathcal{T}}+\mathcal{O}(\mathcal{T}^0). \tag{288}$$

We can use this to find an approximation for the reflected intensity $A^R(\theta_a,\theta_b)$ in the case $m\gg 1$,

$$A^R=\frac{\cos\theta_a}{4\pi m^2}\frac{T_aT_b}{\mu_a\mu_b}\,\gamma(\mu_a,\mu_b). \tag{289}$$

When $m\gg 1$, $T(\mu)\approx 4\mu/m$ (since θ cannot exceed the Brewster angle, which is small at large m), implying

$$A^R=\frac{\cos\theta_a}{4\pi m^2}\frac{4\cos\theta_a}{m}\frac{4\cos\theta_b}{m}\frac{4}{\mathcal{T}}$$

$$\approx\frac{6}{\pi m}\cos^2\theta_a\cos\theta_b. \tag{290}$$

B. Limit intensity and injection depth

The limit intensity $\tau_1(\mu)$ of a semi-infinite space can also be calculated. From Eq. (182) it follows that

$$\tau_1(\mu)=\int_0^\infty d\tau'\, G_S(\infty,\tau')e^{-\tau'/\mu} \tag{291}$$

$$=\frac{1}{D}\int_0^\infty d\tau'\,\Gamma_H(\tau')e^{-\tau'/\mu} \tag{292}$$

$$=\lim_{\mu_b\to\infty}\frac{\gamma(\mu,\mu_b)}{\mu_b} \tag{293}$$

$$=\frac{4\mu}{\mathcal{T}}. \tag{294}$$

The injection depth $z_0=\tau_0 l$ can also be calculated. If we take the (diffusion) approximation $\Gamma_H=\tau_0+\tau\approx\tau_0$ and insert it in the above equality we find

$$\tau_1(\mu)=\frac{\tau_0}{D}\,\mu=\frac{4\mu}{\mathcal{T}}, \tag{295}$$

$$\tau_0\approx\frac{4}{3\mathcal{T}}. \tag{296}$$

Just as in the calculation of G_S we can write the homogeneous solution Γ_H as the sum of three parts:

$$\Gamma_H(\tau)=\frac{4}{3\mathcal{T}}+\Gamma_0(\tau)+\Gamma_1(\tau), \tag{297}$$

$$\Gamma_0(\tau)=\mathcal{O}(1),\quad \Gamma_1(\tau)=\mathcal{O}(\mathcal{T}). \tag{298}$$

We further require that Γ_0 behave as $\tau+\tau_{00}$ for $\tau\to\infty$. The constant τ_{00} is a $\mathcal{O}(1)$ correction to τ_0. For $m\to\infty$ we can use definition Eq. (265) and $\mu\approx 1$, since the Brewster angle is small:

$$N(\tau+\tau')=\int_0^1 \frac{d\mu}{2\mu}\, e^{-(\tau+\tau'')/\mu} T(\mu) \approx \frac{\mathcal{T}}{4}\, e^{-(\tau+\tau')}. \tag{299}$$

Inserting this in the equation for Γ_H and comparing terms up to order $\mathcal{T}^2$, we obtain

$$\Gamma_0 = -e^{-\tau} + \int_0^\infty d\tau' [M_B(\tau-\tau') + M_B(\tau+\tau')]\Gamma_0, \tag{300}$$

while the equation for Γ_1 yields the compatibility relation

$$\int_0^\infty d\tau\, e^{-\tau} \Gamma_0(\tau) = 0. \tag{301}$$

These equations cannot be solved analytically. Numerical analysis yields $\tau_{00} = -1.0357$ (Nieuwenhuizen and Luck, 1993), implying

$$\tau_0^{\text{exact}} = \frac{4}{3\mathcal{T}} - 1.0357 + \mathcal{O}(\mathcal{T}) \quad (m \to \infty). \tag{302}$$

In the limit $m \to 0$ the transmission coefficient is uniformly small, $T(\mu) \approx 3\mathcal{T}\mu/2$. Therefore the term of Eq. (178) arising from the kernel N, defined in Eq. (265), becomes equal to

$$-\frac{3}{2}\,\mathcal{T}\int_0^\infty d\tau'' \int_0^1 \frac{d\mu}{2\mu}\, e^{-(\tau+\tau'')/\mu}\mu\, \frac{4}{\mathcal{T}} = -3\int_0^1 \mu\, d\mu\, e^{-\tau/\mu} \int_0^1 d\mu'\, \mu' \int_0^\infty d\tau\, e^{-\tau/\mu'} J_0(\tau,\mu')$$
$$= 0 \Rightarrow \int_0^1 d\mu\, \mu \int_0^\infty d\tau\, e^{-\tau/\mu} \Gamma_0(\tau). \tag{303}$$

The diffusive shape $\tau+\tau_{00}$ is the exact solution of this equation, with $\tau_{00} = -3/4$. This leads to

$$\tau_0^{\text{exact}} = \frac{4}{3\mathcal{T}} - \frac{3}{4} + \mathcal{O}(\mathcal{T}) \quad (m \to 0). \tag{304}$$

In Fig. 11 numerical values of $\tau_1(1)$, $\gamma(1,1)$, and $3\tau_0$ have been plotted as a function of m. The solid line is $4/\mathcal{T}$, while the dashed line is Eqs. (302)+(304). Notice that these asymptotic expressions work quite well up to $m=1$.

C. Comparison with the improved diffusion approximation

We can compare the exact results for τ_0 with the improved diffusion approximation of Sec. III C. For $m \to \infty$ we can approximate C_1 and C_2 [see Eq. (68)] as

$$C_1 = \frac{1}{3}(1-\mathcal{T}), \quad C_2 \approx \frac{1}{3} - \int_0^1 \mu\, d\mu\, T(\mu) = \frac{1}{3} - \frac{1}{2}\,\mathcal{T}. \tag{305}$$

From Eq. (69) it follows that

$$\tau_0^{\text{diff}} \approx \frac{4}{3\mathcal{T}} - 1, \tag{306}$$

which is very close to the exact value in Eq. (302). Notice that the same result follows when one inserts the diffusion approximation $\Gamma_0(\tau) = \tau + \tau_{00}$ (for all τ) in Eq. (301).

For $m \to 0$, deviations from the diffusion approximation show up only to second order in $\mathcal{T}$,

$$\tau_0^{\text{diff}} = \tau_0^{\text{exact}} = \frac{4}{3\mathcal{T}} - \frac{3}{4} + \mathcal{O}(\mathcal{T}) \quad (m \to 0). \tag{307}$$

To find correction terms in powers of $\mathcal{T}$ is essentially as complicated as solving the Milne equation at finite m. For $m=1$ (no internal reflections), the exact value is known: $\tau_0^{\text{exact}} = 0.710\,44$. This can be compared with the result for the diffusion approximation found in Sec. III.C,

$$\tau_0^{\text{exact}} = 0.710\,44, \tag{308}$$

$$\tau_0^{\text{diff}} = \frac{2}{3} = 0.666\,666. \tag{309}$$

D. Backscatter cone

We now determine the shape of the backscatter cone in the presence of strong internal reflections, in the regime $m \gg 1$. We have to solve

$$\Gamma_C(Q,\tau) = e^{-\tau} + \int_0^\infty d\tau' [M_B(Q,\tau-\tau') + M_B(Q,\tau+\tau')]\Gamma_C(Q,\tau') - \int_0^\infty d\tau' N(Q,\tau+\tau')\Gamma_C(Q,\tau'). \tag{310}$$

For small Q the solution will have the form

$$\Gamma_C(Q,\tau) \approx \gamma_C(Q) e^{-Q\tau}. \tag{311}$$

Integrating Eq. (310) over τ, using for the bulk kernel M_B an eigenvalue $1 - \frac{1}{3}Q^2$, and neglecting the Q dependence of N, we find

$$0=1+\int_0^\infty d\tau\, d\tau' [M_B(Q,\tau-\tau')-M_B(0,\tau-\tau')+M_B(Q,\tau+\tau')-M_B(0,\tau+\tau')]\gamma_C(Q)e^{-Q\tau'} \tag{312}$$

$$-\int_0^\infty d\tau\, d\tau' N(0,\tau+\tau')\gamma_C(Q)e^{-Q\tau} \tag{313}$$

$$=1+\int_0^\infty d\tau[-1+1-\tfrac{1}{3}Q^2]\gamma_C(Q)e^{-Q\tau}-\frac{\mathcal{T}}{4}\gamma_C(Q), \tag{314}$$

yielding

$$\gamma_C(Q)=\frac{4}{\mathcal{T}+\frac{4}{3}Q}=\frac{4}{\mathcal{T}}\frac{1}{1+Q\tau_0}=\frac{3}{Q+1/\tau_0}. \tag{315}$$

In passing, we have recovered the triangular shape of the backscatter cone.

Recently the width of the backscatter cone has been determined experimentally (Den Outer and Lagendijk, 1993). The index ratio m was varied using several types of glass containers. The measurements were compared with the theories of Lagendijk *et al.* (1989), of Zhu *et al.* (1991), and of Nieuwenhuizen and Luck (1993). The first two results have already been discussed in Sec. III.C. The experiments confirmed the theories of Zhu *et al.* (1991) and of Nieuwenhuizen and Luck (1993).

At first sight it may look strange that an experiment with light (vector waves) can be described by a scalar theory. Nieuwenhuizen and Luck (1993) pointed out, however, that for large m only diffusive aspects survive. More subtle properties, such as anisotropic scattering and the vector character lead to subdominant effects. The latter was verified explicitly by Amic *et al.* (1997), indicating why the experiments of den Outer and Lagendijk (1993) are described so well by scalar theories.

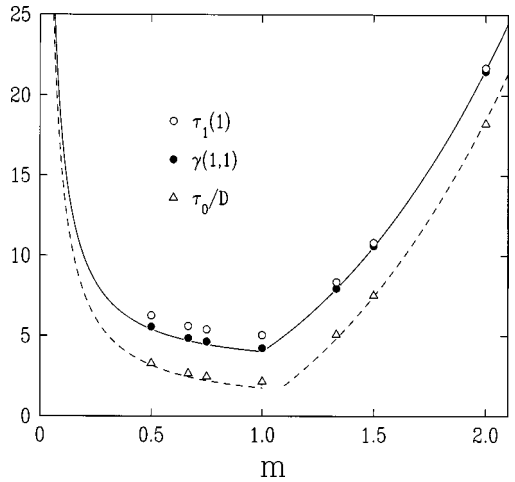

FIG. 11. Comparison of exact values and diffusion approximation for $\tau_1(1)$, $\gamma(1,1)$, and $3\tau_0$: solid line, $4/\mathcal{T}$; dashed line, Eqs. (302)+(304). Even for m close to unity the asymptotic results are quite good.

XII. SEMIBALLISTIC TRANSPORT

Wave propagation through waveguides, quantum wires, films, and double-barrier structures with a modest amount of disorder can be considered within the same approach. The so-called semiballistic regime occurs when in the transverse direction(s) there is almost no scattering, while in the long direction(s) there is so much scattering that the transport is diffusive. Various applications were noted by Nieuwenhuizen (1993) and discussed in detail by Mosk, Nieuwenhuizen, and Barnes (1996). The scattering was considered both in the second-order Born approximation and beyond that approximation. In the latter case it was found that attractive point scatterers in a cavity always have geometric resonances, even for Schrödinger wave scattering.

In the limit of long samples, the transport equation has been solved analytically including geometries such as waveguides, films, and tunneling geometries (for example, Fabry-Pérot interferometers and double-barrier quantum wells). The agreement with numerical data and with experiments is quite satisfactory. In particular, the analysis proved that the large, gate-voltage-independent resonance width of GaAs double-barrier systems, observed by Guéret, Rossel, Marclay, and Meier (1989) can be traced back to scattering from the intrinsically rough GaAs-AlGaAs interfaces.

In the analysis of these systems, the Schwarzschild-Milne equation is decomposed on the cavity modes, thus becoming an evolution equation in the z direction for a matrix. The very same ideas as explained above are used in the solution. Due to the complication of the formalism we shall not present details here. We refer the reader to the original works and the references therein.

XIII. IMAGING OF OBJECTS IMMERSED IN OPAQUE MEDIA

A field of much current interest is the imaging of objects immersed in diffuse media for the purpose of medical imaging. The advantage of imaging with diffuse light is that it is noninvasive and, in contrast to conventional x-ray tomography, it does not cause radiation damage. One application is the detection of breast cancer, another the location of brain regions damaged by stroke (a lot of blood, hence more absorption) or affected by Parkinson's disease (less-than-average blood level, hence greater transparency). In these cases one can shine light

at many locations, and measure the scattered light at many exit points. This information can in principle be used to determine the structure of the scattering medium and to detect possibly abnormal behavior. It is therefore important to know the scattering properties of idealized objects hidden in opaque media. We shall discuss here some instructive cases.

For light waves human tissue is a multiple-scattering medium like those discussed so far, yet the absorption length is short, typically a few tenths of a millimeter. The diffuse transmission through tissue must already have been noticed by our ancestors when they held their hands in front of a candle. On distances much larger than the mean free path, light transport is diffusive and is therefore governed by the Laplace equation. This observation facilitates an analogy with electrostatics: an object deep inside an opaque medium is analogous to a charge configuration at large distance. It is well known that the latter can be expressed in terms of its charge and dipole moment, while higher multipole moments are often negligible. A similar situation occurs in an opaque medium: small objects far from the surface can be described adequately by their charge (which vanishes if there is no absorption) and their dipole moment (which describes to leading order scattering from the object). At large distances the effect of, for instance, a charge will depend on the geometry of the system. As in electrostatics, mirror charges and mirror dipoles can be used in simple geometries. However, solving the boundary problem of complicated geometries like a human head is a hard problem. Close to the object, say, within a few mean free paths, the full radiative transfer is needed, making the problem more complicated than diffusion theory.

Den Outer, Nieuwenhuizen, and Lagendijk (1993) studied the diffuse image of an object embedded in a homogeneous turbid medium and found that it is well described by the diffusion approximation. This framework leads to a prediction of the diffuse image of the object, i.e., the profile of diffuse intensity transmitted through a thick slab near the embedded object. The shapes of the predicted profiles are universal, since they depend only on large distance properties of the problem, and were convincingly observed experimentally for the case of a pencil (absorbing cylinder) and a glass fiber (transparent cylinder). Further results on imaging of objects within the framework of the diffusion approximation can be found in Schotland, Haselgrove, and Leigh (1993), Feng, Zeng, and Chance (1995), Zhu, Wei, Feng, and Chance (1996), and Paasschens and 't Hooft (1998).

A. Spheres

In the diffusion approximation the problem is straightforward. Close to the object (though still many mean free paths away) the intensity can be written as

$$I(\mathbf{r}) = I_0(\mathbf{r}) + \delta I(\mathbf{r}), \tag{316}$$

where $I_0(\mathbf{r})$ is the intensity profile in the absence of the object. Luck and Nieuwenhuizen (1998) have introduced the following notation for the disturbance of the intensity:

$$\delta I(\mathbf{r}) = (q + \mathbf{p}\cdot\nabla)\,\frac{1}{|\mathbf{r}-\mathbf{r}_0|} = \frac{q}{|\mathbf{r}-\mathbf{r}_0|} - \mathbf{p}\cdot\frac{\mathbf{r}-\mathbf{r}_0}{|\mathbf{r}-\mathbf{r}_0|^3}. \tag{317}$$

Here q is called the "charge" and $\mathbf{p}$ the "dipole moment" of the object. The linearity of the problem and the isotropy of the spherical defect imply that the charge q is proportional to the local intensity $I_0(\mathbf{r}_0)$ in the absence of the object, while the dipole moment $\mathbf{p}$ is proportional to its gradient. We therefore set

$$q = -QI_0(\mathbf{r}_0), \quad \mathbf{p} = -P\nabla I_0(\mathbf{r}_0), \tag{318}$$

where Q is called the capacitance of the spherical object, and P its polarizability. These two parameters are intrinsic characteristics of the object. The capacitance Q is nonzero (and positive) only if the sphere is absorbing.

For plane-wave incidence on a slab geometry one has the familiar expression $I_0(\mathbf{r}) = (L-z)I_0/L$. A double set of mirror charges is needed to make $I-(L-z)I_0/L$ vanish at $z=0$ and $z=L$ for all ρ:

$$I = \frac{L-z}{L}I_0 + q\sum_{n=-\infty}^{\infty}\left\{\frac{1}{[(z-z_0+2nL)^2+(\rho-\rho_0)^2]^{1/2}} - \frac{1}{[(z+z_0+2nL)^2+(\rho-\rho_0)^2]^{1/2}}\right\} \tag{319}$$

$$-p\sum_{n=-\infty}^{\infty}\left\{\frac{z-z_0+2nL}{[(z-z_0+2nL)^2+(\rho-\rho_0)^2]^{3/2}} + \frac{z+z_0+2nL}{[(z+z_0+2nL)^2+(\rho-\rho_0)^2]^{3/2}}\right\}. \tag{320}$$

The intensity $T(x,y)$ transmitted through the sample and emitted on the right side ($z=L$), at the point $\rho=(x,y)$, is proportional to the normal derivative of the diffuse intensity at that point:

$$T(x,y) = -Kl\left.\frac{\partial I(x,y,z)}{\partial z}\right|_{z=L}. \tag{321}$$

When there is no embedded object, the transmission is uniform $T_0 = KI_0 l/L$. In the presence of an object one finds

$$T(\rho)=T_0\left(1-2Q(L-z_0)\sum_{n=-\infty}^{+\infty}\frac{L-z_0+2nL}{[(L-z_0+2nL)^2+(\rho-\rho_0)^2]^{3/2}}-2P\sum_{n=-\infty}^{+\infty}\frac{2(L-z_0+2nL)^2-(\rho-\rho_0)^2}{[(L-z_0+2nL)^2+(\rho-\rho_0)^2]^{5/2}}\right). \tag{322}$$

The information on the type of scatterer is coded in its capacitance Q and polarizability P. In experiments on pencils and fibers, $2-d$ analogs of these profiles have been clearly observed (Den Outer *et al.*, 1993). In the same fashion the reflected intensity can be estimated by taking the derivative in Eq. (321) at $z=0$. The rest of this section is devoted to determining Q and P in idealized situations. This amounts to solving the scattering problem with the radiative transfer equation in the presence of an object placed at $\mathbf{r}_0$.

For large objects the diffusion theory can be used, which simplifies the problem. Following Den Outer *et al.* (1993) we consider a macroscopic object of radius R, having diffusion coefficient D_2 and inverse absorption length κ, while the medium is nonabsorbing and has diffusion coefficient D_1. At the boundary of the object one has

$$I_{\rm out}(R^+)=I_{\rm in}(R^-), \tag{323}$$

$$D_1\left.\frac{\partial I_{\rm out}}{\partial n}\right|_{R^+}=D_2\left.\frac{\partial I_{\rm in}}{\partial n}\right|_{R^-}. \tag{324}$$

Near the object one has

$$I_{\rm in}=A\ \mathrm{sinhc}(\kappa r)-\frac{3B}{\kappa^2 r}\left[\mathrm{sinhc}(\kappa r)-\cosh(\kappa r)\right]\frac{z-z_0}{r}, \tag{325}$$

where $\mathrm{sinhc}(x)\equiv\sinh(x)/x$. Matching the solutions gives

$$Q=R\,\frac{D_2(\cosh\,\kappa R-\mathrm{sinhc}\,\kappa R)}{D_1\,\mathrm{sinhc}\,\kappa R+D_2(\cosh\,\kappa R-\mathrm{sinhc}\,\kappa R)}. \tag{326}$$

For a totally absorbing sphere ($\kappa\to\infty$) the result $Q=R$ follows immediately by requiring in Eq. (316) that $I(R)=0$. The polarizability reads

$$P=R^3\,\frac{D_1(\mathrm{sinhc}\,\kappa R-\cosh\,\kappa R)-D_2(2\cosh\,\kappa R-2\,\mathrm{sinhc}\,\kappa R-\kappa R\,\sinh\,\kappa R)}{2D_1(\mathrm{sinhc}\,\kappa R-\cosh\,\kappa R)+D_2(2\cosh\,\kappa R-2\mathrm{sinhc}\,\kappa R-\kappa R\,\sinh\,\kappa R)}. \tag{327}$$

In the absence of absorption this reduces to

$$Q=0,\quad P=R^3\,\frac{D_1-D_2}{2D_1+D_2}. \tag{328}$$

Lancaster and Nieuwenhuizen (1998) consider the limit of small objects: a point scatterer with scattering cross section $\sigma_{\rm sc}$ extinction cross section $\sigma_{\rm ex}$ and albedo $a_e=\sigma_{\rm sc}/\sigma_{\rm ex}$. If diffuse intensity hits the scatterer once, but does not return to it, Q and P read

$$Q_1=\frac{3}{4\pi}\,\frac{\sigma_{\rm abs}}{l},\quad P_1=\frac{1}{4\pi}\,\sigma_{\rm ex}l, \tag{329}$$

where $\sigma_{\rm abs}=\sigma_{\rm ex}-\sigma_{\rm sc}$. The intensity can also return an arbitrary number of times to the scatterer. For point scatterers this boils down to a geometric series expansion for Q and P,

$$Q=\frac{Q_1}{1+Q_1B_1},\quad P=\frac{P_1}{1+P_1B_2}, \tag{330}$$

where B_1 and B_2 are integrals describing the propagation of the diffuse intensity through the medium and the effect of hitting the scatterer another time. These integrals are actually divergent in the limit $kl\to\infty$, which introduces extra internal parameters of the point scatterer.

In contrast to extended objects, for point scatterers the maximally crossed diagrams also contribute. The reason is that the exit and return points coincide, so there is no dephasing. The analysis finally yields

$$Q=\frac{Q_1}{1+Q_1(2B_1-B_1^{(1)})},$$

$$P=\frac{P_1}{1+P_1(2B_2-B_2^{(1)})}, \tag{331}$$

which retains the structure of Eq. (330). Note that there is an additional factor 2, except for the diagrams with one intermediate common scatterer, an effect that is accounted for by subtracting $B_{1,2}^{(1)}$. This is very similar to the fact that the single-scatterer diagram does not contribute to the enhanced backscatter cone; see Eq. (209). Lancaster and Nieuwenhuizen (1998) also considered more realistic situations in an approach involving a partial-wave expansion.

For extended objects it is a highly nontrivial task to go beyond the diffusion approximation. Luck and Nieuwenhuizen (1998) considered the application of the radiative transfer equation to such cases, for which one has to solve the analog of the scattering problem of quantum mechanics. This is generally a hard and still unsolved problem. However, there are three cases in

TABLE III. Capacitance Q and polarizability P of small and large spheres and cylinders immersed in an opaque medium. In column for large radius the diffusion approximation is given by the term outside the brackets. For narrow and wide cylinders the effective radius and the polarizability are presented.

Object	Small-radius behavior ($R \ll l$)	Large-radius behavior ($R \gg l$)
Absorbing sphere	$Q \approx \frac{3R^2}{4l}$	$Q \approx R\left(1-\frac{\tau_0 l}{R}\right)$, $\tau_0 \approx 0.710\,446$
Transparent sphere	$P \approx -\frac{R^3}{3}\left(1+\frac{3R}{4l}\right)$	$P \approx -R^3\left(1-\frac{3\tau_{01}l}{R}\right)$, $\tau_{01} \approx 0.4675$
Reflecting sphere	$P \approx \frac{R^2 l}{4}$	$P \approx \frac{R^3}{2}\left(1+\frac{6l^2}{5R^2}\right)$
Absorbing cylinder	$R_{\text{eff}} \approx al\left(\frac{R}{l}\right)^{16/3\pi^2} e^{-4l/3R}$, $a \approx 1.20$	$R_{\text{eff}} \approx R\left(1-\frac{\tau_0 l}{R}\right)$, $\tau_0 \approx 0.710\,446$
Transparent cylinder	$P \approx -\frac{R^2}{2}\left(1+\frac{R}{l}\right)$	$P \approx -R^2\left(1-\frac{2\tau_{01}l}{R}\right)$, $\tau_{01} \approx 0.2137$
Reflecting cylinder	$P \approx \frac{3Rl}{8}$	$P \approx R^2\left(1+\frac{4l^2}{5R^2}\right)$

which the inside of the scatterer plays a trivial role: a totally absorbing (black) object (having $\kappa=\infty$), a transparent, nonabsorbing object (having $\kappa=0$, $D_2=\infty$), and a totally reflecting, nonabsorbing object (having $\kappa=D_2=0$). For spheres and cylinders of these types, the scattering problem can be reduced to an integral equation in one variable, which is solved exactly in the limits of small and large objects. In the latter case the results of diffusion theory are recovered, and the first-order corrections to diffusion theory are found; see Table III and Figs. 12 and 13. The same approach can be extended, in principle, to more general cases.

B. Cylinders

The use of the radiative transfer approach can be extended to other objects (Luck and Nieuwenhuizen, 1998). Consider a cylinder with radius R with its axis parallel to the x axis. Assume the sample is infinitely long in the x direction, so that both $I_0(\mathbf{r})$ and the disturbance $\delta I(\mathbf{r})$ depend only on the two-dimensional perpendicular component $\mathbf{r}_\perp=(y,z)$. Equation (317) is replaced by

$$\delta I(\mathbf{r}_\perp)=(q+\mathbf{p}\cdot\nabla)\ln\frac{\tilde{R}}{|\mathbf{r}-\mathbf{r}_0|}=q\,\ln\frac{\tilde{R}}{|\mathbf{r}-\mathbf{r}_0|}-\frac{\mathbf{p}\cdot(\mathbf{r}_\perp-\mathbf{r}_{0\perp})}{|\mathbf{r}-\mathbf{r}_0|^2}. \tag{332}$$

The length scale $\tilde{R}$, called for by dimensional analysis, is determined by conditions at the boundaries of the sample, so that it is in general proportional to the sample size. This sensitivity of $\delta I(\mathbf{r})$ to global properties of the sample arises because the logarithmic potential of a point charge in two-dimensional electrostatics is divergent at long distances. As a consequence, the capacitance Q is not intrinsic to the cylinder. An intrinsic quantity is its *effective radius* R_{eff}, defined by the condition that the cylindrically symmetric part of the total intensity, including the charge term, vanish at a distance $r=R_{\text{eff}}$ from the axis of the cylinder. We thus have $I_0(\mathbf{r}_0)+q\,\ln(\tilde{R}/R_{\text{eff}})=0$, hence, with $q=-I(\mathbf{r}_0)Q$,

$$Q=\frac{1}{\ln(\tilde{R}/R_{\text{eff}})}. \tag{333}$$

We observe that R_{eff} and $\tilde{R}$ have the dimension of a length, while the polarizability P has the dimension of an area. As a consequence, the orders of magnitude $R_{\text{eff}}\sim R$ and $P\sim R^2$ can be expected for a cylinder of radius R. For the same physical situations as above, more accurate predictions can be found in Table III. For a cylinder in a slab geometry the transmitted intensity $T(y)$ finally reads in terms of Q and P

$$T(y)=T_0\left[1-Q\pi\left(1-\frac{z_0}{L}\right)\frac{\sin(\pi z_0/L)}{\cos(\pi z_0/L)+\cosh(\pi y/L)}-P\,\frac{\pi^2}{L^2}\frac{1+\cos(\pi z_0/L)\cosh(\pi y/L)}{[\cos(\pi z_0/L)+\cosh(\pi y/L)]^2}\right], \tag{334}$$

where

$$\tilde{R}=\frac{2L}{\pi}\sin\frac{\pi z_0}{L} \tag{335}$$

is indeed of order L, but also depends nontrivially on the aspect ratio z_0/L. These shapes have been observed in the experiments of Den Outer *et al.* (1993).

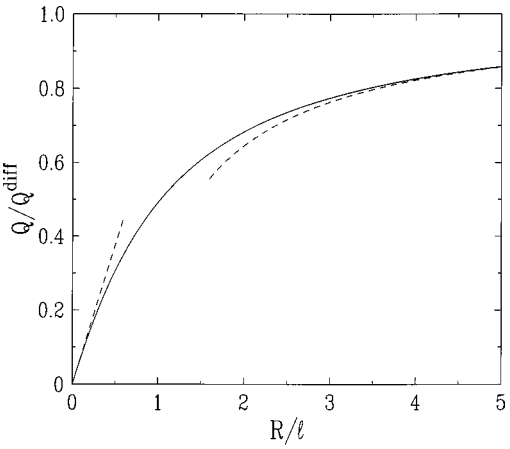

FIG. 12. Plot of the size factor $Q/Q_{\rm diff}$ of the capacitance of an absorbing sphere vs the ratio R/l; solid line, outcome of the numerical analysis; dashed lines, small-radius and large-radius behaviors of Table III.

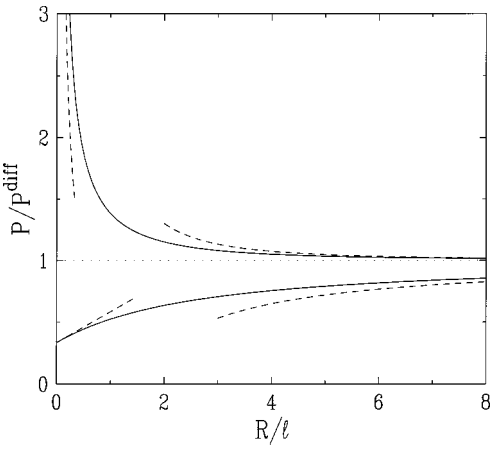

FIG. 13. Plot of the size factor $P/P^{\rm diff}$ of the polarizability of a transparent sphere (lower curves) and a reflecting sphere (upper curves): Solid lines, outcome of the numerical analysis; dashed lines, small-radius and large-radius behaviors of Table III.

XIV. INTERFERENCE OF DIFFUSIONS: HIKAMI VERTICES

So far our discussion has focused on the intensity aspects of wave transport. We now consider interference effects, which are due to the inherent wave nature of the problem. First we have to introduce the concept of interference vertices. These vertices describe the interaction between diffusions. The vertices are named after Hikami, who used them in 1981 (Hikami, 1981) for the calculation of weak-localization corrections to the conductance. Their original introduction dates back two years earlier to the work of Gor'kov, Larkin, and Khmel'nitskii (1979). Remember that each diffusion consists of two amplitudes. The vertices describe the exchange of amplitudes between diffusions, which leads to correlations between the diffusions. It is also possible to represent these processes using the standard impurity diagram technique, as described for instance by Abrikosov, Gor'kov, and Dzyaloshinski (1963), but the interference vertices prove to be more convenient.

A. Calculation of the Hikami four-point vertex

We start with the simplest vertex: the four-point vertex, in which two diffusions interchange an amplitude. The technique for calculating the vertex by means of diagrams is well known (Abrikosov *et al.*, 1963): First, draw the diagrams; second, write down a momentum for each line and use momentum conservation at each vertex; and finally, integrate over the free momenta. The first step, writing down all leading diagrams, requires some care. In Fig. 14 we have drawn the diagrams in the Hikami box to second-order Born approximation. It is important to include *all* leading diagrams, as there will be a cancellation of leading terms. These cancellations are imposed by energy conservation. In the second-order Born approximation one neglects scattering more than twice from the same scatterer; the (dashed) interaction line indicates that the propagators scatter once on the same scatterer. Scattering processes involving just one propagator have already been included, as the propagators are dressed. We have not drawn all diagrams, as one can imagine. First, the box is attached to a diffusion ending with a scatterer (which is consistent with the way we have defined the diffusions). As a result, common scatterings between propagators on the same leg are not allowed in the vertex because they are already included. Second diagrams with two or more scatterers and parallel dashed lines are subleading. They contain loops with two propagators of the *same* type, i.e., integrals like $\int d^3\mathbf{p}G(\mathbf{p}+\mathbf{q})G(\mathbf{p})$, which turn out to be of higher order in $1/(k_0 l)$. Third, diagrams with two crossed dashed lines are also subleading. Finally, we again work in the independent-scatterer approximation.

As an example we calculate the second diagram on the right-hand side of Fig. 14. As usual in the diffusion approximation, the diffuse intensity is assumed to be slowly varying, which allows us to expand the Green's functions as

$$\begin{aligned} G(\mathbf{p}+\mathbf{q},\omega+\tfrac{1}{2}\Delta\omega) &\approx \left[p^2+2\mathbf{p}\cdot\mathbf{q}+q^2-\frac{w^2}{c^2}-\Delta\omega\,\frac{\omega}{c^2}-nt\right]^{-1} \\ &\approx G-\left(2\mathbf{p}\cdot\mathbf{q}+q^2-\Delta\omega\,\frac{\omega}{c^2}\right)G^2+4(\mathbf{p}\cdot\mathbf{q})^2G^3, \end{aligned} \tag{336}$$

with the shorthand notation $G=G(\mathbf{p},\omega)$. The momenta, numbered according to Fig. 14, point towards the vertex. We number the Green's functions also according to the figure. Note that this particular diagram is a product of two loops. To lowest order in q^2 we have

$$H_4^{(b)}=nu^2\int\frac{d^3\mathbf{p}}{(2\pi)^3}\,G_1(\mathbf{p}+\mathbf{q}_1,\omega+\omega_1)G_3(\mathbf{p}-\mathbf{q}_4,\omega+\omega_3)G_4^*(\mathbf{p},\omega+\omega_4)$$
$$\times\int\frac{d^3\mathbf{p}'}{(2\pi)^3}\,G_1(\mathbf{p}'-\mathbf{q}_2,\omega+\omega_1)G_3(\mathbf{p}'+\mathbf{q}_3,\omega+\omega_3)G_2^*(\mathbf{p}',\omega+\omega_2)$$
$$=nu^2\left[I_{2,1}+\frac{4k^2}{3}(q_2^2+q_3^2-\mathbf{q}_2\cdot\mathbf{q}_3)I_{4,1}+\frac{k}{c}(\omega_1+\omega_3-2\omega_4)I_{3,1}\right][I_{2,1}+\cdots],\tag{337}$$

where the $\mathbf{q}_i$ are the momenta of the diffusions, the ω_i are the frequency differences of the diffusions, and u is the scatter potential. The I integrals are given in Appendix A. We take absorption terms into account to lowest order, i.e., only in the leading contributions, the $I_{2,1}$ terms. This yields

$$H_4^{(b)}=\frac{-l^3}{16\pi k^2}+\frac{l^5}{48\pi k^2}\left(-\mathbf{q}_2\cdot\mathbf{q}_3-\mathbf{q}_1\cdot\mathbf{q}_4+\sum q_i^2+\kappa^2\right)$$
$$+\frac{-il^4}{16\pi k^2 c}(\omega_1+\omega_3-\omega_2-\omega_4).\tag{338}$$

Here we made use of the fact that in second-order Born approximation $nu^2=4\pi/l$.

A similar calculation gives $H_4^{(a)}$ and $H_4^{(c)}$. Defining the reduced frequencies of the legs as $\tilde\Omega_1=-(\omega_1-\omega_4)/D$, $\tilde\Omega_2=-(\omega_1-\omega_2)/D$, $\tilde\Omega_3=-(\omega_3-\omega_2)/D$, and $\tilde\Omega_4=-(\omega_3-\omega_4)/D$, we find for the sum of the three diagrams

$$H_4=H_4^{(a)}+H_4^{(b)}+H_4^{(c)}$$
$$=\frac{l^5}{96\pi k^2}\left[-2\mathbf{q}_1\cdot\mathbf{q}_3-2\mathbf{q}_2\cdot\mathbf{q}_4\right.$$
$$\left.+\sum_{i=1}^{4}(\mathbf{q}_i^2+\kappa_i^2+i\tilde\Omega_i)\right]\delta\left(\sum\mathbf{q}_i\right).\tag{339}$$

This is the main result of this section. Note that the leading, constant terms proportional to l^3/k^2 have canceled, which is closely related to the current conservation laws (Kane, Serota, and Lee, 1988).

In Eq. (339) it is important to keep track of the q^2 terms. When the vertex is attached to a diffusion, the q_j^2 terms together with κ and $\tilde\Omega$ yield, according to the diffusion equation, $(q_j^2+\kappa^2+i\tilde\Omega_j)\mathcal{L}_j=12\pi/l^3$. The constant factor on the right-hand side corresponds to a delta function in real space. If we attach external diffusions to the Hikami box, this delta function is nonzero at roughly one mean free path from the surface and its contribution can be neglected, as its effect is of order l/L. As a result, the absorption part and the frequency-dependent part vanish:

$$H_4(\mathbf{q}_1,\mathbf{q}_2,\mathbf{q}_3,\mathbf{q}_4)=-h_4(\mathbf{q}_1\cdot\mathbf{q}_3+\mathbf{q}_2\cdot\mathbf{q}_4)\delta\left(\sum\mathbf{q}_i\right),\tag{340}$$

where we have denoted $h_4=l^5/(48\pi k^2)$. In most calculations, however, we use a Fourier transform in the z direction, because in our slab geometry the $(q_x,q_y,z)=(\mathbf{q}_\perp,z)$ representation is the most convenient. Then the q_z terms become differentiations:

$$H_4=\frac{h_4}{2}\left[2\partial_{z_1}\partial_{z_3}+2\partial_{z_2}\partial_{z_4}-2\mathbf{q}_{\perp_1}\cdot\mathbf{q}_{\perp_3}-2\mathbf{q}_{\perp_2}\cdot\mathbf{q}_{\perp_4}\right.$$
$$\left.+\sum_{i=1}^{4}(-\partial_{z_i}^2+q_{\perp_i}^2+\kappa_i^2+\tilde\Omega_i)\right].\tag{341}$$

The differentiations work on the corresponding diffusions and afterwards z_i should be set equal to z. Formally one has

$$H_4(z;z_1,z_2,z_3,z_4)\mathcal{L}_1(z_1)\mathcal{L}_2(z_2)\mathcal{L}_3(z_3)\mathcal{L}_4(z_4)$$
$$=\frac{h_4}{2}[2\partial_{z_1}\partial_{z_3}+\cdots]\mathcal{L}_1(z_1)\mathcal{L}_2(z_2)\mathcal{L}_3(z_3)\mathcal{L}_4(z_4)|_{z_i=z},\tag{342}$$

but we just write this as $H_4(z)\mathcal{L}_1(z)\mathcal{L}_2(z)\mathcal{L}_3(z)\mathcal{L}_4(z)$. Note that the vertices yield the spatial derivatives of the diffusions, that is, their fluxes. This observation is helpful in estimating the influence of internal reflections, which reduce the spatial derivatives of the diffusions.

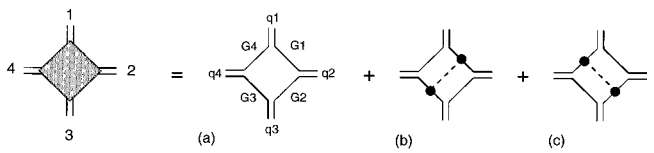

FIG. 14. Hikami four-point vertex. It describes the exchange of amplitudes of two incoming diffusons 1 and 3 into two outgoing diffusons 2 and 4. The dots linked with the dashed line denote an extra scatterer on which both amplitudes scatter. The solid lines are dressed amplitude propagators.

B. Six-point vertex: H_6

We shall also need a second-order diagram for the six-point vertex H_6. Six diffusions are connected to this diagram (Fig. 15). This diagram was calculated by Hikami (1981). Again, the dressings of the diagrams have to be added to the bare diagrams. Taking rotations of the depicted diagrams into account, there are 16 diagrams in the second-order Born approximation. (It is not allowed to dress the bare six-point vertex with a scatterer that connects two opposite propagators. This dressing gives a leading contribution also, but the result-

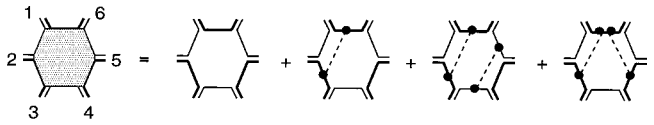

FIG. 15. Six-point vertex H_6, describing the interaction of six diffusons. We did not draw possible rotations of the three right diagrams. In total there are sixteen diagrams.

ing diagram is the same as a composed diagram with two four-point vertices. Therefore it should not be included here, but it will enter in diagrams with two H_4 vertices.) One finds

$$H_6=\frac{-l^7}{96\pi k^4}\left[\mathbf{q}_1\cdot\mathbf{q}_2+\mathbf{q}_2\cdot\mathbf{q}_3+\mathbf{q}_3\cdot\mathbf{q}_4+\mathbf{q}_4\cdot\mathbf{q}_5+\mathbf{q}_5\cdot\mathbf{q}_6+\mathbf{q}_6\cdot\mathbf{q}_1+\sum_{i=1}^{6}\left(\mathbf{q}_i^2+\frac{1}{2}\kappa_i^2+\frac{i}{2}\tilde{\Omega}_i\right)\right]\delta\left(\sum\mathbf{q}_i\right). \tag{343}$$

Apart from the frequency and absorption terms included here, Hikami's original expression can be derived from Eq. (343) using momentum conservation.

C. Beyond the second-order Born approximation

Going beyond the second-order Born approximation in the calculation of the diffusion diagrams meant that in the diagrams the t matrix replaced the potential u. This resulted in a replacement of the mean free path: it became $l\equiv n\bar{tt}/4\pi$ instead of $l\equiv nu^2/4\pi$. However, for the vertices the situation is more subtle. In the previous calculations we worked to second order of the scattering potential, thus neglecting diagrams with more than two scatterings on the same scatterer. Including all orders there are eight diagrams, as in Fig. 16.

The calculation is very similar to that of the second-order Born approximation above. The only difference is that instead of u, the t matrices t and $\bar{t}$ occur (t on G's, $\bar{t}$ on G^*'s). After summing the expressions for the eight diagrams, one finds the same result for the Hikami box as was found previously in second-order Born approximation, Eq. (339). However, the definition of the mean free path is different: $l=n\bar{tt}/4\pi$ instead of $l=nu^2/4\pi$. We conclude that, although extra diagrams were present, only the mean free path was renormalized in extending from second-order Born to the full Born series. This can also be shown more generally in the nonlinear sigma model (Lerner, 1996). For the six-point vertex it was not checked explicitly whether the second and full Born approximations give the same result (there are at least 64 diagrams), but we have no doubt they will.

D. Corrections to the conductivity

In the original works of Gor'kov *et al.* (1979) and Hikami (1981), the vertices were introduced to calculate weak-localization corrections to the conductivity. We have already mentioned that the maximally crossed diagrams give the largest correction to the conductivity, increasing the return probability of the intensity. In the Hikami-vertex formalism these diagrams are drawn in Fig. 17. The correction to the diffusion constant diverges with the sample size in one and two dimensions. This divergence indicates the absence of extended states in one and two dimensions no matter how small the disorder. In three dimensions, however, there is a transition to a localized state at a finite level of disorder. In this work we do not consider such loop effects. We suppose that we are far from localization, so that we can restrict ourselves to the leading processes, and the vertices show up only in the interaction between different diffusions.

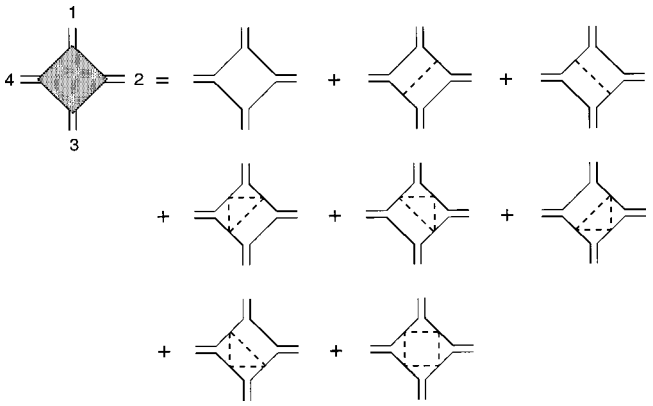

FIG. 16. Four-point vertex, beyond the second-order Born approximation. Instead of three, there are now eight diagrams to be calculated. The resulting expression, however, is apart from a renormalization of the mean free path the same as in the second-order Born approximation.

XV. SHORT RANGE, LONG RANGE, AND CONDUCTANCE CORRELATIONS: C_1, C_2, AND C_3

A nice feature of optical mesoscopic systems, as compared to electronic systems, is that they permit separate measurement of certain parts of the transmission signal. Depending on whether integration over incoming or outgoing directions is performed, one measures fundamentally different quantities. In electronic systems one usually measures the conductance of the sample. This is done by connecting incoming and outgoing sides to a clean electron "bath." All electrons are collected and all angular dependence is lost. In contrast, in optical systems one usually measures the angular resolved transmission, but angular integration is possible. The correlation functions of the different transmission quantities, their magnitudes, their decay rates, and the underlying diagrams are all very different.

In this section we shall discuss correlation functions for all three transmission quantities. See also the review by Berkovits and Feng (1994) for the physical meaning of the correlations. We try to provide all quantitative factors relevant for an experiment. In later sections the same approach will be extended to higher-order correlations.

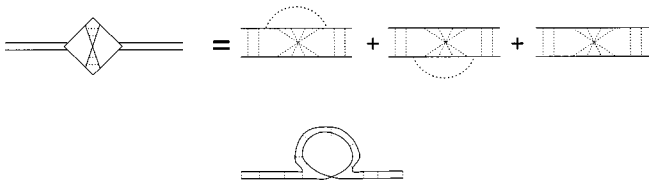

FIG. 17. First-order correction to the conductivity in the Hikami formalism. At the right we have written out the vertices in the second-order Born approximation. On the second line the first diagram in the right-hand side of the upper line is drawn in a different way, showing it is a loop effect.

A. Angle-resolved transmission: the speckle pattern

If a monochromatic plane wave shines through a disordered sample, one sees large-intensity fluctuations in the transmitted beam, so-called "speckles." The speckle pattern is wildly fluctuating (as a function of the frequency of the light or the outgoing angle). The typical diameter of a speckle spot on the outgoing surface is λ. We are interested in the correlation between speckle patterns of two different beams. The beams may have different incoming angles, different frequencies, or different positions.

We denote the transmission from the incoming channel a (wave coming in under angles θ_a, ϕ_a) to the outgoing channel b (waves transmitted into angles θ_b, ϕ_b) as T_{ab}. There are short-, long-, and "infinite"-range contributions to the correlation function of the speckles. The frequency correlation functions can be classified as

$$\frac{\langle T_{ab}(\omega)T_{cd}(\omega+\Delta\omega)\rangle}{\langle T_{ab}(\omega)\rangle\langle T_{cd}(\omega+\Delta\omega)\rangle}=1+C_1^{abcd}(\Delta\omega)+C_2^{abcd}(\Delta\omega)+C_3^{abcd}(\Delta\omega). \tag{344}$$

Feng, Kane, Lee, and Stone (1988) originally put this expression forward as an expansion in $1/g$, where C_1 was of order one, C_2 of order $1/g$, and C_3 of order $1/g^2$. We return to this expansion below. We present a sketchy picture of the diagrams of the different correlations in Fig. 18. The largest contributions to transport are from the independent diffusions, yet correlations are present, mixing diffusions with different frequencies or angles.

The unit contribution in Eq. (344) comes from the uncorrelated product of average intensities. The C_1 term in the correlation function is the leading correlation if the angle-resolved transmission T_{ab} is measured. It is unity if the two incoming directions a and c are the same, the outgoing directions b and d are the same, and $\Delta\omega$ is zero. If one changes the frequency of the incoming beam, the speckles of the outgoing beam deform and eventually the correlation vanishes exponentially. This effect is the short-ranged C_1 contribution. Also of interest is the case of the angular C_1 correlation with the frequency fixed: If the angle of the incoming beam is changed, the speckles change due to two effects. First, the speckle follows the incoming beam. This is also known as the memory effect, which one can even see by the naked eye. Second, the speckle pattern also deforms, i.e., it decorrelates; this is again the C_1 correlation. The C_1 correlation is a sharply peaked function, nonzero only if the angle of the incoming and outgoing channel are changed by the same amount. Diagrammatically, the C_1 factorizes in two disconnected diagrams; see Fig. 18.

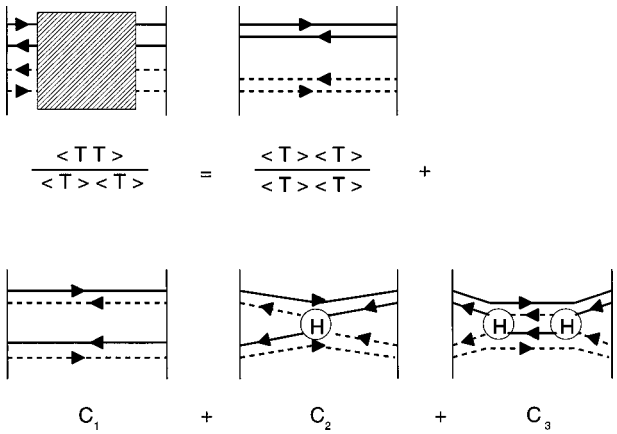

FIG. 18. Schematic picture of the different correlation functions present in the transmission of two intensities. The arrows distinguish between advanced and retarded propagators. Propagators with equal transverse momentum or frequency have the same style of line (dashed or solid). The hatched box contains in principle all contributions to $\langle T_{ab}T_{cd}\rangle$. The main part just factorizes, but correlations are present. The C_1 correlation involves a simple interchange of amplitudes. The C_2 and C_3 correlation involve a Hikami box (circled H); they are a perturbative effect for weak scattering.

Theoretical studies of C_1 were first done by Shapiro (1986). Experimental work on C_1 as a function of angle, explicitly showing the memory effect, was done by Freund, Rosenbluh, and Feng (1988). Van Albada, De Boer, and Lagendijk (1990) studied the frequency dependence of C_1. Later, the effects of absorption and, especially, internal reflection were studied (Freund and Berkovits, 1990; Van Rossum and Nieuwenhuizen, 1993).

B. Total transmission correlation: C_2

The C_2 correlation stands for the long-range correlations in the speckle pattern. Consider again a single-direction-in/single-direction-out experiment. Again the two incoming angles are the same ($a=c$), yet this time we look at the cross correlation of two speckles far apart. As there is an angle difference in the outgoing channel, but not in the incoming beam, the C_1 term is now absent. Instead there is a much weaker correlation. As the frequency shifts, this correlation decays algebraically. This is the C_2 contribution. It describes correlations between speckles that are far apart. In a single-channel-in/single-channel-out experiment it is only possible to see the weak effects of these higher-order correlations in very strongly scattering media, i.e., if the system is rather close to Anderson localization. This type of experiment was done by Genack and Garcia

(1993). The C_2 term can be measured more easily in a setup using one incoming channel and integrating over all outgoing channels. In an experiment the outgoing light is collected with an integrating sphere. Therefore one measures the total transmission $T_a = \Sigma_b T_{ab}$. In this setup the C_2 correlation function, which has a much smaller peak value but is long ranged, contributes for all outgoing angles. The C_2 term is now the leading correlation as the sharply peaked C_1 term is overwhelmed. A precise estimate of the C_1 contribution in C_2 was made by Van Rossum, De Boer, and Nieuwenhuizen (1995). Only outgoing diffusions with no transverse momentum and no frequency difference in their amplitudes are leading in the total transmission, as then the phases of the outgoing amplitudes cancel. From Fig. 18 one sees indeed that it holds for the C_2 diagram (outgoing lines of similar style pair), but not for the C_1 diagram. The long-range character of the C_2 arises due to interference of the diffuse light paths. It is of order g^{-1} and corresponds to a diagram in which the two incoming diffusions interact through a Hikami vertex, where the diffusions exchange amplitudes.

The long-range C_2 correlation function was first studied by Stephen and Cwilich (1987). Zyuzin and Spivak (1987) introduced a Langevin approach to simplify the calculation of correlation functions. Pnini and Shapiro (1989) applied this method to calculate the correlation functions of light transmitted through and reflected from disordered samples. The C_2 correlation functions were measured in several experiments. For optical systems Van Albada *et al.* performed measurements (Van Albada *et al.*, 1990; De Boer, Van Albada, and Lagendijk, 1992). Microwave experiments were performed by Genack, Garcia, and Polkosnik (1990) and Garcia, Genack, Pnini, and Shapiro (1993). In several papers effects of absorption and internal reflections were studied; see Pnini and Shapiro (1991), Lisyansky and Livdan (1992), Zhu *et al.* (1991), and Van Rossum and Nieuwenhuizen (1993). It was shown that absorption and internal reflection, neglected in the earliest calculations, significantly reduce the correlations.

C. Conductance correlation: C_3

Finally, the C_3 term in Eq. (344) is dominant when the incoming beam is diffuse and one collects all outgoing light. Experimentally one can do this using two integrating spheres. Then one measures, just as in electronic systems, the conductance $g = \langle T \rangle = \Sigma_{a,b} T_{ab}$. In that measurement contributions to the correlation are dominant, where the angles a and c are arbitrarily far apart. Though C_3 is of order g^{-2}, it dominates over the C_1 and C_2 terms, as it has contributions from all incoming and outgoing angles. Therefore it is sometimes called the ''infinite''-range correlation. In contrast to the amplitudes for the C_2 term, the amplitudes of the incoming diffusions now must have opposite phases, as can be seen in a diagram where the two incoming diffusions interact twice (see Fig. 18). Note that a loop occurs. Apart from the normalization to the average, C_3 equals the universal conductance fluctuations, or UCF.

The UCF were an important discovery in the study of mesoscopic electron systems. The electronic conductance of mesoscopic samples shows reproducible sample-to-sample fluctuations. This was observed in experiments on mesoscopic electronic samples by Umbach, Washburn, Laibowitz, and Webb (1984). The theoretical explanation was given by Altshuler (1985) and by Lee and Stone (1985). For reviews on the subject see Lee, Stone, and Fukuyama (1987) and the book edited by Altshuler *et al.* (Altshuler, Lee, and Webb, 1991). The discovery of these fluctuations showed that interference effects are important in electronic systems, even far from the localization transition. The variance of the fluctuations is independent of the sample parameters such as the mean free path, the sample thickness, and, most remarkably, the average conductance. Therefore the fluctuations are called universal conductance fluctuations. The conductance fluctuates when the phases of the waves in the dominant paths change. This happens, of course, if one changes the position of the scatterers, e.g., by taking another sample. One may also keep the scatterers fixed but apply a magnetic field or vary the Fermi energy. In all these cases one modifies the phases of scattered waves, so that different propagation paths become dominant. The fluctuations are much larger than one would obtain classically by modeling the system by a random resistor array, in which interference effects are neglected. A classical approach is valid only on a length scale exceeding the phase coherence length, where the fluctuations reduce to their classical value.

Unfortunately, despite some advantages of optical systems, the analog of the UCF has not yet been observed in them. Such experiments turn out to be difficult. Although the magnitude of the fluctuations is universal, they occur on a background of order g, where g is the dimensionless conductance (in optical experiments one typically has $g \sim 10^3$). The value of the fluctuations relative to the background is thus $1/g$, so that the C_3 correlation function is of order $1/g^2$, typically of order 10^{-6}. For electrons this problem does not occur, as smaller values of g are achievable. In the electronic case there have been many observations of the universal conductance fluctuations.

A promising candidate for measuring C_3 is the microwave experiment of Stoytchev and Genack (1997). In such a setup one has good control over the channels. Moreover, one is able to study materials with large disorder, i.e., down to $g = 3$.

In principle the C_2 and C_3 correlations are present as sub-leading terms in the angular correlation function, but there are also other contributions of order $1/g$ and $1/g^2$, respectively, to the correlation Eq. (344). The weak-localization correction (see Sec. XIV.D) is an example of a $1/g$ contribution to C_1. We have drawn a $1/g^2$ contribution to C_2 in Fig. 19. Such corrections are studied by Garcia *et al.* (1993). The interpretation of the C's as an expansion in $1/g$ is misleading. Rather, we define the C_1, C_2, and C_3 as the leading terms in the

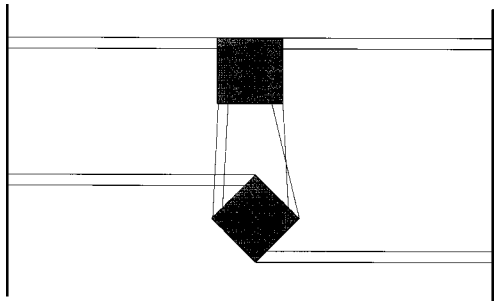

FIG. 19. A contribution of order $1/g^2$ to the C_2 correlation. The boxes are Hikami boxes, the parallel lines are the diffusons. By following the amplitudes, one can check that the incoming pairings ij^* and ji^* change on the outgoing side into pairings ii^* and jj^*. This diagram is thus not contributing to the C_3, which is also of order $1/g^2$ but requires diagrams without amplitude exchange. The exchange in pairing of incoming and outgoing amplitudes means that the diagram is a higher-order C_2 diagram.

correlation of T_{ab}, T_a, and T, respectively. Equivalently, C_1 contains disconnected diagrams; incoming and outgoing amplitudes automatically have the same pairing. The C_2 term contains connected diagrams swapping the initial pairing, and C_3 contains all connected diagrams in which incoming and outgoing pairings are identical.

XVI. CALCULATION OF CORRELATION FUNCTIONS

A. Summary of diffuse intensities

For the calculation of interference effects it is often too complicated to take the precise behavior near the boundaries into account. We therefore approximate the diffuse intensity with its bulk behavior, yet we will use the prefactors and angular dependence, especially τ_0 and τ_1, found with the radiative transfer approach.

The diffuse intensity created from a beam impinging in direction a is

$$\mathcal{L}^a_{\rm in}(z)=\frac{4\pi\tau_1(\mu_a)T(\mu_a)}{klA\mu_a}\frac{L-z}{L}. \tag{345}$$

For uniform illumination of the sample the source term in the transport equation becomes

$$S(z)=\sum_a S_a = A\int_0^k \frac{d\mathbf{q}_{\perp a}}{2\pi} q_{\perp a} S_a$$
$$=\frac{2k}{l}\int_0^1 d\mu\, T(\mu) e^{-z/l\mu}. \tag{346}$$

Using this source term in the Schwarzschild-Milne equation gives the diffuse intensity for a uniform illuminated sample:

$$\mathcal{L}_{\rm in}(z)=\frac{4k}{l}\frac{L+z_0-z}{L+2z_0}. \tag{347}$$

Defining

$$\epsilon_a=\frac{\pi T(\mu_a)\tau_1(\mu_a)}{kA\mu_a}, \tag{348}$$

and comparing the prefactors, one has

$$\mathcal{L}^a_{\rm in}(z)=\epsilon_a\mathcal{L}_{\rm in}(z). \tag{349}$$

Finally, for diffuse propagation between two points in the slab one has

$$-\frac{d^2}{dz^2}\mathcal{L}_{\rm int}(z,z';M)+M^2\mathcal{L}_{\rm int}(z,z';M)$$
$$=\frac{12\pi}{l^3}\delta(z-z'), \tag{350}$$

with the solution

$$\mathcal{L}_{\rm int}(z,z';M)=\frac{12\pi}{l^3}\frac{\sinh Mz_<\sinh M(L-z_>)}{M\sinh ML}. \tag{351}$$

For angle-resolved measurements the outgoing intensity in a certain direction b is, in analogy with Eq. (349),

$$\mathcal{L}^b_{\rm out}(z)=\epsilon_b\mathcal{L}_{\rm out}(z)=\epsilon_b\frac{k}{l}\frac{z}{L}. \tag{352}$$

The angular transmission coefficient reads

$$\langle T_{ab}\rangle=\frac{\pi\tau_1(\mu_a)\tau_1(\mu_b)T(\mu_a)T(\mu_b)l}{3\mu_a\mu_bA(L+2z_0)} \tag{353}$$
$$=\epsilon_a\epsilon_b\langle T\rangle. \tag{354}$$

The total transmission coefficient is

$$\langle T_a\rangle=\frac{\tau_1(\mu_a)T(\mu_a)l}{3\mu_a(L+2z_0)}. \tag{355}$$

The conductance [cf. Eq. (190)] reads

$$g\equiv\langle T\rangle=\int d^3\mathbf{r}\,\mathcal{L}_{\rm out}(z)S(z)$$
$$=\frac{2kA}{2\pi l}\int_0^\infty L_{\rm out}(z)dz\int_0^1 d\mu\, T(\mu)e^{-z/\mu l}$$
$$=\frac{k^2Al}{3\pi(L+2z_0)}=\frac{4Nl}{3(L+2z_0)}. \tag{356}$$

B. Calculation of the C_1 correlation

The calculation of C_1 is rather simple, as it is just the product of two independent diffusons with exchanged partners. Both diffusons consist of one amplitude from one beam and one complex-conjugated amplitude from the other beam. Due to momentum conservation in each diffuson, the perpendicular momentum difference of the two incoming beams, $\mathbf{q}_\perp$, is equal to the difference of the outgoing momenta. Therefore the C_1 is only nonzero if incoming and outgoing angles are shifted equally during the experiment.

We calculate the normalized product of a diffuson with "squared mass" $M^2=q_\perp^2+\kappa^2+i\tilde{\Omega}$ and the complex-conjugated diffuson. This yields

$$C_1(M)=\left|\frac{T_{ab}(M)}{T_{ab}(\kappa)}\right|^2=\left|\frac{\mathcal{L}^{ab}(M)}{\mathcal{L}^{ab}(\kappa)}\right|^2$$
$$=\frac{|M|^2}{\kappa^2}\left|\frac{(1+\kappa^2 z_0^2)\sinh\,\kappa L+2\kappa z_0\,\cosh\,\kappa L}{(1+M^2 z_0^2)\sinh\,ML+2Mz_0\,\cosh\,ML}\right|^2. \tag{357}$$

In Fig. 20 this function is drawn for various situations. In thick samples where $Mz_0\ll 1$ and no absorption is present, the result reduces to (Feng *et al.*, 1988)

$$C_1(M)=\left|\frac{ML}{\sinh\,ML}\right|^2. \tag{358}$$

For large angle or frequency difference ($|M|L\gg 1$), C_1 decays exponentially, as $C_1(M)\sim\exp(-2\,\mathrm{Re}(M)L)$. The spatial correlations of beams can be extracted from the Fourier transform of the angular correlation function.

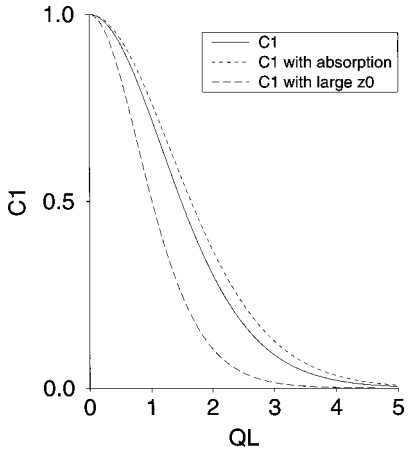

FIG. 20. C_1 angular correlation function plotted against the scaled perpendicular momentum difference: solid line, small z_0, no absorption; short dashed line, absorption ($\kappa=2/L$), small z_0; long dashed line, large skin layers ($z_0=L/3$), no absorption.

C. Calculation of the C_2 correlation

The diagram of the long-range correlation C_2 is depicted in Fig. 21. Remember that C_1 is zero if incoming and outgoing angles are changed unequally, but C_2 is connected, allowing momentum flow from one diffuson to the other. Therefore it is nonzero if one changes incoming and outgoing angles by a different amount. C_2 stems from the interaction between two diffusons, which exchange partners somewhere inside the slab. The Hikami box describes this exchange. We have

$$C_2=\frac{1}{\langle T_a\rangle\langle T_c\rangle}\int_0^L dz\,\mathcal{L}^a_{\rm in}(z,M_1)\mathcal{L}^c_{\rm in}(z,M_3)H_4(z)$$
$$\times\mathcal{L}_{\rm out}(z,M_2)\mathcal{L}_{\rm out}(z,M_4). \tag{359}$$

We have labeled the incoming diffusons with odd numbers and the outgoing diffusons with even numbers, a convention used throughout this work. Attaching diffusons to the Hikami box allows a simplification of the expression for the box. We calculate C_2 by inserting $M^2_{2,4}={q_\perp}^2+\kappa^2\pm i\tilde{\Omega}$, $M_1=M_3=\kappa$. In the z-coordinate representation the box reads (see Sec. XIV)

$$H_4(z_1,z_2,z_3,z_4)=h_4(\partial_{z_1}\partial_{z_3}+\partial_{z_2}\partial_{z_4}+{q_\perp}^2). \tag{360}$$

The above calculation for C_2 is similar to the one obtained in the Langevin approach, as one can see by comparing Eq. (39) of Pnini and Shapiro (1989) to Eqs. (360) and (359) in this section. In the Langevin approach one assumes that there is a macroscopic intensity, which describes the average diffusion and an uncorrelated random-noise current superposed. In our approach we have a slowly varying diffuse intensity, while the pointlike, uncorrelated random interactions originate from the Hikami box.

We discuss some simplified cases. Consider first the case of angular correlations and no absorption but taking the boundary effects into account:

$$C_2(q_\perp)=\frac{3\pi L}{k^2 lA}F_2(q_\perp L), \tag{361}$$

in which we define the dimensionless function F_2,

$$F_2(q_\perp L)=[\sinh 2q_\perp L-2q_\perp+q_\perp z_0(6\sinh^2 q_\perp L-2{q_\perp}^2L^2)+4{q_\perp}^2z_0^2(\sinh 2q_\perp L-q_\perp L)+6{q_\perp}^3z_0^3\sinh^2 q_\perp L$$
$$+{q_\perp}^4z_0^4\sinh 2q_\perp L][2q_\perp L\{(1+{q_\perp}^2z_0^2)\sinh q_\perp L+2q_\perp z_0\cosh q_\perp L\}^2]^{-1}, \tag{362}$$

which decays like $1/q_\perp$ for large $q_\perp$ (i.e., for large angles). However, it still should hold that $q_\perp l\ll 1$, else we probe essentially interference processes within one mean free path from the surface, which is beyond this approach. Neglecting boundary effects, $z_0\ll L$, one recovers (Pnini and Shapiro, 1991)

$$F_2(q_\perp L)=\frac{\sinh(2q_\perp L)-2q_\perp L}{2q_\perp L\,\sinh^2(q_\perp L)}, \tag{363}$$

with $F_2(0)=\frac{2}{3}$. In Fig. 22 we have plotted the F_2 function for various situations.

We have studied the correlation as a function of the two-dimensional momentum $q_\perp$. Similarly, we can study the real-space correlations. The functional form in real space is of roughly similar shape to Fig. 22, with typical decay length L in the x,y direction (Stephen and Cwilich, 1987). One can also obtain frequency correla-

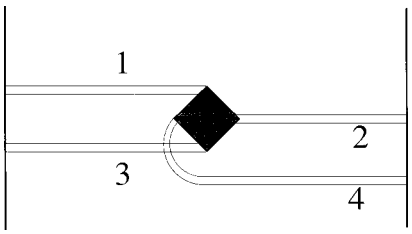

FIG. 21. Diagram of the long-range C_2 correlation function. The shaded box denotes the Hikami four-point vertex depicted in Figs. 15 and 17.

tions. Without absorption, neglecting boundary effects, one finds (De Boer *et al.*, 1992)

$$F_2(\tilde{\Omega})=\frac{2}{\sqrt{2\tilde{\Omega}}L}\left(\frac{\sinh(\sqrt{2\tilde{\Omega}}L)-\sin(\sqrt{2\tilde{\Omega}}L)}{\cosh(\sqrt{2\tilde{\Omega}}L)-\cos(\sqrt{2\tilde{\Omega}}L)}\right). \tag{364}$$

Of special interest is the top of the correlation function. By definition the top of the correlation function corresponds to the second cumulant, or second central moment, of the total transmission distribution function. With a plane wave as incoming beam, all transverse momenta are absent, so we also neglect absorption. These assumptions correspond to all M being equal to zero in Eq. (359). The diffusons are simple linear functions, given by Eqs. (345) and (352). Neglecting internal reflections, one obtains for the second cumulant (Stephen and Cwilich, 1987)

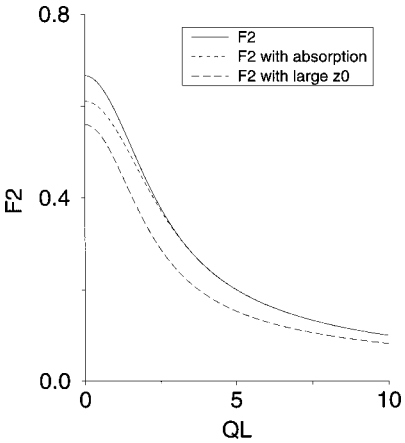

FIG. 22. F_2, the normalized form of the angular correlation function C_2, plotted against the scaled perpendicular momentum difference: solid line, small z_0, no absorption [Eq. (363)]; short dashed line, absorption ($\kappa=2/L$), small z_0; long dashed line, large skin layers ($z_0=L/3$), no absorption.

$$\langle\langle T_a^2\rangle\rangle=\frac{\langle T_a^2\rangle-\langle T_a\rangle^2}{\langle T_a\rangle^2}$$
$$=\frac{1}{\langle T_a\rangle^2}\int\int dx\,dy$$
$$\times\int_0^L dz\,H_4\mathcal{L}_{\rm in}^a(z)\mathcal{L}_{\rm out}(z)\mathcal{L}_{\rm in}^a(z)\mathcal{L}_{\rm out}(z)$$
$$=\frac{1}{gL^3}\int_0^L dz[z^2+(L-z)^2]=\frac{2}{3g}, \tag{365}$$

where double brackets denote cumulants normalized to the average. The correlation is thus proportional to $1/g$. The inverse power of g counts the number of four-point vertices; this power can be looked upon as the probability that two intensities interfere.

One obtains a general expression for C_2 by inserting the appropriate diffusons and the Hikami box Eq. (360) into Eq. (359). The result is rather lengthy and is given by van Rossum and Nieuwenhuizen (1993).

1. Influence of incoming beam profile

We now study the influence of the beam profile on the correlation. In experiments the beam is often focused to a small spot in order to minimize the dimensionless conductance g and therefore to maximize the correlations. Physically it is clear that the correlations increase if the two incoming channels are closer to each other, i.e., if the beam diameter is smaller. If the spot of the incoming beam is finite, amplitudes with different angles, i.e., different transverse momenta, are present. They can combine into incoming diffusons with perpendicular momentum. We suppose that the incoming beam has a Gaussian profile. We decompose it into plane waves defined in Eq. (147) (for convenience we assume the average incidence to be perpendicular),

$$\psi_{\rm in}=\frac{2\pi}{W}\sum_a \phi(q_{\perp_a})\psi_{\rm in}^a,\quad \phi(q_\perp)=\frac{\rho_0}{\sqrt{2\pi}}e^{-q_\perp{}^2\rho_0^2/4}, \tag{366}$$

where ρ_0 is the beam diameter. In order to have two diffusons with momenta $q_\perp$ and $-q_\perp$, we find that the four incoming amplitudes combine to a weight function

$$\int d^2P_1d^2P_3\phi(P_1)\phi^*(P_1+q_\perp)\phi(P_3)\phi^*(P_3-q_\perp)$$
$$=e^{-\rho_0^2q_\perp{}^2/4}. \tag{367}$$

We get the correlation function by integrating the $q_\perp$-dependent correlation function over the momentum with the corresponding weight. Neglecting boundary layers we find for the top of the correlation (De Boer *et al.*, 1992).

$$\langle\langle T_a^2\rangle\rangle=\frac{\rho_0^2}{4\pi g}\int d^2q_\perp e^{-\rho_0^2q_\perp{}^2/4}F_2(q_\perp L), \tag{368}$$

with F_2 as in Eq. (363). If the incoming beam is very broad, $\rho_0\gg L$, only the term $F_2(q_\perp=0)=2/3$ contributes

and one recovers the plane-wave behavior $\langle\langle T_a^2\rangle\rangle = 2/3g$. The second cumulant decreases as $1/\rho_0^2$ at large ρ_0. At smaller beam diameters the top of the correlation is proportional to $1/\rho_0$, and diverges in this approximation, in which $q_\perp l \sim l/\rho_0 \ll 1$.

2. Reflection correlations

We have seen that the transmission corresponds to the diffusons, but in reflection there are two intensity diagrams: the diffusons provide a constant background, while the maximally crossed diagrams yield the enhanced backscatter cone, which is of importance only if incoming and outgoing angles are the same. This leads to more diagrams and to more peaks in the reflection correlation than in the transmission correlation. For the C_1 correlation one can pair diffusons and maximally crossed diagrams (Berkovits and Kaveh, 1990). Indeed, in optical experiments two peaks were seen by Freund and Rosenbluh (1991). The C_2 term in reflection was treated by Berkovits (1990). Measurement of C_2 in reflection by collecting all reflected light is tricky, as it is hard not to interfere with the incoming beam. Nevertheless, measurement may be possible as a long-range component in the angle-resolved reflection (this, however, requires quite small values of g). For neither C_1 nor C_2 in reflection does one expect a very good agreement with theory, the problem being that the precise behavior of the diffuson near the surface is important. The diffusion approximation $ql \ll 1$ is no longer valid, in particular if the indices of refraction match, as then the intensity gradient near the surface is the largest. The calculation of C_1 is probably easily extended, but for C_2 one also would need the Hikami box beyond first order in ql.

D. Conductance fluctuations: C_3

One might think that the calculation of the C_3 or UCF in the above Landauer approach would be straightforward. However, the calculation in the Landauer approach is quite cumbersome, as on short length scales (of the order of the mean free path) divergences show up when one treats the problem on a macroscopic level using diffusons. As an alternative, the Kubo approach is often used in mesoscopic electronic systems (Altshuler, 1985; Lee and Stone, 1985; Lee *et al.*, 1987). The results for the conductance obtained by either the Kubo or the Landauer formalism should be identical (see Fisher and Lee, 1981; Janβen, 1991). Yet the Kubo approach cannot be applied directly to optical systems when absorption is to be included. Studies of C_3 in the Landauer approach were undertaken by Kane *et al.* (1988), Berkovits and Feng (1994), and van Rossum, Nieuwenhuizen, and Vlaming (1995), who show explicitly that all divergences cancel.

The C_3 correlation function, defined in Eq. (344), involves incoming diffusons $\mathcal{L}_{\rm in}^{a,c}$ and outgoing ones $\mathcal{L}_{\rm out}^{b,d}$. Due to the factorization of the external direction dependence [see Eqs. (349), (352), and (356)], this dependence on external parameters cancels for C_3. We can write

$$C_3^{abcd}(\kappa,\tilde{\Omega}) = C_3(\kappa,\tilde{\Omega}) = \frac{1}{\langle T\rangle^2}\sum_{\mathbf{q}_\perp} F(q_\perp,\kappa,\tilde{\Omega}), \tag{369}$$

where $\mathbf{q}_\perp$ is the $(d-1)$-dimensional transverse momentum. The function F is the main object to be determined in this section. We thus calculate it at fixed $q_\perp$ and with external diffusons for diffuse illumination $\mathcal{L}_{\rm in}$ and $\mathcal{L}_{\rm out}$, Eqs. (347) and (352). Depending on dimension we have

$$\sum_{\mathbf{q}_\perp} F(q_\perp,\kappa,\tilde{\Omega}) = F(0,\kappa,\tilde{\Omega}) \quad \text{quasi 1D}, \tag{370}$$

$$= W\int \frac{d\mathbf{q}_\perp}{2\pi} F(q_\perp,\kappa,\tilde{\Omega}) \quad \text{quasi 2D}, \tag{371}$$

$$= W^2\int \frac{d^2\mathbf{q}_\perp}{(2\pi)^2} F(q_\perp,\kappa,\tilde{\Omega}) \quad \text{3D}. \tag{372}$$

In contrast to C_1 and C_2, as a result of the $q_\perp$ integral, C_3 will depend on the dimensionality of the system.

Let us work out in more detail the long-range diagrams of C_3, roughly depicted in Fig. 18. For all diagrams there are two incoming advanced fields, which for the moment call i and j, and two retarded ones, i^* and j^*. Consider an optical experiment with integrating spheres at incoming and outgoing sides. The incoming diffusons cannot have a momentum or frequency difference, and the pairing must be ii^* and jj^*. In Fig. 23(a) the incoming diffusons interfere somewhere in the slab. In diagrammatic language the diffusons interchange a propagator so that the pairing changes into ij^* and ji^*. Propagation continues with these diffusons, which, due to the different pairings, can have nonzero frequency difference and nonzero momentum. Only the outgoing diffusons without a momentum or frequency difference are dominant. Therefore somewhere else in the slab a second interference occurs. Again exchanging an amplitude, the original pairing, ii^* and jj^*, is restored and the two diffusons propagate out [see Fig. 23(a)i]. Other contributions occur as well, yet the incoming and outgoing pairings are always ii^* and jj^*. In Fig. 23(a)ii the first incoming diffuson meets an outgoing diffuson and exchanges amplitudes. These internal diffusion lines meet at a second point where the original pairings are restored. Clearly in this process the intermediate paths are traversed in time-reversed order. Due to time-reversal symmetry they give a contribution similar to Fig. 23(a)i. In Fig. 23(b)i a diffuson breaks up such that one of its amplitudes makes a large detour, returns to the breaking point, and recombines into an outgoing diffuson. The second incoming diffuson crosses the long path of the amplitude, and one of its amplitudes follows the same contour as the first diffuson. Finally, Fig. 23(c) depicts the situation in which only one internal diffuson occurs. Its endpoints must lie within a distance of a few mean free paths. Because of the local character, this class does not show up in the final result; we need it, however,

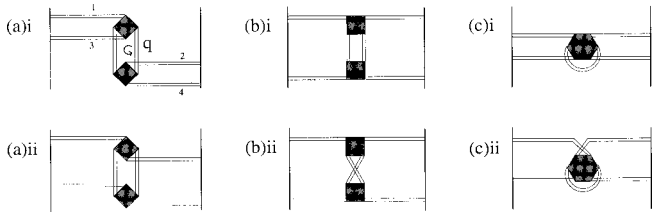

FIG. 23. Leading contributions to the conductance fluctuations apart from short-distance processes. The incoming diffusons from the left interfere twice before they go out on the right. The close parallel lines correspond to diffusons; the shaded boxes are Hikami vertices; **q** denotes the free momentum which is to be integrated over.

since it contains terms that cancel divergences from the other two classes.

E. Calculation of the C_3 correlation function

The diagrams for the conductance fluctuations contain a loop; the two internal diffusons have a free momentum, over which one has to integrate. In Fig. 23(a) we denote this momentum as **q**. Physically, one expects important contributions to the conductance fluctuations if the distance between the two interference vertices ranges from the mean free path to the sample size. Yet the **q** integral diverges for large momentum, i.e., when the two interference processes are close to each other. The standard picture of diffuse transport with diffusons and interference described by Hikami vertices, which works so well for loopless diagrams such as the C_2 correlation function (Sec. XV) or the third cumulant of the total transmission (Sec. XVII), is spoiled by these divergences.

As an example we calculate the diagram presented in Fig. 23(a)i. This diagram was first depicted by Feng *et al.* (1988) and considered in detail by Berkovits and Feng (1994). These authors pointed out that a short-distance divergency appears. They found a cubic divergency in three dimensions and, in general, a d-dimensional divergency in d dimensions. Let us see how it appears. For simplicity we consider a quasi-one-dimensional system for which frequency differences and absorption are absent, so that the decay rate vanishes, i.e., $M=0$ for all diffusons. From Fig. 23(a)i one directly reads off its corresponding expression $F_{a.i}$,

$$F_{a.i}=\int\int dz\,dz'\,\mathcal{L}_{\rm in}^2(z)H_4(z)\mathcal{L}_{\rm int}^2(z,z')H_4(z')\mathcal{L}_{\rm out}^2(z). \tag{373}$$

After performing some partial integrations and using the diffusion equation (350) one finds

$$\begin{aligned}F_{a.i}=&\frac{l^4}{4k^4}\,\delta(0)\int dz\,\mathcal{L}_{\rm in}^2(z)\mathcal{L}_{\rm out}^2(z)+\frac{h_4 l^2}{k^2}\int dz\,\mathcal{L}_{\rm int}(z,z)\\&\times[\mathcal{L}_{\rm in}'^2(z)\mathcal{L}_{\rm out}^2(z)+\mathcal{L}_{\rm in}^2(z)\mathcal{L}_{\rm out}'^2(z)\\&+2\mathcal{L}_{\rm in}'(z)\mathcal{L}_{\rm out}'(z)\mathcal{L}_{\rm in}(z)\mathcal{L}_{\rm out}(z)]+4h_4^2\int dz'\\&\times\int dz\,\mathcal{L}_{\rm int}^2(z,z')\mathcal{L}_{\rm in}'^2(z)\mathcal{L}_{\rm out}'^2(z'),\end{aligned} \tag{374}$$

where the spatial derivative of $\mathcal{L}(z)$ is denoted as $\mathcal{L}'$. The divergency is clearly present in the $\delta(0)$. It comes about as follows: For the case of zero external momenta, the Hikami box yields $H_4(\mathbf{q},0,-\mathbf{q},0)=2h_4q^2$, while the internal diffuson has the form $\mathcal{L}_{\rm int}(q)=12\pi/(l^3q^2)$. Omitting the external lines, we find that the diagram leads to

$$\begin{aligned}&\int\frac{dq}{(2\pi)}\,H_4^2(\mathbf{q},0,-\mathbf{q},0)\mathcal{L}_{\rm int}^2(q)\\&=\frac{l^4}{4k^4}\int\frac{d^3q}{(2\pi)^3}\,q^0\\&=\frac{l^4}{4k^4}\,\delta(r=0).\end{aligned} \tag{375}$$

We label the expressions according to the diagrams in Fig. 23, F_a, F_b, and F_c and sum them. For the 1D case we find

$$F_a+F_b+F_c=-\frac{2}{15}\,\delta(0)L+\frac{2}{15}. \tag{376}$$

The second term in Eq. (376) is exactly equal to the well-known result for the UCF in one dimension. (Note that the prefactors of the diffusons and the Hikami boxes have canceled precisely. This is a manifestation of the universal character of conductance fluctuations.) But a singular part is annoyingly present. The term $\delta(0)$ is a linear divergency. In the three-dimensional case one has to integrate over the transverse momenta, yielding a cubic divergency.

The cancellation of this divergence is very involved and requires a number of special short-range diagrams, which resist a general classification or treatment (Van Rossum, Nieuwenhuizen, and Vlaming, 1995). Here we only make use of the fact that the special short-range diagrams do, in the end, cancel the divergences, while giving no long-range contribution. The nondivergent part of the diagrams of Fig. 23 is the only remainder. It reads

$$\begin{aligned}F(q_\perp,\kappa,\tilde\Omega)=&4h_4^2\int\int dz\,dz'\,\mathcal{L}_{\rm int}(z,z';M)\mathcal{L}_{\rm int}(z,z';M^*)[\mathcal{L}_{\rm in}'^2(z)\mathcal{L}_{\rm out}'^2(z')+\mathcal{L}_{\rm in}'(z)\mathcal{L}_{\rm out}'(z)\mathcal{L}_{\rm in}'(z')\mathcal{L}_{\rm out}'(z')]\\&+\frac{h_4^2}{2}\int\int dz\,dz'[\mathcal{L}_{\rm int}^2(z,z';M)+\mathcal{L}_{\rm int}^2(z,z';M^*)]\,\frac{d^2}{dz^2}[\mathcal{L}_{\rm in}(z)\mathcal{L}_{\rm out}(z)]\,\frac{d^2}{dz'^2}[\mathcal{L}_{\rm in}(z')\mathcal{L}_{\rm out}(z')],\end{aligned} \tag{377}$$

in which again $M^2=q_\perp^2+\kappa^2+i\tilde{\Omega}$. The upper line of Eq. (377) corresponds to the diagrams of Fig. 23(a), whereas the lower line corresponds to the diagrams of Fig. 23(b). Finally, using Eq. (372), we find that the value at vanishing transverse momentum gives the variance of the conductance in one dimension, whereas integration over the transverse momentum yields the correlation in two and three dimensions.

By using Eqs. (377) and (372) and inserting the appropriate diffusons, we can study various cases. Consider the case of fully transmitting surfaces; neglecting absorption and frequency differences one finds

$$F(q_\perp)=\frac{3}{2}\frac{2+2{q_\perp}^2L^2-2\cosh 2q_\perp L+q_\perp L\,\sinh 2q_\perp L}{{q_\perp}^4L^4\,\sinh^2 q_\perp L}, \tag{378}$$

which decays for large momenta as $q_\perp^{-3}$, thus converging in three or fewer dimensions. The subsequent integration over the loop momentum finally yields

$$\langle T^2\rangle_c=\frac{2}{15}\approx 0.133, \quad \text{quasi 1D} \tag{379}$$

$$=\frac{3}{\pi^3}\,\zeta(3)\,\frac{A}{L}\approx 0.116\,\frac{A}{L}, \quad \text{quasi 2D} \tag{380}$$

$$=\frac{1}{2\pi}\,\frac{A}{L^2}\approx 0.159\,\frac{A}{L^2} \quad \text{3D}, \tag{381}$$

in which ζ is Riemann's zeta function. These values are for wide slabs. For cubic samples Lee *et al.* (1987) find in 2D that $\langle T^2\rangle_c=0.186$ and in 3D 0.296 (the value in 1D is of course the same). One can also determine the frequency dependence of the correlation using Eq. (377), which is of importance as it determines the frequency range of the light needed to see the fluctuations (Van Rossum, Nieuwenhuizen, and Vlaming, 1995). By inserting the appropriate diffusons one can also study the case of partial reflection at the surfaces of the sample. It is physically clear that the internal reflections lead to a less steep diffuse intensity in the sample as a function of the depth. The fluctuations are proportional to the space derivatives and thus reduce. We present the results in Fig. 24, where we have plotted the correlation function for various values of the ratio between extrapolation length and sample thickness. One sees that the correlation is lower than without internal reflections. We note that neither the variance (the value at vanishing $\tilde{\Omega}$), nor the form of the correlations is fully universal.

XVII. THIRD CUMULANT OF THE TOTAL TRANSMISSION

So far we have considered correlations between intensities defined as

$$\frac{\langle T_{ab}T_{cd}\rangle}{\langle T_{ab}\rangle\langle T_{cd}\rangle}=1+C_1+C_2+C_3. \tag{382}$$

The $C_1(q_\perp,\tilde{\Omega})$, $C_2(q_\perp,\tilde{\Omega})$, and $C_3(\tilde{\Omega})$ correlation functions describe correlations between two intensities. By definition their value at zero frequency and zero momentum difference, i.e., the peak value, is the second cumulant of the distribution functions of the transmission quantities. An obvious question is how higher cumulants behave. The size of the fluctuations and the shape of the distribution relates to the "distance" from the localization transition. Far from localization, diffusion channels are almost uncorrelated and fluctuations are small (except the optical speckle pattern in the angle-resolved transmission). The correlation between the channels increases if localization is approached. The relevant parameter is the inverse dimensionless conductance $1/g$, which can be interpreted as the probability that two channels will interfere. Close to Anderson localization g approaches unity, and fluctuations increase.

A. Cumulants of the probability distribution

We first study the third cumulant of the total transmission. The total transmission is a constant superposed with fluctuations. To first order in g^{-1} the fluctuations have a Gaussian distribution (De Boer *et al.*, 1992; Kogan, Kaveh, Baumgartner, and Berkovits, 1993). The relative variance of this distribution, the top of C_2, is proportional to g^{-1}, and thus a factor of g larger than for the conductance fluctuations. This sensitivity of the total transmission to interference processes and its simple limiting behavior (as compared to the angle-resolved transmission) make it an ideal quantity for studying mesoscopic effects in its distribution. The third cumulant of the distribution was determined in very precise experiments by De Boer, Van Rossum, Van Albada, Nieuwenhuizen, and Lagendijk (1994). In this section we calculate its theoretical value. Using the diagrammatic approach we relate the third cumulant normalized to the average total transmission, $\langle\langle T_a^3\rangle\rangle$, to the normalized second cumulant $\langle\langle T_a^2\rangle\rangle$.

The moments of the probability distribution can be extracted from the distribution $P(T_a)$ as

$$\langle T_a^k\rangle=\int dT_a P(T_a)T_a^k. \tag{383}$$

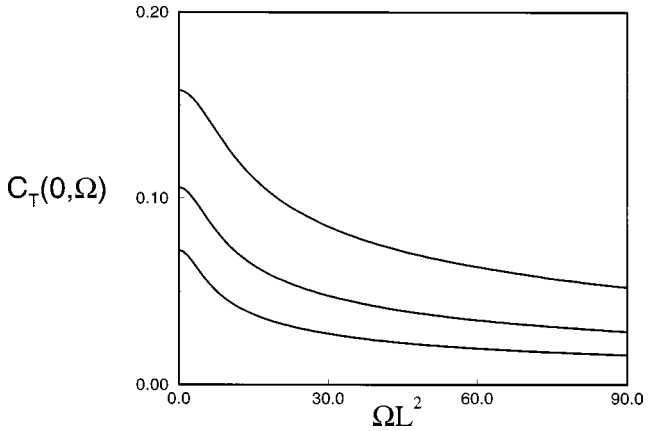

FIG. 24. The C_3 frequency correlation in 3D as a function of frequency difference, with different internal reflection values: upper curve, $z_0=0$; middle curve, $z_0=L/10$; lower curve $z_0=L/5$; no absorption.

In a diagrammatic approach the kth moment can be represented by a diagram with k diffusons on both incoming and outgoing sides. The $k=1$ term is the average total transmission $\langle T_a\rangle$, as given by the Schwarzschild-Milne equation in Eq. (355), it corresponds to a single diffuson and is thus independent of channel-to-channel correlations. The second moment can be decomposed in the first two cumulants:

$$\frac{\langle T_a^2\rangle}{\langle T_a\rangle^2}=\frac{\langle T_a\rangle^2}{\langle T_a\rangle^2}+\frac{\langle T_a^2\rangle_{\rm cum}}{\langle T_a\rangle^2}=1+\langle\langle T_a^2\rangle\rangle, \tag{384}$$

where the double brackets denote cumulants normalized to the average. Diagrammatically we depict the second moment in Fig. 25. The decomposition in cumulants proves useful, as each cumulant corresponds to a different number of interactions between the diffusons. The first term, in Fig. 25(a), contains no interference; it factorizes in the average transmission squared. The second term, Fig. 25(b), is the second cumulant $\langle\langle T_a^2\rangle\rangle$. It gives the variance of the fluctuations. This is just a special case of the C_2 correlation function, $\langle\langle T_a^2\rangle\rangle=C_2(0)$.

Likewise, one can distinguish three different contributions to the third moment,

$$\frac{\langle T_a^3\rangle}{\langle T_a\rangle^3}=1+3\langle\langle T_a^2\rangle\rangle+\langle\langle T_a^3\rangle\rangle. \tag{385}$$

We have drawn the corresponding leading diagrams in Fig. 26. The first term, Fig. 26(a), again corresponds to transmission without interference. The second term, Fig. 26(b), is the product of a single diffuson and a second cumulant diagram. From the figure it is clear that this decomposition can be done in three ways, which determine the combinatorical prefactor of $\langle\langle T_a^2\rangle\rangle$ in Eq. (385). The third contribution stands for the third cumulant of the distribution and expresses the leading deviation from the Gaussian distribution. This is the term we are mainly interested in. It consists of two related diagrams: Fig. 26(c) and 26(d). The three intensities can interfere twice two by two, or the intensities can interact all three together, with a Hikami six-point vertex. Both contributions will prove to be of the same order of magnitude. The strength of the effect can be easily estimated using the interpretation of $1/g$ as an interaction probability. By looking at the diagram, we see that the third cumulant is proportional to the probability of two diffusons meeting twice, and thus is of the order $1/g^2$. We have thus found the estimate

$$\langle\langle T_a^3\rangle\rangle\propto\langle\langle T_a^2\rangle\rangle^2. \tag{386}$$

Finally, we note that there is another contribution to both second and third cumulant. Because there is only a finite number of channels in an experiment, the intensity distribution will always have nonzero width. We have verified that this effect brings a negligible contribution to the measured second and third cumulants (Van Rossum, de Boer, and Nieuwenhuizen, 1995).

B. The calculation of the third cumulant

Two processes contribute to the third cumulant. One with two four-point vertices, which we term $\langle\langle T_a^3\rangle\rangle_c$,

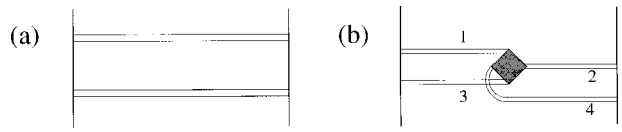

FIG. 25. The two contributions to the second moment of the total transmission. (a) Independent transmission channels. This process is of order unity and is almost completely reducible to the mean value squared. (b) Two interfering channels; this is the second cumulant or C_2 diagram of order $1/g$. The close parallel lines are diffusons.

and one with a six-point vertex $\langle\langle T_a^3\rangle\rangle_d$, where we have chosen the subscripts according to Fig. 26.

1. Interference via two four-point vertices

First consider the diagram in Fig. 26(c). We have labeled the incoming diffusons with odd numbers, the outgoing ones with even numbers. Two incoming diffusons, $\mathcal{L}_1$ and $\mathcal{L}_3$, meet at position z; in a Hikami box they interfere into $\mathcal{L}_2$ and an internal diffuson $\mathcal{L}_{78}^{\rm int}$. $\mathcal{L}_2$ propagates out, whereas $\mathcal{L}_{78}^{\rm int}$ interferes again at z' with the incoming diffuson $\mathcal{L}_5$ into two outgoing ones, $\mathcal{L}_4$ and $\mathcal{L}_6$. Apart from this process, three other sequences of interference are possible. This means that the diffusons can also be permuted as $(\mathcal{L}_1,\mathcal{L}_3,\mathcal{L}_5,\mathcal{L}_2,\mathcal{L}_4,\mathcal{L}_6)\rightarrow(\mathcal{L}_3,\mathcal{L}_5,\mathcal{L}_1,\mathcal{L}_4,\mathcal{L}_6,\mathcal{L}_2)\rightarrow(\mathcal{L}_5,\mathcal{L}_1,\mathcal{L}_3,\mathcal{L}_6,\mathcal{L}_2,\mathcal{L}_4)$. We denote the sum over these permutations as $\Sigma_{\rm per}$. As the diagrams can also be complex conjugated, there is a combinatorial factor of 2 for all diagrams. (Note that this is different from the C_2 calculation; the second cumulant diagram is identical to its complex conjugate and thus there is no such factor.) The expression for the diagram of Fig. 26(c) is now

$$\langle\langle T_a^3\rangle\rangle_c=\langle T_a\rangle^{-3}2\sum_{\rm per}A\int_0^L dz\int_0^L dz' H_4(z)H_4(z')\mathcal{L}_1(z)\times\mathcal{L}_2(z)\mathcal{L}_3(z)\mathcal{L}_4(z')\mathcal{L}_5(z')\mathcal{L}_6(z')\mathcal{L}_{78}^{\rm int}(z,z'). \tag{387}$$

It turns out that it is useful to rewrite the form of the Hikami boxes as introduced in Eq. (339) into an equiva-

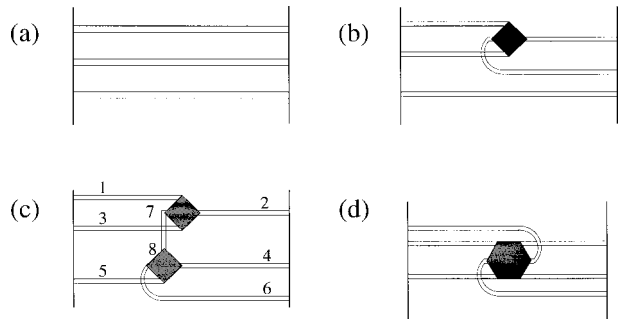

FIG. 26. The three contributions to the third moment of the total transmission: (a) independent transmission channels; contribution is of order 1; (b) correlation which can be decomposed into the second cumulant, contribution is of order g^{-1}; (c) and (d) contributions to the third cumulant, $O(g^{-2})$.

lent expression, using momentum conservation, $\mathbf{q}_a+\mathbf{q}_{a'}+\mathbf{q}_b+\mathbf{q}_{b'}=0$. In real space the use of momentum conservation corresponds to partial integration. The Hikami box is again simplified using the fact that there are no transverse momentum terms, or $q_\perp$ terms, for the outgoing diffusons. Using the numbering in Fig. 26, we obtain

$$H_4(z)=-h_4[2\partial_{z_1}\partial_{z_2}+2\partial_{z_2}\partial_{z_3}],$$
$$H_4(z')=h_4[2\partial_{z_4}\partial_{z_6}-\partial_{z_8}^2+{q_{\perp_8}}^2]. \tag{388}$$

Source terms, i.e., q_i^2 terms, of the incoming and outgoing diffusons were again neglected, but the source term of the diffuson between the vertices is important. As one sees with the diffusion equation (350), it produces

$$(-\partial_{z_8}^2+{q_{\perp_8}}^2)\mathcal{L}_{78}^{\rm in}(z,z')=\frac{l^3}{12\pi}\,\delta(z-z'). \tag{389}$$

The contribution from the source term, i.e., $H_4(z')\propto -\partial_{z_8}^2+{q_{\perp_8}}^2$, $H_4(z)\propto\partial_{z_1}\partial_{z_2}+\partial_{z_2}\partial_{z_3}$, is

$$\frac{-h_4 l^2 A}{k^2}\int_0^L dz[\partial_{z_1}\partial_{z_2}+\partial_{z_2}\partial_{z_3}+\cdots+\partial_{z_6}\partial_{z_1}]\mathcal{L}_1\ldots\mathcal{L}_6. \tag{390}$$

Although this corresponds to a local process (just one z coordinate is involved), it is of leading order. Together with the expression coming from $H_4(z')$, proportional to $\partial_{z_4}\partial_{z_6}$, we find for the total contribution of the process in Fig. 26(c)

$$\langle\langle T_a^3\rangle\rangle_c=\frac{8h_4^2}{\langle T_a\rangle^3}\sum_{\rm per}A\int_0^L dz\,\mathcal{L}_1(z)\mathcal{L}_2'(z)\mathcal{L}_3(z)\int_0^L dz'\,\mathcal{L}_4'(z')\mathcal{L}_5(z')\mathcal{L}_6'(z')\partial_z\mathcal{L}^{\rm int}(z,z')-\frac{l^7A}{48\pi k^4\langle T_a\rangle^3}$$
$$\times\int_0^L dz[\partial_{z_1}\partial_{z_2}+\partial_{z_2}\partial_{z_3}+\partial_{z_3}\partial_{z_4}+\partial_{z_4}\partial_{z_5}+\partial_{z_5}\partial_{z_6}+\partial_{z_6}\partial_{z_1}]\mathcal{L}_1(z)\mathcal{L}_2(z)\mathcal{L}_3(z)\mathcal{L}_4(z)\mathcal{L}_5(z)\mathcal{L}_6(z), \tag{391}$$

where $\mathcal{L}'(z)$ denotes the z derivative of $\mathcal{L}(z)$. When this is calculated for a plane wave, one finds

$$\langle\langle T_a^3\rangle\rangle_c=\frac{28}{15g^2}, \tag{392}$$

which is indeed proportional to g^{-2}, as predicted.

2. Contribution of the six-point vertex

The other diagram contributing to the third cumulant is depicted in Fig. 26(d). The hexagon is again the Hikami six-point vertex H_6. It can be thought of in the following way: the use of the Hikami box assumes that the outgoing legs scatter at least once before they propagate out or interfere again. This is a reasonable assumption for the outgoing diffusons, but for the internal diffuson $\mathcal{L}_{78}^{\rm int}$ it is also possible that coming from z it interferes again at z' directly, i.e., without scattering. This process was not included in the calculation of the previous subsection and has to be studied separately. The unscattered intensity decays exponentially over one mean free path. Therefore this process is important only if z and z' are within one mean free path of each other. As the diagrams can also be complex conjugated, there is also a factor of 2 for all diagrams.

After a Fourier transformation in the z direction the six-point vertex yields a contribution to the third cumulant

$$\langle\langle T_a^3\rangle\rangle_d=\frac{h_4 l^2 A}{k^2\langle T_a\rangle^3}\int_0^L dz[\partial_{z_1}\partial_{z_2}+\partial_{z_2}\partial_{z_3}+\partial_{z_3}\partial_{z_4}+\partial_{z_4}\partial_{z_5}+\partial_{z_5}\partial_{z_6}+\partial_{z_6}\partial_{z_1}]$$
$$\times\mathcal{L}_1(z)\mathcal{L}_2(z)\mathcal{L}_3(z)\mathcal{L}_4(z)\mathcal{L}_5(z)\mathcal{L}_6(z), \tag{393}$$

where again the notation of Eq. (342) is implied. We used the fact that all outgoing diffusons have zero transverse momentum. Therefore all $q_{\perp_i}q_{\perp_j}$ terms are absent. In case of an incoming plane wave we find a contribution to the third cumulant $\langle\langle T_a^3\rangle\rangle_d=-4/(5g^2)$. The contribution from the source term, i.e., Eq. (390) of the previous subsection, exactly cancels the contribution from the six-point vertex. The cancellation seems plausible, as one does not expect short-distance properties to be important in the total process. Nevertheless, this cancellation depends on the precise form of the Hikami four-point vertex in Eq. (388). If we use other equivalent forms of the Hikami box the contributions of the single and double integral in Eq. (391) shift with respect to each other and there is not a full cancellation. Of course, neither the result for Eq. (391) nor the final result for $\langle\langle T_a^3\rangle\rangle$ relies on this choice. One obtains for the third cumulant

$$\langle\langle T_a^3\rangle\rangle=\langle\langle T_a^3\rangle\rangle_c+\langle\langle T_a^3\rangle\rangle_d$$
$$=\frac{8h_4^2Ak^2}{\langle T_a\rangle^3}\sum_{\rm per}\int_0^L dz\,\mathcal{L}_1(z)\mathcal{L}_2'(z)\mathcal{L}_3(z)$$
$$\times\int_0^L dz'\,\mathcal{L}_4'(z')\mathcal{L}_5(z')\mathcal{L}_6'(z')\partial_z\mathcal{L}^{\rm int}(z,z'). \tag{394}$$

C. Influence of incoming beam profile

Now that we know the leading interference processes, we can insert the diffusons and obtain the final value of the third cumulant. We first consider the simple case of incoming plane waves. As there can be no transverse momentum difference in the incoming amplitudes, all

$q_{\perp_i}$ vanish. As a result all diffusons are linear functions of z. We find from Eq. (394)

$$\langle\langle T_a^3\rangle\rangle = \frac{16}{15g^2} = \frac{12}{5}\langle\langle T_a^2\rangle\rangle^2 \quad \text{plane wave;} \quad \rho_0 \gg L. \tag{395}$$

In practice, however, one often deals with a Gaussian beam with limited spot size, influencing the cumulants in two ways. First, if the spot size decreases to values comparable to the sample thickness we have to convolute over a range of incoming momenta, just as we did when calculating the second cumulant. Second, the Gaussian profile contributes an extra geometrical factor, as will be shown below. The expression for the diagrams with diffusons with arbitrary momentum is calculated as follows. Because of momentum conservation and phase condition on the outgoing diffusons, the transverse momentum $\mathbf{q}_{\perp_7}$ of the diffuson connecting the two four-boxes must equal $\mathbf{q}_{\perp_5}$. The integration over the possible momenta results again in a Gaussian weight function $\exp(-\rho_0^2(q_{\perp_1}^2+q_{\perp_3}^2+q_{\perp_5}^2)/8)$. The third cumulant is obtained by inserting the momentum-dependent diffusons into Eq. (394). This gives

$$\langle\langle T_a^3\rangle\rangle = \frac{\rho_0^4}{16\pi^2 g^2}\int d^2\mathbf{q}_{\perp_1} d^2\mathbf{q}_{\perp_3} e^{-\rho_0^2[q_{\perp_1}^2+q_{\perp_3}^2+(q_{\perp_1}+q_{\perp_3})^2]/8} F_3(q_{\perp_1}L, q_{\perp_3}L, |\mathbf{q}_{\perp_1}+\mathbf{q}_{\perp_3}|L), \tag{396}$$

with

$$\begin{aligned} F_3(x_1,x_3,x_5) = \sum_{\text{per}} \Bigg(& \frac{(x_1+x_3)^2 x_5\cosh(x_1+x_3)}{(x_1+x_3+x_5)^2(x_1+x_3-x_5)^2} - \frac{(x_1-x_3)^2 x_5\cosh(x_1-x_3)}{(x_1-x_3+x_5)^2(x_1-x_3-x_5)^2} - \frac{(x_1+x_3)x_5\sinh(x_1+x_3)}{(x_1+x_3+x_5)(x_1+x_3-x_5)} \\ & + \frac{(x_1-x_3)x_5\sinh(x_1-x_3)}{(x_1-x_3+x_5)(x_1-x_3-x_5)} + \frac{(x_1+x_3)\cosh(x_1+x_3+2x_5)}{4(x_1+x_3+x_5)^2} - \frac{(x_1+x_3)\cosh(x_1+x_3-2x_5)}{4(x_1+x_3-x_5)^2} \\ & - \frac{(x_1-x_3)\cosh(x_1-x_3+2x_5)}{4(x_1-x_3+x_5)^2} + \frac{(x_1-x_3)\cosh(x_1-x_3-2x_5)}{4(x_1-x_3-x_5)^2} \Bigg) [x_5\sinh(x_1)\sinh(x_3)\sinh^2(x_5)]^{-1}. \end{aligned} \tag{397}$$

If the beam diameters are wide ($\rho_0 \gg L$), one finds $F_3(0,0,0) = \frac{16}{15}$, which means for the third cumulant $\langle\langle T_a^3\rangle\rangle = 4F_3(0,0,0)/3g^2$, or

$$\langle\langle T_a^3\rangle\rangle = \frac{16}{5}\langle\langle T_a^2\rangle\rangle^2 \quad \text{(Gaussian profile;} \quad \rho_0 \gg L), \tag{398}$$

which differs by a factor of $\frac{4}{3}$ from the plane-wave limit Eq. (395). This is a geometrical effect, depending on the profile of the incoming beam. In a real-space picture one understands this effect most easily: The correlation depends on the distance. It is strongest if the incoming beams are close together. Therefore it is not surprising to see the influence of their overlap. In the next section we calculate this geometrical factor for higher cumulants as well. For the experimentally relevant case when the beam diameter is roughly equal to the thickness, it turns out that the behavior of Eq. (398) is found for a large range of beam diameters. The increase of the correlation for smaller beams turns out to be roughly the same for both the third cumulant and the second cumulant squared.

Van Rossum, De Boer, and Nieuwenhuizen (1995) extensively compared theory with the experiment reported by De Boer *et al.* (1994). Apart from the correction for the finite beam diameter, as discussed above, two other experimental corrections were included—internal reflections and contributions from disconnected diagrams. All corrections to Eq. (398) turn out to be relatively small. By presenting the results as the ratio between the second cumulant squared and the third cumulant, errors in the sample thickness and the mean free path cancel. For the experimental data it was found that $\langle\langle T_a^3\rangle\rangle = (3.3 \pm 0.6)\langle\langle T_a^2\rangle\rangle^2$, in good agreement with Eq. (398).

Stoytchev and Genack (1997) performed microwave scattering on systems with values of g approaching unity. In that case the plane-wave prediction applies. They found $\langle\langle T_a^3\rangle\rangle = (2.38 \pm 0.05)\langle\langle T_a^2\rangle\rangle^2$, indeed in good agreement with Eq. (395).

The extension of the calculation to higher cumulants is straightforward. The nth cumulant will contain $(n-1)$ Hikami four-point vertices. So the contribution is $\langle\langle T_a^n\rangle\rangle \propto g^{1-n}$. But it is clear that the calculation becomes laborious at large n. We take another approach to this problem in Sec. XVIII.

D. Third cumulant of the conductance

The reader will not be surprised to learn that the third cumulant of the conductance can also be calculated using a diagrammatic approach (Van Rossum, Lerner, Altshuler, and Nieuwenhuizen, 1997). This third cumulant is notable for vanishing in one dimension (Macêdo, 1994). We already saw that in the mesoscopic regime the conductance shows universal fluctuations (UCF). The conductance being a random variable showing large

fluctuations, one should consider its full distribution. It was soon clear that the first higher cumulants of the conductance are proportional to (Altshuler, Kravtsov, and Lerner, 1986)

$$\langle g^n\rangle_{\rm cum} \propto \langle g\rangle^{2-n}, \quad n < g_0, \quad \langle g\rangle > 1. \tag{399}$$

Here g_0 is the mean conductance at the scale l. In the metallic regime far from localization, where $\langle g\rangle \gg 1$, the higher cumulants are probably small, and the distribution of the conductance is roughly Gaussian. However, for $n \gtrsim g_0$ the decrease in magnitude of the cumulants, as described by Eq. (399), is changed into a very rapid increase ($\propto \exp[g_0^{-1} n^2]$). This leads to log-normal tails of the distribution (Altshuler *et al.*, 1986). With increasing disorder, the log-normal tails become more important. The full conductance distribution at the threshold of localization ($\langle g\rangle \sim 1$) is at present unknown, but it is quite plausible that the whole distribution crosses over to a log-normal shape in the strongly localized regime [see Shapiro (1990) and Altshuler, Kravtsov, and Lerner (1991) for a discussion]. Indeed, it is well known that in the strongly localized regime in one dimension the conductance is given by the product of transmission amplitudes, yielding a log-normal distribution (Anderson, Thouless, Abrahams, and Fisher, 1980; Abrikosov, 1981; Economou and Soukoulis, 1981; Mel'nikov, 1981).

Although higher-order cumulants govern the tails of the distribution, they do not affect it near the center. A deviation from the Gaussian distribution near the center is revealed, first of all, in the lowest nontrivial cumulants. An important step in this direction was the calculation of the third cumulant of the distribution using random-matrix theory by Macêdo (1994). He found for the orthogonal ($\beta=1$) and symplectic ensemble ($\beta=4$) that the third cumulant of the conductance is proportional to $1/g^2$. Thus the leading term given by Eq. (399) vanishes [see, for instance, Mehta (1967) for the definitions of the ensembles]. For the unitary ensemble ($\beta=2$) even this sub-leading term vanishes, and the behavior is $1/g^3$ (Macêdo, 1994). The physical reason behind this is not clear. [We recently learned that the same result in quasi one dimension was found Tartakovski (1996) using the scaling method described by Tartakovski (1995).] However, random-matrix theory is only valid in quasi-one-dimensional systems. Therefore it was not known whether such a cancellation also occurred in higher dimensions. If this is indeed the case, it might indicate an overlooked symmetry of the system, as is suggested by the fact that the leading-order contribution to the third cumulant of the density of states vanishes in two dimensions (Altshuler *et al.*, 1986). The question we thus wish to consider is whether or not a cancellation occurs for the third cumulant of the conductance in two and three dimensions.

We rewrite Eq. (399) into a relation for the relative cumulants: $\langle g^n\rangle_c / \langle g\rangle^n \propto \langle g\rangle^{2-2n}$. The inverse powers of $\langle g\rangle$ on the right-hand side can be interpreted as the number of Hikami four-boxes in the diagrams; hence the third cumulant diagram contains four Hikami four-boxes. Indeed, it proves impossible to draw $\langle g^3\rangle_c$ diagrams with three boxes. Diagrams with more boxes are sub-leading as they are of higher power in $1/\langle g\rangle$. The diagrams are represented in Fig. 27. In the figure there are diagrams of the same order with one six-box and two four-boxes. They can be obtained by contracting one diffusion in the diagrams with four-boxes. In physical terms the six-box diagrams correspond to processes in which, after an interference process, the amplitudes do not combine into a diffuson, but instead interact directly again without being scattered.

The diagrams were evaluated using the Kubo approach, which offers the advantage that no divergences emerge; treatment of absorption is difficult, though, as indicated in the discussion on C_3. The evaluation of the diagrams is a painful but straightforward exercise. The diagrams have two or three free-momentum loops, of which one is eliminated due to momentum conservation. In one dimension, where the diffusons are simple linear functions, the diagrams can be evaluated analytically. Numerical evaluation of the integrals in $d=2$ and $d=3$ yield

$$\begin{aligned}
&\langle g^3\rangle_c = 0 \quad \text{(quasi 1D)},\\
&\langle g^3\rangle_c = -0.0020\langle g\rangle^{-1} \quad \text{(quasi 2D, square)},\\
&\langle g^3\rangle_c = +0.0076\langle g\rangle^{-1} \quad \text{(3D, cubic)}.
\end{aligned} \tag{400}$$

Thus the leading contribution to the third cumulant in one dimension vanishes. This confirms the random-matrix theory result (Macêdo, 1994) diagrammatically. It is seen that there is no cancellation in higher dimensions. The results for rectangular samples are given in Fig. 28, where we multiplied the third cumulant by the average of the dimensionless conductance. The third cumulant for wide slabs ($L_x \gg L_z$, $L_y \gg L_z$) is proportional to $(L_x L_y/\langle g\rangle)$. In the figure, due to the multiplication by $\langle g\rangle$, there is proportionality to $(L_x L_y)^2/L_z^4$ for wide slabs. Note that the third cumulant passes through zero when going from 2D to 3D at a sample size of $0.46 L_z \times L_z \times L_z$. For very narrow slabs the correct quasi-2D limit is recovered.

The random-matrix result that the third cumulant vanishes in one dimension is also found in the diagrammatic approach. In two and three dimensions, however, there is no cancellation; the leading contribution to the third cumulant is negative in two dimensions and positive in three dimensions. The fact that the third cumulant changes sign is surprising. The third cumulant is also known as the skewness of a distribution. One would have expected a positive third cumulant of the conductance in analogy with the third cumulant of the total transmission, or if the distribution would be tending to log-normal. Instead, we find that all possible values occur: negative, positive, and zero. Experiments measuring the conductance distribution could shed some light on this point.

XVIII. FULL DISTRIBUTION FUNCTIONS

In this section we calculate the full distribution of the total transmission and the angle-resolved transmission;

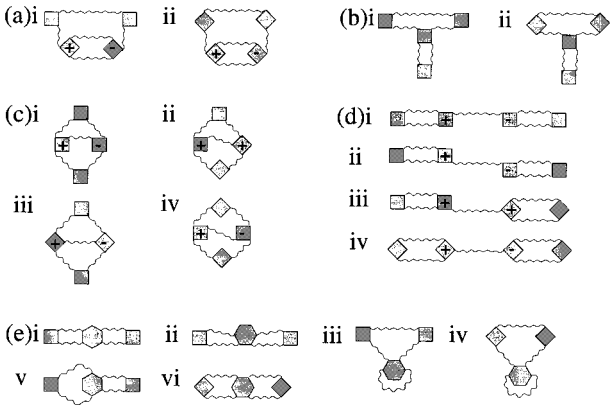

FIG. 27. Set of diagrams for the third cumulant of the conductance. The wavy lines denote diffusons (in the Kubo approach).

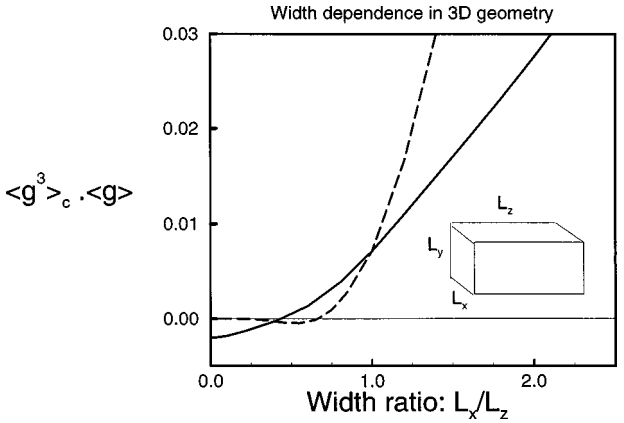

FIG. 28. Third cumulant multiplied by the average conductance in a 3D sample, plotted against the transverse size L_x. The geometry is $L_x \times L_z \times L_z$ for the solid line. Note that the sign changes in going from a quasi-2D to a 3D sample. The dashed line corresponds to the geometry $L_x \times L_x \times L_z$.

both can be mapped on the eigenvalue distribution of the transmission matrix. Before we discuss the distribution in the mesoscopic regime, let us first consider the "classical" situation, which is the limit of large g. There are no correlations between intensities. Here the angle-resolved transmission, or speckle intensity, is distributed according to Rayleigh's law (Goodman, 1975),

$$P(T_{ab}) = \frac{1}{\langle T_{ab} \rangle} e^{-T_{ab}/\langle T_{ab} \rangle}. \tag{401}$$

Anyone who has ever seen a laser speckle pattern on the wall will remember the wild pattern with both bright and dark spots, due to this distribution. Rayleigh's law can be derived in the context of the ladder diagrams (Shapiro, 1986). The nth moment of the speckle intensities is made up of n amplitudes and n complex-conjugated amplitudes. As stated before, there is no restriction on the pairing of two amplitudes into a diffuson for this type of measurement. The amplitudes $\{a_1^*, a_2^*, a_3^*, \ldots, a_n^*\}$ have $n!$ possibilities of pairing with the amplitudes $\{a_1, a_2, a_3, \ldots, a_n\}$. Thus

$$\langle T_{ab}^n \rangle = n! \langle T_{ab} \rangle^n, \tag{402}$$

which corresponds with Rayleigh's law. Yet, as we know from the example of a laser beam reflecting from a rough wall, multiple scattering is not essential for Rayleigh's law to operate. Indeed, Rayleigh's original derivation goes as follows (Goodman, 1975): The field ψ at a given position on the outgoing side is the sum of many fields, and therefore the real and imaginary parts each have an independent Gaussian distribution. The intensity I is the amplitude squared and thus has an exponential distribution,

$$P \sim e^{-[(\mathrm{Re}\ \psi)^2 + (\mathrm{Im}\ \psi)^2]/2\sigma^2} \sim e^{-I/\langle I \rangle}. \tag{403}$$

Thus reflection from a rough wall will also work.

Kogan and Kaveh (1995) addressed the question of the speckle statistics of (optically) very thin samples. In optically thin samples a considerable fraction of the light does not scatter at all, but is transmitted coherently. In the limit of zero thickness, i.e., only coherent light, the distribution becomes a delta function. In the intermediate regime a simple counting argument yields the distribution, which interpolates between the delta distribution and Rayleigh's law. In the opposite case of strong scattering, the mesoscopic regime, interferences modify the speckle distribution. The leading correction was derived by Shnerb and Kaveh (1991). Genack and Garcia observed a deviation from Rayleigh's law at large intensities (Garcia and Genack, 1989; Genack and Garcia, 1993). A crossover to stretched exponential behavior was derived by Kogan *et al.* (1993).

For the total transmission and the conductance, the distributions are similar in the large-g limit. For both quantities the outgoing diffusons are frequency and momentum independent, as we explained in Sec. XV. As there is no interaction between the diffusons in this limit, only one type of pairing is possible for both quantities. This yields, in principle, a delta distribution if one probes an infinite number of channels. In practice, of course, only a limited number of channels are probed, and the law of large numbers predicts a narrow Gaussian distribution.

A. Eigenvalues of the transmission matrix

In mesoscopic systems the observables are random quantities and are therefore not always characterized by their mean values, but their entire distribution function is of interest. This is particularly true in the distribution of eigenvalues of the transmission matrix. Assuming that all eigenvalues contribute equally to the conductance, one would expect a Gaussian distribution. As there are N eigenmodes, the eigenvalue distribution should be peaked around $g/N = l/L$. But this picture proves wrong, as was first observed by Dorokhov (1984) and later by Imry (1986). It is not the eigenvalues, but the inverse localization lengths $1/\xi_n$ that are uniformly distributed (Pendry, MacKinnon, and Pretre, 1990; Stone *et al.*, 1991). As a result the eigenvalues T_n of the transmission matrix $t^\dagger t$ can be expressed as

$$T_n = \cosh^{-2}(L/\xi_n), \tag{404}$$

implying that

$$\langle \mathrm{Tr}(tt^\dagger)^j \rangle = \left\langle \sum_{n=1}^{N} T_n^j \right\rangle = g \int_0^1 \frac{dT}{2T\sqrt{1-T}}\, T^j. \tag{405}$$

This distribution is plotted in Fig. 29. The first derivations of the distribution used random-matrix theory and were therefore valid only in quasi 1D (Mello, Pereyra, and Kumar, 1988). However, Nazarov (1994) showed that it is true not only in quasi 1D, but also under very general conditions. Note that the normalization of the distribution is ill defined—the distribution should be understood in the sense that all its moments are defined. This problem can be avoided by adjusting the lower boundary of the integral to something other than 0. The minimal value corresponds to the decay of unscattered intensity. Therefore $T_n \geqslant \cosh^{-2}(L/l) \approx \exp(-2L/l)$, normalizing the distribution Eq. (405). Although this cutoff is important for the normalization of the distribution, its influence on the momenta is very small, and we refrain from it. The distribution Eq. (405) is valid only in the regime where g is not too small. Loop effects near the Anderson transition, where $g \sim 1$, will change it, as we discuss below.

The concept of open and closed channels explains the physical meaning of this curious distribution function. An eigenmode of the transmission matrix is, according to this distribution, either essentially blocked or, with a much smaller probability, essentially conducting. This picture has been confirmed in various computer simulations (Pendry *et al.*, 1990; Pendry, MacKinnon, and Roberts, 1992; Oakeshott and MacKinnon, 1994). The eigenvalue distribution also provides us with a nice picture explaining why the correlations in mesoscopic systems are so large. If all the channels are equally conducting, fluctuations of the channels average out by the law of large numbers. Yet if only a few channels are conducting, fluctuations in one channel will be clearly seen. The probability distribution of the total transmission and deviations from Rayleigh's law will be explained below using these concepts.

We should point out that for the UCF the same argument does not apply. The variance in the conductance Nl/L is caused by the finiteness of the number of channels N. In the picture of either closed or open channels the number of open channels N_{eff} equals roughly $Nl/L \ll N$. The conductance would thus fluctuate according the law of large numbers with a variance: $\langle \Sigma_n T_n^2 \rangle = \frac{2}{3} g$. However, this is incorrect, as we know that $\langle \Sigma_n T_n^2 \rangle \sim O(1)$; see Sec. XVI.D. For the UCF the interaction between the eigenmodes is essential.

In practice it is difficult, if not impossible, to measure the eigenmodes and eigenvalues directly. As they are the eigenmodes of the very large random-transmission matrix, they have a very complex structure. Nevertheless, the eigenvalue distribution has observable consequences. It was shown by Beenakker and Büttiker (1992) that the shot noise of electronic conductors universally reduces by a factor of 3 because of this distribution. Shot noise occurs only in electronic systems and thus is not of much interest for us. Instead, we shall show that the total transmission and speckle-intensity distribution function are related to the eigenvalue distribution function.

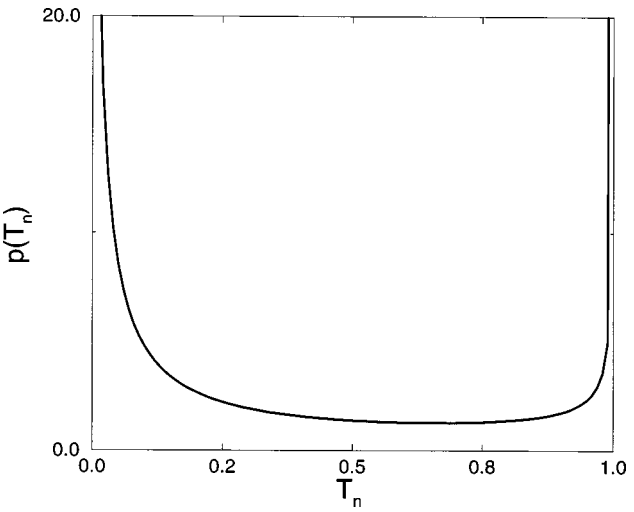

FIG. 29. Bimodal eigenvalue distribution of transmission matrix. The average value occurs with only a small probability. The eigenvalues are almost all either 0 or 1.

B. Distribution of total transmission

We first calculate the probability distribution of the total transmission. From the distribution without interference effects we saw that it has a simpler distribution (in the sense of cumulants) than the speckle distribution. We neglect corrections such as absorption, skin layers, and disconnected diagrams. Consider again an incoming plane wave in direction μ_a (μ denotes again the cosine with respect to the z axis). The wave is transmitted into the outgoing channel b with transmission amplitude t_{ab} and transmission probability $T_{ab} \equiv |t_{ab}|^2$. The speckle and total transmission factorize as $\langle T_a \rangle = \epsilon_n g$ and $\langle T_{ab} \rangle = \epsilon_a \epsilon_b g$.

We consider the jth cumulant of T_a. In a diagrammatic approach this object has j transmission amplitudes t_{ab} and an equal number of Hermitian conjugates $t_{ba}^\dagger = t_{ab}^*$. The explicit calculation of the second cumulant C_2 (Sec. XV) and third cumulant (Sec. XVII) showed that the leading diagrams are connected and have no loops.

Let us fix the external diffusions in the term $t_{ab_1} t_{b_1 a}^\dagger t_{ab_2} \ldots t_{ab_j} t_{b_j a}^\dagger$. Contributions to the sum over b_i come only from diagrams with outgoing diffusons that have no transverse momentum. These are the diagrams in which the lines with equal b_i pair into diffusons. We indicate this pairing of the outgoing diffusons with brackets,

$$(t_{ab_1}t^\dagger_{b_1a})(t_{ab_2}t^\dagger_{b_2a})\ldots(t_{ab_j}t^\dagger_{b_ja}). \tag{406}$$

The outgoing diffusons are now fixed. At the incoming side it is convenient to keep the t_{ab}'s fixed, while the $t^\dagger_{ab}$'s are permuted among them. This leaves $j!$ possibilities for the incoming side in total, but of these only $(j-1)!$ permutations correspond to connected diagrams (these diagrams contain $j-1$ Hikami boxes. The C_2 diagram contained one box, the third cumulant diagram two boxes). Next we factor out the incoming and outgoing diffusons and group the remainder of the diagrams into a skeleton K. Making use of Eq. (349) we obtain

$$\langle T_a^j\rangle_{\rm con}=\epsilon_a^j(j-1)!\int d\mathbf{r}_1 d\mathbf{r}_1'\ldots d\mathbf{r}_j d\mathbf{r}_j'\,\mathcal{L}_{\rm in}(\mathbf{r}_1)\times\mathcal{L}_{\rm out}(\mathbf{r}_1')\ldots\mathcal{L}_{\rm in}(\mathbf{r}_j)\mathcal{L}_{\rm out}(\mathbf{r}_j')K(\mathbf{r}_1,\mathbf{r}_1',\ldots,\mathbf{r}_j,\mathbf{r}_j'). \tag{407}$$

The integral just describes

$$\langle{\rm Tr}(tt^\dagger)^j\rangle\equiv{\rm Tr}\sum_{b_1,a_2,b_2,\ldots,a_j,b_j}\langle t_{a_1b_1}t^\dagger_{b_1a_2}t_{a_2b_2}\ldots t_{a_jb_j}t^\dagger_{b_ja_1}\rangle = \sum_{a_1,b_1,\ldots,a_j,b_j}\langle t_{a_1b_1}t^\dagger_{b_1a_2}t_{a_2b_2}\ldots t_{a_jb_j}t^\dagger_{b_ja_1}\rangle. \tag{408}$$

There is only one way to attach incoming and outgoing diffusons to K. The sums over the indices lead exactly to the total flux diffusons in Eq. (407). One finds the following important relation between the moments of the eigenvalue distribution and the connected total transmission diagrams:

$$\langle T_a^j\rangle_{\rm con}=(j-1)!\,\epsilon_a^j\langle{\rm Tr}(tt^\dagger)^j\rangle. \tag{409}$$

Normalizing with respect to the average, we introduce $s_a=T_a/\langle T_a\rangle$. The generating function of the connected diagrams is easily calculated:

$$\Phi_{\rm con}(x)\equiv\sum_{j=1}^{\infty}\frac{(-1)^{j+1}x^j}{j!}\langle s_a^j\rangle_{\rm con} = g\,\log^2(\sqrt{1+x/g}+\sqrt{x/g}). \tag{410}$$

Since the cumulants are given solely by connected diagrams, the distribution of s_a follows as (Nieuwenhuizen and Van Rossum, 1995)

$$P(s_a)=\int_{-i\infty}^{i\infty}\frac{dx}{2\pi i}\exp[xs_a-\Phi_{\rm con}(x)]. \tag{411}$$

Let us examine some properties of this distribution. For limiting values of s_a we use a saddle-point analysis. The saddle point is found by the condition $(d/dx)[xs_a-\Phi_{\rm con}(x)]=0$. Thus we find

$$s_a=\frac{\log(\sqrt{1+x/g}+\sqrt{x/g})}{\sqrt{x/g(1+x/g)}}. \tag{412}$$

The right-hand side of Eq. (412) diverges if x approaches $-g$ (from above) and decreases monotonically for larger x. Thus for large $s_a\gg1$ we find the saddle point near $x=-g$. By inserting the saddle point one finds a simple exponential tail,

$$P(s_a)\approx\exp\left(-gs_a+g\,\frac{\pi^2}{4}\right),\quad s_a\gg1. \tag{413}$$

The saddle point also dominates the shape for small $s_a\ll1$ (and large g). One finds essentially log-normal growth:

$$P(s_a)\sim\exp\left[\frac{g}{4}-\frac{g}{4}\left(\log\frac{2}{s_a}+\log\log\frac{2}{s_a}-1\right)^2\right]. \tag{414}$$

In Fig. 30 the solid curves depict the distribution equation (411) for some values of g. At moderate g we can clearly see the deviation from a Gaussian. In interesting, recent experiments on quasi-1d microwave scattering, Stoytchev and Genack (1997) measured the total transmission distribution for conductances as low as $g\sim3$. Although one would expect important loop contributions for such low values of g, excellent agreement with the above prediction was found. To obtain the fit, the value of g had to be extracted from the variance of the distribution rather than from the measured conductance. This adjustment is probably necessary because of the strong absorption occurring in waveguides. The effect of absorption was calculated by Brouwer (1997) for a waveguide. For strong absorption the total transmission had a log-normal distribution, while the ratio of $\ll T_a^3\gg/\ll T_a^2\gg^2$ became 3.0 instead of 2.4.

C. Influence of beam profile

We have considered above the case of an incoming plane wave. Again in optical systems a Gaussian intensity profile is more realistic. For the third cumulant we saw a nontrivial dependence on the incoming beam profile, suggesting that higher cumulants are also sensitive to this effect. For perpendicular incidence the incoming amplitude is $\psi_{\rm in}(\mathbf{r})=W^{-1}\Sigma_a\phi(q_a)\psi^a_{\rm in}(\mathbf{r})$, where $\psi^a_{\rm in}(\mathbf{r})$ is the plane wave of Eq. (147), and where

$$\phi(q_a)=\sqrt{2\pi}\rho_0\,\exp(-\tfrac{1}{4}\rho_0^2q_a^2). \tag{415}$$

We consider the limit in which the beam is much broader than the sample thickness ($\rho_0\gg L$) but still much smaller than the transverse size of the slab ($\rho_0\ll W$). With a smaller beam diameter, the incoming transverse momenta, which are of order $1/\rho_0$, are of the order of $1/L$. The diffusons will then become the well-known cosh functions (Sec. XVI.A). Here the momentum dependence of the diffusons can be neglected; apart from a geometrical factor, the diffusons are identical to the plane-wave case. Due to the integration over the center of gravity, each diagram involves a factor $A\,\delta_{\Sigma q,\Sigma q'}$. In the jth-order term there occurs a factor

$$F_j=\frac{A}{A^{2j}}\sum_{q_1q_1'\ldots q_jq_j'}\phi(q_1)\phi^*(q_1')\ldots\phi(q_j)\phi^*(q_j')\,\delta_{\Sigma q,\Sigma q'} = \int d^2\rho|\phi(\rho)|^{2j}. \tag{416}$$

For a plane wave we have $|\phi(\rho)|=\sqrt{A}$, and $F_j=A^{1-j}$. For our Gaussian beam we obtain

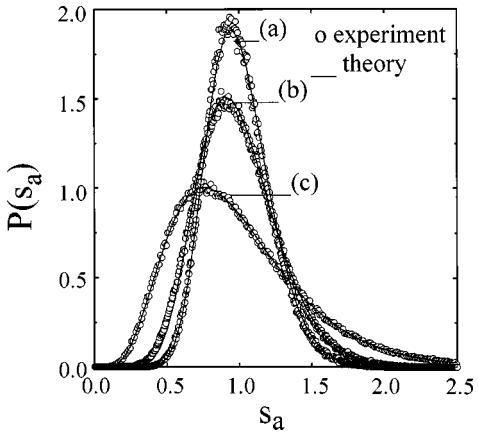

FIG. 30. Distribution of the total transmission vs normalized intensity s_a. Theory and microwave experiments for three different sample sizes (*a,b,c*) from Stoychev and Genack (1997). For curve (c), the conductance is the lowest at 3.06 (absorption corrected). Reproduced with kind permission of the authors.

$$F_j=\frac{1}{j}\left(\frac{\pi\rho_0^2}{2}\right)^{1-j}. \tag{417}$$

It is thus convenient to identify $A_G=\frac{1}{2}\pi\rho_0^2$ with the effective area of a Gaussian beam. (This definition is different from the one used in previous sections, where $A_G=\pi\rho_0^2$). As compared to the plane-wave case, the jth-order term is smaller by a factor of $1/j$ for a Gaussian profile. This implies for the generating function of the connected diagrams

$$\Phi_{\rm con}(x)=g\int_0^1\frac{dy}{y}\log^2\left(\sqrt{1+\frac{xy}{g}}+\sqrt{\frac{xy}{g}}\right). \tag{418}$$

For small s_a (and large g), there is again a log-normal saddle point. For large s_a, the dominant shape of the decay is given by the singularity at $x=-g$ and again yields $P(s_a)\sim\exp(-gs_a)$. The shape of the distribution is quite similar to the plane-wave case. Expanding the generating function we recover the results for the second and third cumulant obtained in Secs. XV and XVII.

D. Speckle intensity distribution

We apply the same method to obtain the distribution of the angular transmission coefficient. The angular and total transmission distributions are related to each other in a fairly simple way, because the interference processes are dominated by the same type of diagrams: loopless connected diagrams. The different distribution for total transmission and speckle is the consequence of a counting argument only. In the plane-wave situation the average angular transmission reads $\langle T_{ab}\rangle=\epsilon_a\epsilon_b g$. Let us count the number of connected loopless diagrams that contribute to $T_{ab}^j=t_{ab}t_{ba}^\dagger t_{ab}\ldots t_{ab}t_{ba}^\dagger$. Now not only massless outgoing diffusons, but all pairings into outgoing diffusons contribute. This yields an extra combinatorial factor $j!$ in the jth moment:

$$\langle T_{ab}^j\rangle_{\rm con}=j!(j-1)!\,\epsilon_a^j\epsilon_b^j\langle{\rm Tr}(t^\dagger t)^j\rangle. \tag{419}$$

For the normalized angular transmission coefficient $s_{ab}=T_{ab}/\langle T_{ab}\rangle$, we define the generating function of the connected diagrams as (Nieuwenhuizen and Van Rossum, 1995)

$$\Phi_{\rm con}(x)\equiv\sum_{j=1}^{\infty}\frac{(-1)^{j-1}x^j}{j!^2}\langle s_{ab}^j\rangle_{\rm con}, \tag{420}$$

with $\Phi_{\rm con}$ given by Eq. (410) for plane-wave incidence and by Eq. (418) for a broad Gaussian beam, respectively. In contrast to the total transmission distribution, the cumulants are not only given by the connected diagrams. Kogan *et al.* (1993) showed that the extra summation of the disconnected diagrams corresponds to an additional integral, which finally yields a Bessel function:

$$P(s_{ab})=\int_{-i\infty}^{i\infty}\frac{dx}{\pi i}\,K_0(2\sqrt{-s_{ab}x})\exp(-\Phi_{\rm con}(x)). \tag{421}$$

The integral can be evaluated numerically. The speckle intensity distribution is shown in Fig. 31 for an incoming plane wave.

For large g and moderate s_{ab}, one has $\Phi_{\rm con}(x)\approx x$ and we recover Rayleigh's law: $P(s_{ab})=\exp(-s_{ab})$. The leading correction is found by expanding in $1/g$,

$$P(s_{ab})=e^{-s_{ab}}\left[1+\frac{1}{3g}(s_{ab}^2-4s_{ab}+2)\right]. \tag{422}$$

A similar equation was derived previously by Shnerb and Kaveh (1991).

For obtaining the tail of the distribution, one can again apply steepest descent, which yields

$$P(s_{ab})\exp(-2\sqrt{gs_{ab}}). \tag{423}$$

This stretched exponential tail of the distribution was observed as early as 1989 by Garcia and Genack in microwave experiments, but unfortunately their dynamic range was rather small. The fit of the stretched exponential was therefore rather imprecise. The maximum intensity was five times the average where one does not expect to see the tail behavior, but rather observes a crossover behavior. Using Eq. (418) one easily derives the speckle distribution due to an incoming beam with Gaussian profile. This leads to a different distribution with the same asymptotic behavior.

E. Joint distribution

It turns out that the speckle distribution and the total transmission distribution of a given incoming direction are related. This is not surprising as a large total transmission for a given incoming direction will also be reflected in the individual speckles. The moments of the joint distribution are

$$\langle s_{ab}^k s_a^l\rangle_{\rm con}=(k+l-1)!k!\langle{\rm Tr}(tt^\dagger)^{k+l}\rangle. \tag{424}$$

The combinatorial factor $k!$ is for the speckle pattern, the factor $(k+l-1)!$ is the number of possible pairings of incoming beam. Defining σ_{ab} as $s_{ab}=\sigma_{ab}s_a$, one obtains $\langle\sigma_{ab}^k s_a^m\rangle=k!(m-1)!\langle T_n^m\rangle$ with $m=k+l$. Thus

$P(\sigma_{ab},s_a)=\exp(-\sigma_{ab})P(s_a)$. This shows that σ_{ab} and s_a are independent variables. Nevertheless, s_{ab} and s_a are dependent. Their joint distribution is

$$P(s_{ab},s_a)=\frac{\exp(-s_{ab}/s_a)}{s_a}\times\int\frac{dx}{2\pi i}\exp(xs_a-\Phi_{\rm con}(x)). \tag{425}$$

Integration over s_a or s_{ab} yields the distribution $P(s_{ab})$, or $P(s_a)$, respectively. This is somewhat surprising. Indeed, as the right-hand side of Eq. (425) contains only connected diagrams, and thus the same holds for the left-hand side. This seems to contradict our earlier remark that $P(s_{ab})$ contained both connected and disconnected diagrams. However, in deriving Eq. (425) we have tacitly performed an analytic continuation for negative l values. By performing the integration over s_a we find the correct expression for $P(s_{ab})$.

In conclusion we have derived the full distribution function of both the total transmission and the angular transmission coefficients by mapping it to the distribution of eigenvalues of T_{ab}. But at least for the lowest cumulants one can use this mapping the other way around. First, experiments on the distribution functions confirm the eigenvalue distribution. Secondly, from our detailed evaluation of the low-order diagrams, i.e., the second and third cumulants, we can gain insight on the eigenvalue distribution. It is clear from those calculations that the eigenvalue distribution is also based on loopless connected diagrams.

The effect of absorption has been neglected here. Our explicit calculation of second and third cumulants and the experimental data show that the effects of absorption and skin layers can be incorporated to a large extent by considering normalized cumulants, such as $\langle T_a^3\rangle_c/\langle T_a^2\rangle_c^2$. Indeed, in the presence of strong absorption these dimensionless ratios are similar to the values calculated without absorption (Stoytchev and Genack, 1997). A theoretical analysis of absorption effects has been carried out by Brouwer (1997).

The distribution of the conductance cannot be calculated using the above technique. The correlations in the conductance correspond to these in the eigenvalues. These correlations were not included, as we used only the distribution of a single eigenvalue, and not the joint distribution of multiple eigenvalues.

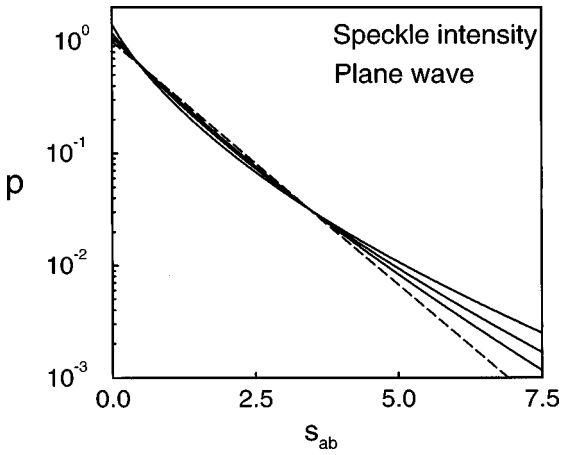

FIG. 31. Distribution of speckles vs the normalized intensity s_{ab} for an incoming plane wave, $g=2$, 4, and 8 (upper to lower curve at $s_{ab}=5$). The dashed line corresponds to Rayleigh's law ($g=\infty$).

ACKNOWLEDGMENTS

We have been stimulated by the continuous interest in our work of A. Z. Genack, H. C. van de Hulst, I. V. Lerner, J. M. Luck, and G. Maret. We have gained many insights on this subject from discussion and collaboration with our co-workers M. P. van Albada, B. L. Altshuler, E. Amic, J. F. de Boer, A. L. Burin, Zh. S. Gevorkian, E. Hofstetter, Yu. M. Kagan, A. Lagendijk, D. J. Lancaster, I. V. Lerner, J. M. Luck, R. Maynard, A. Mosk, P. N. den Outer, M. Schreiber, G. V. Shlyapnikov, B. A. van Tiggelen, and R. Vlaming. Further we should like to thank C. W. J. Beenakker, P. W. Brouwer, the late S. Feng, J. J. M. Franse, N. N. Garcia, T. R. Kirkpatrick, E. Kogan, Yu. Nazarov, M. Nieto-Vesperinas, J. L. Pichard, I. Ya. Polishchuk, J. Ricka, J. J. Saens, R. Sprik, M. Stoytchev, A. Tip, P. de Vries, and G. H. Wegdam. This research was supported by the EEC HCM-Network ERBCHRXCT930373 and by NATO (Grant number CRG 921399).

APPENDIX: LOOP INTEGRALS

The same loop momentum integrals recur often in the diagram calculations:

$$I_{k,l}\equiv\int\frac{d^3\mathbf{p}}{(2\pi)^3}G^k(\mathbf{p})G^{*l}(\mathbf{p}), \tag{A1}$$

where $G(\mathbf{p})=[\mathbf{p}^2-k^2-nt]^{-1}$. For the simplest integral, $I_{1,1}$, we find

$$I_{1,1}=\int\frac{d^3\mathbf{p}}{(2\pi)^3}G(\mathbf{p})G^*(\mathbf{p})=\int_{-\infty}^{\infty}\frac{dp}{(2\pi)^2}\frac{p^2}{(p^2+\mu^2)(p^2+\bar{\mu}^2)}, \tag{A2}$$

where $\mu^2=-k^2-nt$. The sum of the residues yields $1/[4\pi(\mu+\bar{\mu})]$, and without absorption the optical theorem gives

$$\mu+\bar{\mu}=\frac{n\ \mathrm{Im}\ t}{k}=\frac{1}{l}. \tag{A3}$$

Therefore

$$I_{1,1}=\frac{l}{4\pi}. \tag{A4}$$

The general $I_{k,l}$ integral can be found from the $I_{1,1}$ integral using

$$I_{k+1,l}=\frac{-1}{2k\mu}\frac{d}{d\mu}I_{k,l};$$

$$I_{k,l+1}=\frac{-1}{2l\overline{\mu}}\frac{d}{d\overline{\mu}}I_{k,l}. \tag{A5}$$

For example, $I_{1,2}=-I_{2,1}=-il^2/(8\pi k)$ and $I_{2,2}=l^3/(8\pi k^2)$. We shall also use

$$\int \frac{d^3\mathbf{p}}{(2\pi)^3}(\mathbf{p}\cdot\mathbf{q})^2 G^k(\mathbf{p})G^{*l}(\mathbf{p})=\frac{1}{3}k^2q^2I_{k,l}, \tag{A6}$$

where the factor of 1/3 comes from the angular integral. If absorption is present $\mu+\overline{\mu}=[l(1-\kappa^2l^2/3)]^{-1}$, and thus

$$I_{1,1}=\frac{1}{4\pi(\mu+\overline{\mu})}=\frac{l}{4\pi}\left(1-\frac{1}{3}\kappa^2l^2\right). \tag{A7}$$

In general there is a prefactor

$$I_{n,m}\propto(1-\kappa^2l^2/3)^{n+m-1}, \tag{A8}$$

where we have assumed that $\kappa l\ll 1$. However, this prefactor need only be included for terms not proportional to q or $\tilde{\Omega}$, as we work to first order of (Ml).

REFERENCES

Abrahams, E., P. W. Anderson, D. C. Licciardello, and T. V. Ramakrishnan, 1979, Phys. Rev. Lett. **42**, 673.

Abrikosov, A. A., 1981, Solid State Commun. **37**, 997.

Abrikosov, A. A., L. P. Gor'kov, and I. E. Dzyaloshinski, 1963, *Methods of Quantum Field Theory in Statistical Physics* (Dover, New York).

Altshuler, B. L., 1985, Pis'ma Zh. Éksp. Teor. Fiz. **41**, 530 [JETP Lett. **41**, 648].

Altshuler, B. L., A. G. Aronov, and B. Z. Spivak, 1981, Pis'ma Zh. Éksp. Teor. Fiz. **33**, 101 [JETP Lett. **33**, 94].

Altshuler, B. L., V. E. Kravtsov, and I. V. Lerner, 1986, Zh. Éksp. Teor. Fiz. **91**, 2276 [Sov. Phys. JETP **64**, 1352].

Altshuler, B. L., V. E. Kravtsov, and I. V. Lerner, 1991, in *Mesoscopic Phenomena in Solids*, edited by B. L. Altshuler, P. A. Lee, and R. A. Webb, Modern Problems in Condensed Matter Sciences No. 30 (North-Holland, Amsterdam), p. 449.

Altshuler, B. L., P. A. Lee, and R. A. Webb, 1991, Eds., *Mesoscopic Phenomena in Solids*, Modern Problems in Condensed Matter Sciences No. 30 (North-Holland, Amsterdam).

Ambartsumian, V. A., 1943, Dokl Akad. Nauk SSSR **38**, 257.

Amic, E., J. M. Luck, and T. M. Nieuwenhuizen, 1996, J. Phys. A **29**, 4915.

Amic, E., J. M. Luck, and T. M. Nieuwenhuizen, 1997, J. Phys. I **17**, 445.

Anderson, P. W., 1958, Phys. Rev. **109**, 1492.

Anderson, P. W., D. J. Thouless, E. Abrahams, and D. S. Fisher, 1980, Phys. Rev. B **22**, 3519.

Ando, T., and H. Fukuyama, 1988, Eds., *Anderson Localization*, Springer Proceedings in Physics No. 28 (Springer, Berlin).

Barabanenkov, Y. N., 1973, Izv. Vyssh. Uchebn. Zaved. Radiofiz. **16**, 88.

Beenakker, C. W. J., 1997, Rev. Mod. Phys. **69**, 731.

Beenakker, C. W. J., and M. Büttiker, 1992, Phys. Rev. B **46**, 1889.

Berkovits, R., 1990, Phys. Rev. B **42**, 10750.

Berkovits, R., and S. Feng, 1994, Phys. Rep. **238**, 135.

Berkovits, R., and M. Kaveh, 1990, Europhys. Lett. **13**, 97.

Brouwer, P. W., 1997, Phys. Rev. B **57**, 10526.

Chandrasekhar, S., 1960, *Radiative Transfer* (Dover, New York).

de Boer, J. F., M. P. van Albada, and A. Lagendijk, 1992, Phys. Rev. B **45**, 658.

de Boer, J. F., M. C. W. van Rossum, M. P. van Albada, T. M. Nieuwenhuizen, and A. Lagendijk, 1994, Phys. Rev. Lett. **73**, 2567.

den Outer, P. N., and A. Lagendijk, 1993, Opt. Commun. **103**, 169.

den Outer, P. N., T. M. Nieuwenhuizen, and A. Lagendijk, 1993, J. Opt. Soc. Am. A **10**, 1209.

Dorokhov, O. N., 1984, Solid State Commun. **51**, 381.

Economou, E. N., 1990, *Green's Functions in Quantum Physics* (Springer, Berlin).

Economou, E. N., and C. M. Soukoulis, 1981, Phys. Rev. Lett. **46**, 618.

Efetov, K. N., 1983, Adv. Phys. **32**, 53.

Feng, S., C. Kane, P. Lee, and A. D. Stone, 1988, Phys. Rev. Lett. **61**, 834.

Feng, S., F. A. Zeng, and B. Chance, 1995, Appl. Opt. **34**, 3826.

Fisher, D. S., and P. A. Lee, 1981, Phys. Rev. B **23**, 6851.

Freund, I., and R. Berkovits, 1990, Phys. Rev. B **41**, 496.

Freund, I., and M. Rosenbluh, 1991, Opt. Commun. **82**, 362.

Freund, I., M. Rosenbluh, and S. Feng, 1988, Phys. Rev. Lett. **61**, 2328.

Garcia, N., and A. Z. Genack, 1989, Phys. Rev. Lett. **63**, 1678.

Garcia, N., A. Z. Genack, R. Pnini, and B. Shapiro, 1993, Phys. Lett. A **176**, 458.

Genack, A. Z., and N. Garcia, 1993, Europhys. Lett. **21**, 753.

Genack, A. Z., N. Garcia, and W. Polkosnik, 1990, Phys. Rev. Lett. **65**, 2129.

Gevorkian, Zh. S., 1998, Phys. Rev. E **57**, 2338.

Gevorkian, Zh. S., and Th. M. Nieuwenhuizen, 1998, Phys. Rev. E (in press).

Goodman, J. W., 1975, in *Laser Speckle and Related Phenomena*, edited by J. C. Dainty, (Springer, Berlin), Vol. 9, p. 9.

Gor'kov, L. P., A. I. Larkin, and D. E. Khmel'nitskii, 1979, Pis'ma Zh. Éksp. Teor. Fiz. **30**, 248 [JETP Lett. **30**, 228].

Gorodnichev, E., S. Dudarev, and D. Rogozkin, 1990, Phys. Lett. A **144**, 48.

Guéret, P., C. Rossel, E. Marclay, and H. Meier, 1989, J. Appl. Phys. **66**, 278.

Halperin, B. I., 1965, Phys. Rev. A **139**, 104.

Hanke, W., and Y. V. Kopaev, 1992, Eds., *Electronic Phase Transitions*, Modern Problems in Condensed Matter Sciences No. 32 (North-Holland, Amsterdam).

Hikami, S., 1981, Phys. Rev. B **24**, 2671.

Imry, Y., 1986, Europhys. Lett. **1**, 249.

Ioffe, A. F., and A. R. Regel, 1960, Prog. Semicond. **4**, 237.

Ishimaru, A., 1978, *Wave Propagation and Scattering in Random Media, Vols. 1 and 2* (Academic, New York).

Janβen, M., 1991, Solid State Commun. **79**, 1073.

Kagiwada, H. H., R. Kalaba, and S. Ueno, 1975, *Multiple Scattering Processes: Inverse and Direct*, Applied Mathematics and Computation No. 8 (Addison-Wesley, Reading, MA).

Kane, C. L., R. A. Serota, and P. A. Lee, 1988, Phys. Rev. B **37**, 6701.

Kaveh, M., 1991, in *Analogies in Optics and Micro-Electronics*, edited by W. van Haeringen and D. Lenstra (Kluwer Academic, Haarlem).
Kirkpatrick, T. R., 1985, Phys. Rev. B **31**, 5746.
Kogan, E., and M. Kaveh, 1995, Phys. Rev. B **51**, 16400.
Kogan, E., M. Kaveh, R. Baumgartner, and R. Berkovits, 1993, Phys. Rev. B **48**, 9404.
Kramer, B., and G. Schön, 1990, Eds., *Anderson Transition and Mesoscopic Fluctuations*, Physica A **167** (special issue).
Kroha, J., 1990, Physica A **167**, 231.
Kroha, J., T. Kopp, and P. Wölfe, 1990, Phys. Rev. B **41**, 888.
Kuga, Y., and A. Ishimaru, 1985, J. Opt. Soc. Am. A **1**, 831.
Lagendijk, A., and B. A. van Tiggelen, 1996, Phys. Rep. **270**, 143.
Lagendijk, A., R. Vreeker, and P. de Vries, 1989, Phys. Lett. A **136**, 81.
Lancaster, D., and T. M. Nieuwenhuizen, 1998, Physica A **256**, 417.
Landauer, R., 1975, Z. Phys. B **21**, 247.
Lee, P. A., and T. V. Ramakrishnan, 1985, Rev. Mod. Phys. **57**, 291.
Lee, P. A., and A. D. Stone, 1985, Phys. Rev. Lett. **55**, 1622.
Lee, P. A., A. D. Stone, and H. Fukuyama, 1987, Phys. Rev. B **35**, 1039.
Lerner, I. V., 1996, private communication.
Lisyansky, A. A., and D. Livdan, 1992, Phys. Lett. A **170**, 53.
Luck, J. M., 1997, unpublished.
Luck, J. M., and T. M. Nieuwenhuizen, 1998, Phys. Rev. E (in press).
Macêdo, A. M. S., 1994, Phys. Rev. B **49**, 1858.
MacKintosh, F., and S. John, 1988, Phys. Rev. B **37**, 1884.
MacKintosh, F., and S. John, 1989, Phys. Rev. B **40**, 2383.
Mehta, M. L., 1967, *Random Matrices and the Statistical Theory of Energy Levels* (Academic, New York).
Mello, P. A., P. Pereyra, and N. Kumar, 1988, Ann. Phys. (N.Y.) **181**, 290.
Mel'nikov, V. I., 1981, Sov. Phys. Solid State **23**, 444.
Merzbacher, E., 1970, *Quantum Mechanics* (Wiley, New York).
Mie, G., 1908, Ann. Phys. (Leipzig) **25**, 377.
Mosk, A., T. M. Nieuwenhuizen, and C. Barnes, 1996, Phys. Rev. B **53**, 15914.
Mott, N. F., 1990, *Metal-Insulator Transitions* (Taylor and Francis, London).
Nagaoka, Y., and H. Fukuyama, 1982, Eds., *Anderson Localization*, Springer Series in Solid State Sciences No. 8 (Springer, Berlin).
Nazarov, Y. V., 1994, Phys. Rev. Lett. **73**, 134.
Nieuwenhuizen, T. M., 1983, Physica A **120**, 197.
Nieuwenhuizen, T. M., 1984, Physica A **125**, 468.
Nieuwenhuizen, T. M., 1993, Europhys. Lett. **24**, 269.
Nieuwenhuizen, T. M., 1993, unpublished.
Nieuwenhuizen, T. M., A. L. Burin, Y. Kagan, and G. V. Shlyapnikov, 1994, Phys. Lett. A **184**, 360.
Nieuwenhuizen, T. M., and J. M. Luck, 1993, Phys. Rev. E **48**, 560.
Nieuwenhuizen, T. M., and M. C. W. van Rossum, 1995, Phys. Rev. Lett. **74**, 2674.
Oakeshott, R. B. S., and A. MacKinnon, 1994, J. Phys.: Condens. Matter **6**, 1513.
Ospeck, M., and S. Fraden, 1994, Phys. Rev. E **49**, 4578.
Paasschens, J. C. J., and G. W. 't Hooft, 1998, J. Opt. Soc. Am. (in press).
Pendry, J. B., A. MacKinnon, and A. B. Pretre, 1990, Physica A **168**, 400.
Pendry, J. B., A. MacKinnon, and P. J. Roberts, 1992, Proc. R. Soc. London, Ser. A **437**, 67.
Peters, K., 1992, Phys. Rev. B **46**, 801.
Pnini, R., and B. Shapiro, 1989, Phys. Rev. B **39**, 6986.
Pnini, R., and B. Shapiro, 1991, Phys. Lett. A **157**, 265.
Polishchuk, I., A. L. Burin, and L. A. Maksimov, 1990, Pis'ma Zh. Éksp. Teor. Fiz. **51**, 644 [JETP Lett. **51**, 731].
Rayleigh, (Lord), J. W. S., 1980, Philos. Mag. **1**, 491 [in *Scientific papers I*, p. 53 (1964) Dover, New York].
Rikken, G. L. J. A., and B. A. van Tiggelen, 1996, Nature (London) **381**, 54.
Schotland, J. C., J. C. Haselgrove, and J. S. Leigh, 1993, Appl. Opt. **32**, 448.
Shapiro, B., 1986, Phys. Rev. Lett. **57**, 2168.
Shapiro, B., 1990, Phys. Rev. Lett. **65**, 1510.
Sharvin, Y., and Y. Sharvin, 1981, Pis'ma Zh. Éksp. Teor. Fiz. **34**, 285 [JETP Lett. **34**, 272].
Sheng, P., 1990, Ed., *Classical Wave Localization* (World Scientific, Singapore).
Shnerb, N., and M. Kaveh, 1991, Phys. Rev. B **43**, 1279.
Soukoulis, C. M., 1993, Ed., *Photonic Band Gaps and Localization* (Plenum, New York).
Stephen, M. J., and G. Cwilich, 1987, Phys. Rev. Lett. **59**, 285.
Stone, A. D., P. A. Mello, K. A. Muttalib, and J.-L. Pichard, 1991, in *Mesoscopic Phenomena in Solids*, edited by B. L. Altshuler, P. A. Lee, and R. A. Webb, Modern Problems in Condensed Matter Sciences No. 30 (North-Holland, Amsterdam), p. 369.
Stoytchev, M., and A. Z. Genack, 1997, Phys. Rev. Lett. **79**, 309.
Tartakovski, A. V., 1995, Phys. Rev. B **52**, 2704.
Tartakovski, A. V., 1996, private communication.
Thouless, D. J., 1974, Phys. Rep., Phys. Lett. **13C**, 93.
Thouless, D. J., 1977, Phys. Rev. Lett. **39**, 1167.
Umbach, C. P., S. Washburn, R. B. Laibowitz, and R. A. Webb, 1984, Phys. Rev. B **30**, 4048.
van Albada, M. P., and A. Lagendijk, 1985, Phys. Rev. Lett. **55**, 2692.
van Albada, M. P., B. A. van Tiggelen, A. Lagendijk, and A. Tip, 1991, Phys. Rev. Lett. **66**, 3132.
van Albada, M. P., J. F. de Boer, and A. Lagendijk, 1990, Phys. Rev. Lett. **64**, 2787.
van de Hulst, H. C., 1980, *Multiple Light Scattering, Vols. 1 and 2* (Academic, New York).
van de Hulst, H. C., 1997, private communication.
van de Hulst, H. C., and R. Stark, 1990, Astron. Astrophys. **235**, 511.
van der Mark, M. B., M. P. van Albada, and A. Lagendijk, 1988, Phys. Rev. B **37**, 3575.
van Haeringen, W., and D. Lenstra, 1990, Eds., *Analogies in Optics and Micro Electronics* (Kluwer Academic, Haarlem).
van Haeringen, W., and D. Lenstra, 1991, Eds., *Analogies in Optics and Micro Electronics* (Kluwer Academic, Haarlem).
van Rossum, M. C. W., J. F. de Boer, and Th. M. Nieuwenhuizen, 1995, Phys. Rev. E **52**, 2053.
van Rossum, M. C. W., I. V. Lerner, B. L. Altshuler, and T. M. Nieuwenhuizen, 1997, Phys. Rev. B **55**, 4710.
van Rossum, M. C. W., and T. M. Nieuwenhuizen, 1993, Phys. Lett. A **177**, 452.
van Rossum, M. C. W., T. M. Nieuwenhuizen, and R. Vlaming, 1995, Phys. Rev. E **51**, 6158.

van Tiggelen, B. A., 1995, Phys. Rev. Lett. **75**, 422.
van Tiggelen, B. A., R. Maynard, and T. M. Nieuwenhuizen, 1996, Phys. Rev. E **53**, 2881.
Vdovin, Y. A., and V. M. Galitskii, 1967, Zh. Éksp. Teor. Fiz. **52**, 1345 [Sov. Phys. JETP **25**, 894].
Vollhardt, D., and P. Wölfle, 1980a, Phys. Rev. Lett. **45**, 842.
Vollhardt, D., and P. Wölfle, 1980b, Phys. Rev. B **22**, 4666.
Vollhardt, D., and P. Wölfle, 1992, in *Electronic Phase Transitions*, Modern Problems in Condensed Matter Sciences No. 32, edited by W. Hanke and Y. V. Kopaev (North-Holland, Amsterdam), p. 1.
Wegner, F., 1976, Z. Phys. B **25**, 327.
Wegner, F., 1979, Z. Phys. B **35**, 207.
Wolf, P. E., and G. Maret, 1985, Phys. Rev. Lett. **55**, 2696.
Zhu, J. X., D. J. Pine, and D. A. Weitz, 1991, Phys. Rev. A **44**, 3948.
Zhu, X. D., S. P. Wei, S. Feng, and B. Chance, 1996, J. Opt. Soc. Am. A **13**, 494.
Zyuzin, A. Y., and B. Z. Spivak, 1987, Sov. Phys. JETP **66**, 560.